A TURBULENT BOUNDARY LAYER WITH SLOT INJECTION OF DRAG REDUCING POLYMER

A THESIS

Presented to

The Faculty of the Graduate Division

by

Dermot Joseph Collins

In Partial Fulfillment

of the Requirements for the Degree

Doctor of Philosophy in the School of Chemical Engineering

Georgia Institute of Technology

July 1973

A TURBULENT BOUNDARY LAYER WITH SLOT INJECTION

OF DRAG REDUCING POLYMER

Approved:

Dr. C. W. Gorton, Chairman

Professor J. E. Hubbartt

Dr. J. D. Muzzy

Date Approved by Chairman: July 17, 1973

ACKNOWLEDGMENTS

I wish to thank my thesis advisor, Dr. C. W. Gorton, for his considerable help throughout my graduate study. His patient and understanding guidance helped me in both the field of science and the game of life.

I am appreciative to my reading committee, Professor J. E. Hubbartt and Dr. J. D. Muzzy for their time and counsel. A special acknowledgment is due the late Dr. William Meese Newton, who was my thesis advisor for the early part of this investigation.

I am grateful to Gulf Oil, DuPont, Union Camp and Allied Chemical corporations for fellowships during my stay at Georgia Tech.

I should like to acknowledge Mr. C. E. Anderson for assistance in taking concentration data, Mr. and Mrs. L. R. Faulkner for help in preparing the illustrations, Mr. C. R. Blackwood and Mr. E. E. Weaver for aid in fabricating equipment components; Mr. L. W. Elston for help in developing analytical procedures and providing laboratory space, and Mrs. Nancy Price for her good work in preparing this manuscript. I also appreciate the stimulating conversations, scientific and otherwise, with Messrs. Weaver, Elston and K. A. Rogers.

I cannot thank my wife Paula enough. She helped in different phases of my research -- data taking and analyses, typing and proofreading of my writing, and constant encouragement and understanding when the going was tough (which was only too frequent).

TABLE OF CONTENTS

TABLE OF CONTENTS (Continued)

LIST OF TABLES

LIST OF TABLES (Continued)

LIST OF ILLUSTRATIONS

LIST OF ILLUSTRATIONS(Continued)

NOMENCLATURE

a	constant in equations that result from least squares analysis
A	reciprocal of von Karman Constant
$\tilde{A}$	constant in the "ultimate profile" Equation (3-8)
b	constant in equations that result from least squares analysis
B	constant in law of the wall Equation (2-12)
$\tilde{B}$	constant in the "ultimate profile" Equation (3-8)
B_1	Parameter in Equation (2-14)
c	constant in equations that result from least squares analysis
C	polymer concentration (ppm)
C_f	total skin-friction coefficient
C_f'	local skin-friction coefficient
C_i	concentration of injected solution (ppm)
C_p	pressure coefficient defined by Equation (3-10)
f,F	general parameter to indicate functional relationship
F_1	general parameter to indicate functional relationship Equation (2-22)
g	general parameter to indicate functional relationship Equation (2-10)
G	boundary layer parameter defined by Equation (2-24)
G_1	function for deviation from law of the wall (Equation(2-22))
H	velocity profile ratio defined by Equation (2-8)
k	von Karman Constant
K	constant for Equation (2-25)
K_m	minimum torque on rotating disk, used in Equation (3-9)

NOMENCLATURE (Continued)

L_δ	boundary layer growth parameter defined by Equation (2-29)
L_λ	concentration plume growth parameter defined by Equation (2-30)
M	molecular weight
n,N	general purpose integer constant
ΔP_s	measured difference between total and static pressure Equation (3-10)
Q_s	sublayer discharge defined in Equation (3-20)
R	pipe radius
R_e	Reynolds number based on pipe radius
R_θ	Reynolds number based on momentum thickness
R_x	Reynolds number based on length
u	mean velocity in the x direction
u'	time dependent velocity in the x direction
u_*	friction velocity, $u_* \sqrt{\tau_w/\rho}$
u_*^c	friction velocity below which drag reduction does not occur
U	free stream velocity in x direction
U_t	true towing velocity, Equation (3-10)
v	mean velocity in the y direction
v'	time dependent velocity in the y direction
w	parameter in equation (2-16)
x	coordinate parallel to the test surface
y	coordinate normal to the test surface
y_+	non-dimensional distance, $y_+ = yu_*/\nu$
z	parameter defined by Equation (3-16)

NOMENCLATURE (Continued)

SUPERSCRIPTS

o	in the pure solvent
p	in the polymer solution

SUBSCRIPTS

w	at the wall
45	x=45
66	x=66

GREEK LETTERS

α	fluid property parameter associated with drag reducing fluids
β	relative rate parameter, defined in Equation (2-31)
Δ	boundary layer parameter defined by Equation (2-23)
δ	boundary layer thickness δ = y(.99 U)
δ_∞	boundary layer thickness δ = y(U)
δ_{ave}	boundary layer thickness averaged over a number of runs
δ_{red}	reduction in boundary layer growth defined in Equation (6-3)
δ_1	displacement thickness defined in Equation (2-7)
ς	non-dimensional distance - $\xi = y/\lambda$
γ	defined in Equation (3-14), $\gamma = U/u_*$
λ	characteristic concentration plume height - y(0.5 C_w)
$[\eta]$	intrinsic viscosity defined by Equation (4-2)
μ	viscosity
ρ	density
Π	equilibrium boundary layer parameter
τ	shear stress

NOMENCLATURE (Concluded)

τ_1	maximum relaxation time of polymer molecules
θ	momentum thickness, defined in Equation (2-6)
ν	kinematic viscosity
σ	sublayer thickness $u_*/\nu = 11.6$

SUMMARY

An experimental study involving velocity profile and polymer concentration measurements was made in a developing channel boundary layer. Pure water and aqueous solutions of Poly (ethylene oxide), Polyox WSR-301, of 500, 1000, and 2000 ppm were injected into the boundary layer downstream from the origin through two rows of holes at an angle of 15^{o} with the plate. Channel dimensions were 12 in. by 3 in.;in the test section the boundary layer thickness and free stream velocity were approximately one inch and 2.6 ft/sec respectively. Both concentration and velocity profiles were measured at test stations 3,6,9, and 15 inches downstream from the injection source for injection rates of 250, 350, 500 and 1000 cc/min. The last rate corresponds to the "sublayer discharge" for pure water flow.

Velocity profiles were measured with a Pitot tube. Wall shear stress data for the pure water boundary layer were obtained using the "law of the wall". The presence of PEO caused large errors in velocity measurements close to the wall. Consequently, the law of the wall method could not be applied to compute wall shear. The pure water velocity defects were plotted for all four test stations. The results showed that the flow approximated an equilibrium turbulent boundary layer. This plot was assumed valid when polymer solutions were injected, and wall shear was calculated from velocity measurements taken in that portion of the boundary layer where no polymer had diffused. Although the results are imprecise they predicted drag increase rather than drag reduction.

However, for all polymer injections studied boundary layer growth rate was reduced, indicating a reduction in drag. These contradictory results led to the conclusion that for the flow situation studied, the wake section of the boundary layer did not have the same velocity defect relationship when polymer was injected.

Concentration profiles were obtained by adding a tracer (150 ppm of Rhodamine B dye) to the injected concentrate. Samples were withdrawn through the same Pitot tube used for velocity data, and dye intensity was measured colorimetrically. The results showed that injection of polymer solution caused supressed turbulent diffusion. For water injection the initial zone of turbulent diffusion lasted approximately three inches from the source. For injection of 500 ppm solutions the initial zone was extended to 15 inches. Injections of 1000 and 2000 ppm solutions resulted in all 21 inches of the test section being in the initial zone. To date, these are the only experimental concentration data in the literature for the "initial zone" of turbulent diffusion. The results also showed that slot injection was more efficient for higher injection concentrations.

CHAPTER I

INTRODUCTION

Very small concentrations, on the order of a few parts per million by weight, of certain dissolved high molecular weight polymers can reduce the frictional resistance in turbulent flow to as low as one fourth that of the pure solvent. Many investigators have noted this behavior experimentally. Since these solutions have a higher viscosity than the pure solvent, the reduction of turbulent skin friction is somewhat surprising.

Toms[1], in 1948, was the first to publish data on this friction reducing effect. He studied a system of polymethyl methacrylate in monochlorobenezene. This phenomenon is sometimes called the "Toms' effect". However, this is a misnomer since there is at least one instance of much earlier work in this area[2]. During World War II, research was done concerning the characteristics of gasoline thickened with aluminum soaps. In turbulent pipe flow the head loss was less for the thickened solution than for that of the pure gasoline.

In the late 1950's, Shaver[3] and Dodge[4] reported reduced friction in solutions of sodium carboxymethylcellulose (CMC). Shaver also observed a repressed formation of horseshoe vortices in turbulent flow. In 1961, Ousterhout and Hall[5] obtained large friction reductions in hydraulic fracturing of oil wells by adding both a natural gum polymer and a synthetic polymer to the water or brine. Possible naval applications led to government support which resulted in increased activity in the study of drag reduction. Vogel and Patterson[6] were the first to obtain

drag reduction from ejection of polymeric solutions into a boundary layer.

Fabula[7] discovered the friction reducing ability of poly (ethylene oxide), (PEO), and was the first to notice drag reduction in the parts per million range. To date, PEO remains the most effective drag reducing material known. Only a few parts per million are required for appreciable friction reduction PEO has become a standard material for studies of friction reduction.

From the mid 1960's to date there has been a considerable amount of research done in the area of drag reduction. This work has been concerned with confirming and extending the basic ideas outlined earlier, and examining possible new applications for friction reduction. Many experiments and theoretical studies with various polymer-solvent systems have been reported. In turbulent shear flows dilute polymer solutions behave differently from pure solvent. Some examples are turbulent flow in both rough and smooth pipes, couette flow, spinning disks, heat and mass transfer, and Pitot tubes. A rigorous explanation has not yet been advanced.

Considerable research is being directed toward engineering applications of the drag reduction phenomenon. In the oil industry, applications presently used are in the drilling of oil wells, in well fracturing operations, and the pumping of crude oil. In the area of naval applications, continuous ejection from a ship may not be economical. Kowalski[8] estimated that several tons of polymer would be required per hour to maintain a uniform 20 ppm polymer concentration throughout the boundary layer on a ship 450 feet long. However, recent studies suggest it is only necessary to have polymer in the sublayer, and that major reductions of polymer

costs and more efficient ejection schemes are necessary for commercial ship application to be feasible. Experiments with a fire department pumper and hose[9] showed head loss was considerably reduced when 200 ppm of PEO was added. Along with greater flow, or less pressure drop in the line, Green[10] has shown that the polymer jet from the nozzle spreads less, is more resistant to wind break-up, and concentrates the water in a smaller area. These factors may be important in fire fighting.

The purpose of the present study was to investigate experimentally changes in various boundary layer parameters resulting from slot ejection of polymer solution concentrate into a two-dimensional developing turbulent boundary layer in channel flow. Experimentally measured velocity and concentration profiles were used to evaluate the effect of injection concentration and rate on the velocity and concentration boundary layers. These data were also used to develop and evaluate a technique based on the velocity defect concept for using the velocity profile to calculate wall shear in a turbulent boundary layer injected with polymer solution.

It is well known that turbulent flow cannot be successfully analyzed for all flow details. For laminar flow, the shear stress can be computed from the velocity profile. In the case of turbulent flow, there is no universal expression known relating the Reynolds stresses to the mean velocity distribution; hence no exact solutions for the boundary layer equations are possible. Completion of the above objectives, however, will provide a contribution to understanding the effect of injecting drag reducing polymer concentrate on the mean flow structure of a turbulent boundary layer.

CHAPTER II

DIFFUSION AND WALL SHEAR IN A TURBULENT BOUNDARY LAYER

2.1 The Turbulent Boundary Layer

2.1.1 The Basic Equations of the Turbulent Boundary Layer

For two-dimensional flow, the steady-state turbulent boundary-layer equations, written in terms of the usual rectangular Cartesian co-ordinates are[11,12,13]

$$u \frac{\partial u}{\partial x} + v \frac{\partial u}{\partial y} = U \frac{dU}{dx} + \frac{1}{\rho} \frac{\partial \tau}{\partial y} - \frac{\partial \overline{u'}^2}{\partial x} \qquad (2\text{-}1)$$

In Equation (2-1) the shear stress τ is given by:

$$\tau = -\rho \overline{u'v'} + \mu \frac{\partial u}{\partial y} \qquad (2\text{-}2)$$

The continuity equation for the mean flow,

$$\frac{\partial u}{\partial x} + \frac{\partial v}{\partial y} = 0 \qquad (2\text{-}3)$$

also applies. For most flows, the last term in Equation (2-1) may be neglected; hence the equation of motion becomes:

$$u \frac{\partial u}{\partial x} + v \frac{\partial v}{\partial y} = U \frac{dU}{dx} + \frac{1}{\rho} \frac{\partial \tau}{\partial y} \qquad (2\text{-}4)$$

For laminar flow, the existence of a known relationship between the shear stress and the velocity gradient completes the set of partial differential equations and an exact solution of the boundary layer equations is mathematically possible. Analytic solutions have been obtained

for some simple boundary conditions. These solutions are so-called similar solutions. The numerical solution of any general problem has always been possible in principle, but has only become practical with the advent of high-speed automatic computers. Relatively simple methods of calculations, for example the Pohlhausen method, which is sufficiently accurate for engineering applications, have been developed which satisfy the equations of motion only on the average. They make use of integrated forms satisfying suitable local boundary conditions.

In the case of turbulent flows, no universal expression is known relating the Reynolds stresses to the mean velocity distribution, and no exact solutions of the boundary-layer equations are possible. The problem can be dealt with in two ways, which both require an essentially empirical assumption for the missing relationship. First, there are a restricted range of flows where conditions are such that approximate similarity solutions may be obtained, and second are methods of solution based upon the integral relationships.

2.1.2 Similarity Solutions

For laminar flow, exact similarity solutions are possible for a wide range of external pressure distributions since the whole velocity distribution can be represented by one choice of length and velocity scales. This is possible for the turbulent layer on a smooth surface only as an approximation in special flow situations. The turbulent layer may be assumed to be composed of two regions: an inner one depending solely upon local conditions, and an outer one dependent upon the upstream history of the flow.

The assumption of a constant eddy viscosity (in normal direction) in the outer region allows for a similarity solution for this part of the layer. However, the inner region provides the boundary conditions for this solution and strict similarity must be relaxed if matching of the two different regions is to be possible. This leads to a solution in the form of predictions for nearly similar (generally termed 'equilibrium' or 'self-preserving') boundary layers.

2.1.3 Integral Methods

The boundary layer equation may be integrated after eliminating v by means of the continuity equation:

$$\frac{d\theta}{dx} = \frac{\tau_w}{\rho U^2} - (H + 2)\frac{\theta}{U}\frac{dU}{dx} \qquad (2\text{-}5)$$

where

$$\theta = \int_o^\infty \frac{u}{U}\left(1 - \frac{u}{U}\right) dy \qquad (2\text{-}6)$$

$$\delta_1 = \int_o^\infty \left(1 - \frac{u}{U}\right) dy \qquad (2\text{-}7)$$

$$H = \delta_1/\theta \qquad (2\text{-}8)$$

Equation (2-5) is commonly called the "momentum equation", and is valid for both laminar and turbulent flows.

For laminar flow, the assumption of a suitable velocity profile (e.g. Pohlhausen) enables θ and H to be calculated. Since τ_w is related to the velocity profile, the momentum equation (2-5) may be solved, given the inviscid flow solution U(x). The only difficulty arises at the forward stagnation point. (Schlichting[11] outlines the Pohlhausen approach in

great detail.)

The wall shear for turbulent flow is found from some empirical equation, for example, the Ludweig-Tillmann equation:

$$\frac{\tau_w}{\rho U^2} = 0.123\, e^{-1.561\, H} \left(\frac{U\theta}{\nu}\right)^{-0.268} \qquad (2\text{-}9)$$

The assumption of a velocity profile of the form $f(y/\delta)$ for turbulent flow does not give good results. Hence, an extra equation is required to calculate H(x). This equation, usually called the auxiliary equation, is of the form:

$$\theta \frac{dH}{dx} = g\left(H,\ R_\theta,\ \frac{\theta}{U}\ \frac{dU}{dx}\right) \qquad (2\text{-}10)$$

Considerable effort has been put forth to determine the best method of calculating H(x) for air flow. Schlichting[11] outlines some of these equations. The early auxiliary equations were strictly empirical. Later, semi-empirical equations were developed. Some of these are the Energy Equation (Truckenbrodt[11]) Moment of Momentum (Granville[11]) and the Entrainment Equation (Head[14]). As the result of an exhaustive study[15], it has been concluded that there are a number of competitive auxiliary equations for calculating turbulent boundary layers.

2.2 Velocity Profiles in the Turbulent Boundary Layer

The constant-pressure, turbulent layer is markedly different from its laminar counterpart. For laminar flow, a plot of experimental values of $\frac{u}{U}$ versus y/δ reveals a single profile, the Balsius profile. This is true regardless of the Reynolds number and skin friction for most of the laminar region. For turbulent layers no single universal profile

exists. For lack of anything better it was generally assumed that turbulent profiles followed a single 1/nth power curve, with n accepted as approximately 7. However, this n is Reynolds number dependent, and experimental data[16] show n varying from 3 to 10.

For turbulent shear flows, there are two regions of similarity in the velocity profile. Near the wall there is the inner law of the "law of the wall" and in the outer region of the layer is the "velocity defect law". These provide relations between the velocity profile and wall shear stress.

2.2.1 The Law of the Wall

Experimental evidence with turbulent shear flow shows that there is a considerable region near the surface where:

$$\frac{u}{u_*} = f\left(\frac{yu_*}{\nu}\right) \tag{2-11}$$

The earliest formulations were based on pipe flow data. Ludwieg and Tillmann[17] suggested that this law of the wall existed in all cases of turbulent flow past a smooth surface. For the special case of two-dimensional incompressible flow, the law of the wall is well established:

$$\frac{u}{u_*} = \frac{1}{k} \ln\left(\frac{yu_*}{\nu}\right) + B \tag{2-12}$$

where k and B are constants. k is generally accepted as being Von Karman's constant, 0.4. B is assigned values varying from 4.9 (Clauser[16]) to 5.5 (Schlichting[11]). Hinze[12] concludes that because of scatter in experimental data, any value in this range is admissible. For flow past rough surfaces this law applies with k remaining the same and B decreasing with

increasing roughness height. The law of the wall is valid from the outer edge of the buffer zone (usually taken as $yu_*/\nu \approx 25$) for approximately 15-25 percent of the boundary layer. For fully developed pipe flows, Schlichting[11] indicates that this law is valid for all of the turbulent core up to the pipe radius.

Clauser[16] compared velocity profiles for turbulent boundary layers, pipes, and channels such that the logarithmic portions coincide. His results showed that deviation from the logarithmic curve was different for each flow situation.

2.2.2 Velocity Defect Law

Far away from the wall the velocity defect ($\frac{U-u}{u_*}$) has been found experimentally to be independent of viscosity and a function of wall shear, density, and distance from the outer edge of the layer. Independence of viscosity is consistent with the notion of a turbulent rather than a viscous process. The profile similarity may be stated:

$$\frac{U-u}{u_*} = F\,(y/\delta) \qquad (2\text{-}13)$$

This was originally deduced from flat plate, channel and pipe flow data. Clauser[18] showed experimentally the existence of boundary layers that exhibited similarity relationships (2-13) in tailored adverse pressure gradients. Clauser called layers that follow a defect law "equilibrium boundary layers".

There is region in which both methods of correlation overlap, hence a relationship exists between the parameters of both laws. It can be shown (Clauser[16]) that in the overlap zone:

$$\frac{U-u}{u_*} = \frac{-1}{k} \ln\left(\frac{y}{\delta}\right) + B_1 \tag{2-14}$$

From equation 2-12 and 2-14, we get:

$$\frac{U}{u_*} = \frac{1}{k} \ln \frac{\delta u_*}{\nu} + B - B_1 \tag{2-15}$$

Coles[19] suggests the following form of the velocity profile in the outer portion of the layer:

$$\frac{u}{u_*} = f\left(\frac{yu_*}{\nu}\right) + \frac{\Pi}{k} w\,(y/\delta) \tag{2-16}$$

where Π is a parameter independent of x and y; w is called the wake function, and $f\left(\frac{yu_*}{\nu}\right)$ is given by the right hand side of equation 2-12. Under this treatment, the velocity defect law is a deviation from the law of the wall. Coles normalized the wake function by subjecting the following conditions:

$$\begin{aligned} w(0) &= 0 \\ w(1) &= 2 \\ \int_0^2 (y/\delta)\, dw &= 1 \end{aligned} \tag{2-17}$$

Therefore, from conditions at the edge of the layer and the relations (2-17):

$$\frac{U-u}{u_*} = \frac{-1}{k} \ln (y/\delta) + \frac{\Pi}{k} \left[2 - w\,(y/\delta) \right] \tag{2-18}$$

Coles then relates the parameter Π to the local skin friction by:

$$\frac{U}{u_*} = \frac{1}{k} \ln \frac{\delta u_*}{\nu} + B + \frac{2\Pi}{k} \qquad (2\text{-}19)$$

Coles defined the boundary layer thickness in terms of δ by the conditions (2-17) rather than the usual definition ($u/U = .99$). Coles tabulated values of the wake function from his survey of various experimental work. Later authors (Fabula and Burns[20], Hinze[12]) give an approximate equation for $w(y/\delta)$; this is:

$$w(y/\delta) = 2 \sin^2 \left(\frac{\pi}{2} \frac{y}{\delta} \right) \qquad (2\text{-}20)$$

or

$$w(y/\delta) = 1 + \sin \left[\frac{2(y/\delta) - 1}{2} \right] \pi \qquad (2\text{-}21)$$

Π is constant in a given type of equilibrium layer. For flat plate flows, Coles suggests that Π is approximately 0.55.

Clauser[16] also proposed a defect law as a deviation from the law of the wall. He suggests:

$$\frac{u}{u_*} = F_1 \left(\frac{yu_*}{\nu} \right) + G_1 (y/\delta) \qquad (2\text{-}22)$$

where F_1 is the logarithmic law of the wall function, (equation 2-12, with $K = 0.41$ and $B = 4.9$) and G_1 represents the deviation from the logarithmic line. Clauser developed a plot of the function G_1, based on the data of seven experimenters, for both smooth and rough walls. Clauser defines δ as the "thickness of the layer to nominal outer edge". Clauser shows the result for previous work[18] for equilibrium pressure gradients and demonstrates that similarity exists between $(U-u)/u_*$ and y/δ for each set of flow conditions. The functional relation between these appears

to be pressure gradient dependent. Clauser defines the following quantities:

$$\Delta = \delta \int_0^\infty \frac{U - u}{u} \, d\,(y/\delta) \tag{2-23}$$

$$G = \int_0^\infty \left(\frac{U - u}{u_*}\right)^2 d\,(y/\delta) \tag{2-24}$$

He indicates that for constant pressure layers $G = 6.8$ and $\Delta/\delta = 3.6$. For non-zero pressure gradient equilibrium flows, both G and Δ are dependent on pressure gradient and can be used to designate a set of equilibrium profiles.

Hama[21] has proposed the following simple formula for the mean velocity distribution for $y/\delta > 0.15$:

$$\frac{U-u}{u_*} = K\,(1-y/\delta)^2 \tag{2-25}$$

Hinze indicates that this form of equation gives adequate agreement for practical purposes. Hama gives K as 9.6 whereas Granville[22] gives K as 9.87 for flat plates and 7.52 for pipes.

2.2.3 Effect of Polymer on Velocity Profile

On the basis of his own pipe flow experiments, Meyer[23] suggests that the following equation for velocity profiles in pipe flow of dilute polymer solutions:

$$\frac{u}{u_*} = \frac{1}{k} \ln \frac{yu_*}{\nu} + B + \Delta B \tag{2-26}$$

$$\Delta B = \alpha \ln \frac{u_*}{u_*}_c \tag{2-27}$$

That is, the profile has the same slope but a different intercept and may be treated as a "negative roughness". This shift in profile has been noticed also by Wetzel and Ripken[24] and Hulsebos[25] in channel flow. For dilute solutions, u_*^c is independent of concentration and peculiar to a given polymer. Poreh and Hsu[26] claim that for PEO α appears proportional to concentration for values of ΔB up to 28; above this value ΔB changes only slightly with concentration. White[27] gives the following relation for PEO:

$$\alpha = 2.3 \sqrt{C} \qquad (2\text{-}28)$$

He indicates that the maximum value of α is 11, for both guar gum and PEO.

For approximately the inner 15% of the boundary layer of dilute polymer solution flow, the modified law of the wall (2-26) is usually assumed valid. In the outer regions of the layer, the velocity defect law is assumed to remain the same since viscosity does not affect the profile in this region. The experiments of Wetzel and Ripken[24] confirm this assumption. More discussion on velocity profiles in dilute polymer flow is in section 3.1.3.

2.3 Diffusion in a Turbulent Boundary Layer

An experimental study of diffusion of ammonia from a slot into a turbulent air boundary layer serves as the basis for characterizing turbulent diffusion. Poreh and Cermak[28] found a series of four stages or zones in the development of a concentration boundary layer. They defined a characteristic plume height, λ, as the distance from the wall where the concentration is one half the maximum (or wall) concentration. They defined a relative rate parameter, β, to differentiate between zones:

$$L_\delta = \delta / \frac{d\delta}{dx} \tag{2-29}$$

$$L_\lambda = \lambda / \frac{d\lambda}{dx} \tag{2-30}$$

$$\beta = L_\lambda / L_\delta \tag{2-31}$$

2.3.1 Initial Zone

In this region closest to the source, the concentration boundary layer grows slowly by molecular diffusion through the laminar sublayer. The characteristic height, λ, is the same order of magnitude as the laminar sublayer. Large concentration gradients make it extremely difficult to obtain reliable data close to the point of injection.

2.3.2 Intermediate Zone

In this zone there is very rapid growth due to high turbulence intensity near the wall. The diffusing plume is submerged in the boundary layer, and is considerably larger than the laminar sublayer. Axial concentration gradients are much smaller than vertical gradients, and the ratio β is small. The mean concentration profiles can be described by the following dimensionless curve:

$$\frac{C}{C_{max}} = f(\xi) \tag{2-32}$$

where $\xi = y/\lambda$. The function $f(\xi)$ is independent of both external velocity and boundary layer thickness for the range studies. Poreh and Cermak found from their data the following empirical equation for the plume growth:

$$\lambda = 0.076\ x^{0.8} \tag{2-33}$$

where λ and x are in cm and x is the distance from the source. They also found in this region that the wall concentration, C_{max}, varied inversely with the external velocity. They indicated that there is not a universal curve for β versus x because β depends somewhat on the location of the source relative to the boundary layer origin. After approximately 18 boundary layer thicknesses from the source, they found deviation from the quasi similar function, f (ξ).

2.3.3 Transition Zone

In this region, the plume growth rate is slowed because of less turbulence in the outer region of the boundary layer. The profile begins to gradually change shape. This region begins approximately 18 boundary layer thicknesses from the source and ends at 60. At the end of this zone β increases to unity, and the value of λ/δ approaches 0.64.

2.3.4 The Final Zone

In the "final zone" the concentration boundary layer coincides with the shear layer. The concentration profiles can be expressed by a quasi-similar equation:

$$\frac{C}{C_{max}} = f\ (y/\delta) \qquad (2\text{-}34)$$

The value of λ/δ remains constant at 0.64.

2.3.5 Equations for Concentration Profiles

Based on an eddy diffusion analysis, Morkovin[29] proposed the following equations to represent the non-dimensionalized concentration profile in the "intermediate" and "final" zones, respectively:

$$\frac{C}{C_w} = \text{EXP}\left\{-0.693\ (y/\lambda)^{1.5}\right\} \tag{2-35}$$

$$\frac{C}{C_w} = \text{EXP}\left\{-0.693\ (y/\lambda)^{2.15}\right\} \tag{2-36}$$

Morkovin's curves agreed well with the experimental data of Poreh and Cermak[28].

CHAPTER III

PREVIOUS STUDIES OF DRAG REDUCTION

Important reviews on the status of the drag reduction effect are in the literature[2,30,31] and Granville[32,33,34] gives an annual summary of progress in the area. This annual summary is given in terms of highlights, laboratory activities, and bibliographic entries for the year. Of special importance is the work of Hoyt[2], whose summary is the most complete review done to date. A complete survey of the literature concerning the "Tom's Effect" would require considerable space and would be covering material encompassed by Hoyt's work. Hence, the aim of this chapter is to briefly discuss pipe flow of polymer solutions, flow around rotating disks and cylinders, and comprehensively review material relevent to this investigation.

3.1 General Drag Reduction Background

There are many polymer/solvent systems which exhibit less friction than the pure solvent. Only the more important industrial systems will be discussed. The effects of reduced drag in pipe flow will be outlined. Each of these effects is an area for considerable research.

3.1.1 Pipe Flow of Dilute Polymer Solutions

Guar is a complex polysaccharide derived from a plant raised commercially as a food additive and thickener. Guar is mostly used in oil well fracturing operations, and technology in this use has progressed such that Pruitt *et al.*[35] developed a design procedure for minimizing pumping costs in fracturing operations.

As mentioned in the introduction, Fabula[7] was the first investigator to use poly (ethylene oxide), (PEO), and to recognize that only a few ppm were sufficient to yield large reductions in drag. Another early contributor to the study of PEO solutions was Virk[36], who found a large effect on pressure drop in pipes with concentrations as low as five ppm. Goren and Norbury[37] found maximum effectiveness at 10 ppm from extensive tests in a 2 inch pipe. At low concentrations density and viscosity are the same as water. Although most investigations involve water, PEO is effective in other solvents.PEO, the most effective drag reducing agent, has the disadvantages of being slow to dissolve and degrades easily under shear.

The first water-soluble friction-reducing material studied in the literature was sodium carboxymethylcellulose (CMC)[3,4]. Ripkin and Piltch[38] and Pruitt and Crawford[39] were among the first to make comprehensive studies of turbulent flow of CMC solutions. Other flow data on CMC solutions have been published by Ernst[40,41]. He experimentally measured fully developed turbulent flow in circular tubes. Both pressure drop and velocity profile measurements were made over a wide range of Reynolds numbers. CMC is less effective on a weight basis than most drag reducing agents[2].

Polyacrylamides are excellent friction reducers, and have the advantages of being less susceptable to shear degradation and dissolving more rapidly than PEO. Metzner and Park[42] worked with dilute solutions of polyacrylamide J-100 (Dow) which they found gave drag reductions at dilute concentrations. Using Separan AP-30 (Dow) and J2-FP (Western Co.) a guar-type polymer, Witsitt et al.[43] carried out flow tests in pipes

over a wide range of concentration and pipe diameter. They found that as a drag reducer polyacrylamides appeared better than guar, but were not as effective as PEO. White[44] arrived at similar conclusions.

3.1.2 Special Effects in Pipe Flow of Dilute Polymer Solutions

The study of turbulent-friction coefficients in pipe flow has uncovered numerous attributes of flowing polymer solutions. Each of these effects is in itself an area for extensive investigation.

It has been noted that increasing pipe size greatly reduces the percentage of drag reduction given a constant Reynolds number. Savins[45] was perhaps the first to point this out. Savins found that his data, along with that of Toms[1], Dodge and Metzner[4], and Shaver and Merrill[3] all showed a similar dependence on tube size. At higher Reynolds numbers, the diameter effect becomes less significant.

All drag-reducing polymers have a concentration such that friction reduction for a given Reynolds number is a maximum. Hoyt and Fabula[46] were first to show this maximum; the concept was later confirmed by other investigators. Virk et al.[47] correlated the results of nine investigators to obtain this analytical expression of the asymptotic limit for maximum drag reduction in smooth pipes:

$$\sqrt{C_f} = 19.0 \log_{10} (Re\sqrt{C_f}) - 32.4 \qquad (3\text{-}1)$$

In comparison the Newtonian turbulent-friction law in smooth pipes:

$$\frac{1}{\sqrt{C_f}} = 4.0 \log_{10} (Re\sqrt{C_f}) - 0.4 \qquad (3\text{-}2)$$

There appears to be a "threshold" shear stress below which no friction reduction takes place. Virk[48] was among the first to notice

this threshold shear stress concept. The results of most authors indicate[2] that the onset shear stress is peculiar for each polymer and is not dependent on flow rate, pipe size, or polymer concentration. Substances with higher molecular weights have lower onset shear stress[2].

When the onset shear stress occurs in the laminar flow regime, the friction factor-Reynolds number plot is an extension of the laminar line[2]. This can be considered as transition delay, transition being defined as the point of departure from the laminar friction line. White and McEligot[49] and Castro and Squire[50] both found extensive transition delay. In larger pipes, where the onset shear stress is not reached until the turbulent regime, no effect of polymer on transition is evident[2].

Hoyt and Fabula[46] first showed that additives were effective on rough surfaces. Many workers since then have used commercial pipes of nominal roughness in their experiments. Virk[51] gave the best data on polymer drag reduction in rough pipes, because he characterized both the test pipes and polymer solution. He found the friction coefficient of even the roughest pipes could be lowered to the value of drag-reduced smooth pipes. Virk showed also that onset of drag reduction occurred at the same wall shear stress in rough and smooth pipes.

White[44] studied pressure drop in turbulent dilute polymer flow over a 33°C temperature range. He found the drag reducing effectiveness is not a direct function of temperature for the range covered. However, there is an indirect effect in that temperature changed solvent viscosity. This can lead to an apparent difference in effectiveness unless the comparison is made at a common Reynolds number.

Both mass and heat transfer rates are reduced by the addition of

a drag reducing agent. Wells[52] developed a correlation to predict heat transfer rates from pressure drop data in drag reducing fluids. He followed the Reynolds analogy approach, using the equation of Meyer for skin friction. Good comparison was indicated with experimental data. Sidahmed and Griskey[53] indicate the effect on mass transfer is comparable to heat transfer.

3.1.3 Velocity Profiles in Pipe Flow

Many investigators have studied the velocity distribution across pipes flowing dilute polymer solutions. All results generally agree, the profiles being much flatter than those of water. The turbulent velocity profile in a pipe can be expressed by

$$\frac{u}{u_*} = A \ln \frac{yu_*}{\nu} + B \qquad (3\text{-}3)$$

where A = 2.5 for Newtonian fluids

B = 5.5 for Newtonian fluids

A new constant, ΔB, can be added to reflect the increase in the local velocity ratio, u/u_*, when the drag reducing solution is present. Hence:

$$\frac{u}{u_*} = A \ln \frac{yu_*}{\nu} + B + \Delta B \qquad (3\text{-}4)$$

Most workers agree that the constant A is unchanged in dilute polymer flows. These important results were first shown by Meyer[23] and confirmed by Ernst[41], Elata et al.[54], and Goren and Norbury[37], among others. ΔB is a complicated function of the polymer molecule's characteristics and concentration. As was discussed in Section 2.2.3, ΔB was found by Meyer[23] to be of the form:

$$\Delta B = \alpha \ln \frac{u_*}{u_*^c} \tag{3-5}$$

where u_*^c is the critical or onset shear stress. For dilute solutions u_*^c depends upon the type of additive and is independent of concentration. White[27], based on the work of five investigators, proposed the following relations for guar and PEO respectively:

$$\begin{aligned} \alpha &= 0.006\ C \\ u_*^c &= .23 \pm .02 \text{ ft/sec} \end{aligned} \tag{3-6}$$

$$\begin{aligned} \alpha &= 2.3\ \sqrt{c} \\ u_*^c &= .08 \pm .02 \text{ ft/sec} \end{aligned} \tag{3-7}$$

For both polymers, the data suggested the maximum value of α to be 11. Poreh and Hsu[26] state that α is proportional to concentration with the maximum value of ΔB to be 28.

There appears to be conflicting evidence concerning the velocity defect in pipe flow. The data of Virk[36] suggest one universal defect law. However, the results of Goren and Norbury[37] show considerable scatter near the wall ($y/R < 0.3$) when plotted in defect form ($\frac{U-u}{u_*}$ vs y/R).

Virk[47] postulates three zones in the turbulent pipe flow profile: the viscous sublayer, the interactive zone characteristic of drag reduction, and a Newtonian turbulent core. The interactive layer corresponds to the Newtonian Buffer Zone. The Newtonian plug is given by Equation (3-4). Virk gives the interactive zone profile by

$$\frac{u}{u_*} = \tilde{A} \ln \frac{y u_*}{\nu} + \tilde{B} \tag{3-8}$$

Virk gives $\tilde{A}$ = 11.7 and $\tilde{B}$ = 17.0. Virk calls Equation 3-8 the "ultimate profile", since this profile is inferred from the ultimate asymptote for drag reduction, Equation 3-1. Granville[55] indicates that other authors have experimentally found this thickened buffer zone, and noted logarithmic profiles in it.

3.1.4 Flow Around Rotating Disks and Cylinders

The external flow of polymers on rotating disks and cylinders offers an opportunity to examine drag reduction in boundary layers.

Hoyt and Fabula[46] contributed some early experimental data on the turbulent flow of drag reducing fluids around rotating disks. Disks were rotated such that turbulent flow extended over most of the disk. A key result of their work is that the maximum torque reduction obtained was similar for different polymers. That is, the same maximum torque reduction can be obtained for a given Reynolds number, regardless of the polymer. Gilbert and Ripken[56] investigated both smooth and rough disks rotating in various concentrations of guar gum. They found maximum reductions of 60% for the smooth disks. Giles[57], using empirical velocity profiles from pipe pressure drop data, developed the following relation where K_m indicates the minimum torque on both sides of the rotating disk:

$$K_m = 0.684\ Re^{-0.362} \qquad (3\text{-}9)$$

His expression has been effective in predicting minimum disk friction to within about 8%. This discrepancy is attributed to end effects in the test arrangement.

Since rotating cylinder viscometers are frequently used in polymer characterization, many studies have been made using couette flow devices.

Shin[58] did the most thorough experiments in turbulent couette flow of polymer solutions. He used PEO in both fresh and sea water and polyisobutylene in cyclohexane and decalin. He found maximum friction reduction at about 80 ppm. By varying the gap in the system he found that the optimum concentration remained about the same. However, the maximum drag reduction at the optimum concentration changed.

3.2 Velocity Measurement

Although this may be considered of minor importance in most drag reduction studies, velocity measurement is a prime factor here. Astarita and Nicodemo[59] were among the first to examine descrepencies between measured and true velocities in viscoelastic flow. They postulated that Pitot tube reading consisted of three components: a first normal stress contribution; an integral normal stress contribution; and a kinetic contribution. For a Newtonian fluid, only the kinetic contribution is non zero. Since both normal stress contributions are negative, they theorized the true velocity should always exceed the measured velocity. Experimentally, they computed total flow from Pitot tubes surveys, and found the measured flow rate to be considerably less than the true. Metzner and Astarita[60] attributed the impact tube errors in polymer fluids to (a) the influence of normal stress terms; (b) the time average of the fluctuation stresses are not simply related to the time average of the velocity distribution; and (c) the boundary layer thickness on the probe may be much larger than the probe size. A large instrument is desirable to reduce errors. However, this results in less precision in the velocity surveys due to averaging over a large probe area. Also,

using a large probe, it is impossible to obtain velocity measurements near a wall.

Wetzel and Tsai[61] give calibration curves for three different impact tubes in PEO WSR-301 solutions of various concentrations. The impact tubes were towed in a laboratory towing facility. Two of the tubes were square ended flattened tubes and one had a hemispherical nose. The towing velocity was varied from one to sixteen feet per second, and polyox concentration varied up to 750 ppm. They found that as the polymer concentration increased, so did the difference between the measured and true velocity. They also found that for the range of velocities covered the pressure coefficient defined below, was independent of velocity:

$$C_p = \frac{\Delta P_s}{\frac{1}{2} \rho U_t^2} \tag{3-10}$$

where ΔP_s = measured difference between total and static pressure

U_t = true velocity

Fruman, Sulmont, and Loiseau[62] tested five different probes in PEO WSR-301 solutions varying from 50 to 200 ppm. They towed the probes in a circular basin, varying the velocity from two to eleven meters per second. They were unable to correlate their calibrations except for the 200 ppm data.

Gilbert and Ripken[56] as part of their work on rotating disks, tried to calibrate their Pitot-static probe. They determined the pressure coefficient for the probe in water and 500 and 1000 ppm guar gum solutions aged up to two weeks. They found the error for one day old guar solutions was quite small, and that the error increased with concentra-

tion, the maximum being about 10%. These discrepencies were less than those obtained by Wetzel and Tsai[61].

Frieke and Schwarz[63] performed experiments with both Pitot tubes and anemometers in polyacrylamide concentrations from 10 to 300 ppm. The velocity was measured independently by the hydrogen bubble technqiue. The results indicated that Pitot tubes adequately measured the local velocity, cylindrical hot-film probes cannot be used to measure velocity under certain conditions, and that conical probes gave better results than cylindrical ones.

The polymer type and concentration, probe dimensions, and fluid velocity all interact together to make estimation of velocity using a Pitot tube an extremely complicated undertaking. It is evident more research is needed in this area.

3.3 Flow Over Flat Plates-Analytical Solutions

Since there is considerably more experimental data for flow in pipes, analytical solutions for flat plate flow in dilute polymer solutions are based on similarity relationships. Granville[22] developed similarity laws for homogenous solutions from a dimensional analysis of the inner similarity law (law of the wall), which was modified for polymer solution flow, and the outer similarity law (velocity defect law) which remained the same as for pure solvent flow. The overlapping of the inner and outer laws resulted in a linear logarithmic relation with von Karman's constant unchanged and the intercept factors a function of polymer characteristics and shear velocity. Various integral relations were developed to calculate displacement thickness, momentum thickness, and shape parameter of flat plate flow. Formulas were developed

for total resistance coefficients of flat plates in homogenous polymer solutions as a function of Reynolds number. A numerical example is given for a sample concentration of guar gum.

Giles[57] developed a new Blasius type law of friction for minimum frictional resistance from empirical pipe data. Following a method similar to Prandtl, he developed a modified 1/nth power velocity distribution and relations for displacement and momentum thickness. Using an integral momentum technique he developed a formula for total skin friction of a flat plate:

$$C_f = 0.315\ R_x^{-0.362} \tag{3-11}$$

Combining his previous flat plate analysis[22] with the interactive layer concept of Virk[47], Equation (3-8), Granville[64] developed a relation for maximum drag reduction on a flat plate. He assumed that maximum drag reduction occurs when the shear layer is reduced to a laminar sub-layer and the interactive layer. That is, the velocity profile throughout the layer is represented by Equation (3-8). Granville derived the following form for maximum drag reduction, limited to high Reynolds numbers flows:

$$\ln (R_x C_f) = \frac{\sqrt{2}}{\tilde{A}} \frac{1}{\sqrt{C_f}} + 1 - \frac{\tilde{B}}{\tilde{A}} + \ln (2\tilde{A}) - \frac{5}{2\sqrt{2}} \sqrt{C_f} \tag{3-12}$$

Granville plotted his result and the power-law relation of Giles[57] and found good agreement between them.

White[27] assumed the modified law of the wall, Equation (2-26), to hold throughout the boundary layer. Using an integral momentum analysis, White derived a relationship for shear stress:

$$\frac{Ux}{\nu} = \frac{0.1108}{k^3} e^{k\gamma} \left(\frac{u_*}{u_*}_o \right)^{-k\gamma} \left[k^2\gamma^2 - 4k\gamma + 6 + k\alpha\,(k\gamma - 3) \right] \quad (3\text{-}13)$$

where

$$\gamma = \frac{U}{u_*} = \left(\frac{2}{c_f'} \right)^{\frac{1}{2}} \quad (3\text{-}14)$$

Following this theory further, White noted that polymer friction reduction for a plate is confined to near the leading edge. Some drag results are plotted, and showed the polymer effectiveness was decreased at large plate-length Reynolds numbers. Using his relation for α (Equation 3-7), White compares his results with the experiments of Levy and Davis,[65] showing fairly good agreement. He also outlined an extension of his methods to flows with pressure gradients.

McCarthy[65] and Granville[67] extended Granville's[22] formulation of the uniform polymer concentration-flat plate problem to include polymer injection near the leading edge, for high Reynolds number flow. The analyses were restricted to the final zone of turbulent diffusion where the polymer plume fills the boundary layer (section 2.3.4). Both McCarthy and Granville assumed that this zone commenced at the injection point. In carrying over the velocity similarity laws from the uniform to the injected case both authors assumed that there is a local effective polymer concentration independent of distance from the wall. This was taken to be the local wall concentration, and was used to determine the ΔB of the modified law of the wall for drag reduced flow. McCarthy gave numerical results for water-polyox solutions with either uniform concentration or injection. Granville's analysis was for an ejected solution

of 2000 ppm of guar gum, which was also compared to a uniform concentration of 2000 ppm.

Granville[55] advanced his previous analysis using similarity-law correlation for drag reduction, and showed that a sufficiently thick turbulent shear layer was required. He showed that the similarity law correlation should not be used if the shear layer is too thin, as in a capillary tube.

Elata[68], following the approach of Prandtl, assumed the following velocity profile for homogeneous solution flat plate flow:

$$\frac{u}{u_*} = A \ln z \tag{3-15}$$

$$z = B' \frac{yu_*}{\nu} \left(\frac{u_*^2 \tau_1}{\nu} \right)^C + 1.0 \tag{3-16}$$

where τ_1 is the maximum relaxation time of the polymer molecules; τ_1 depends on molecular weight and intrinsic viscosity, and C is the concentration in ppm for PEO. From the momentum equation, he developed the following relation for skin friction:

$$\frac{1}{\sqrt{C_f}} \approx 4.13 \log \left[\frac{Ux}{\nu} \left(\frac{U^2 \tau_1}{\nu} \right)^C C_f^{1+C} \right] + 1 - 4.13 \log 2^C \tag{3-17}$$

He extended his analysis to ejection by assuming the polymer was diluted as follows:

$$\delta C_w = \text{constant} \tag{3-18}$$

Elata used numerical integration to compute the total friction along the flat plate. Elata compared his results to experiments of other inves-

tigators and found his analysis predicted a monotonic increase in drag reduction while experiments showed a maximum drag reduction.

White[69] outlines a method of interpreting boundary layer behavior from pipe experimental data. Wall shear data, from pipes of differing diameter, were plotted on double logarithmic coordinates. This method of plotting, first proposed by Gadd, yielded the following simple relationship:

$$\left(\frac{\tau_w^p}{\tau_w^o} \right) = \left(\frac{\tau_w^o}{\tau_w^C} \right)^N \qquad (3\text{-}19)$$

The value N depends upon the concentration of the polymer in the solution. Combining this relation with equations for wall shear and boundary layer thickness for Newtonian fluid developed from the 1/5th power law, he applied the momentum equation to obtain values of these parameters as a function of length, for drag reduced flat plate flow. His analysis showed that drag reduction increases with free stream velocity, decreases with increasing τ_w^C, and increases with length. For 100 ppm guar gum solution, analysis predicted a 30% drag reduction.

Poreh and Hsu[70,71] modified a method based on the Lagrangian similarity hypothesis to develop a numerical scheme for calculating diffusion from a line source. The analysis is limited to predicting maximum concentration and development of the diffusion boundary layer thickness. It is further restricted to the intermediate zone of diffusion in a developing concentration turbulent boundary layer (Section 2.3.2). Their results[71] agreed well with experimental data on diffusion from a line source.[28] They extended their analysis to include the growth

of the diffusion boundary layer in flow past a rough boundary and in flow of drag reducing polymer past a smooth boundary. Polymer injection from a line source was considered further[70].

They assumed a simple velocity profile (Equation 2-25) for the outer portion of the boundary layer. For the inner 15%, they modified the law of the wall, using the ΔB approach. Local values of ΔB were calculated by assuming ΔB was proportional to the concentration of polymer at the wall. Drag reduction, maximum concentration and concentration boundary layer growth are presented for various mass rates of polymer injected into a flat plate boundary layer. Only a free stream velocity of 5 m/sec was considered. Their analysis showed that for drag reduced flows, diffusion rates decreased in comparison with pure water diffusion.

Fabula and Burns[20] analyzed the drag reduction and mixing of polymer solution injected into a two-dimensional flat plate turbulent boundary layer. They assumed that the velocity defect similarity law of Coles[19] approximated the velocity profile throughout the boundary layer. Restricting the analysis to the final zone of turbulent diffusion (Section 2.3.4), they used the expression of Morkovin (Equation 2-36) to describe the concentration profile. Combining these relations, an equation for wall concentration was developed. Comparing their results to the experiments of Wetzel and Ripken[24] they found the "negative roughness" concept for dilute polymer solutions to be valid. Predicted values of the concentration profiles, for both water and polymer injection, differed considerably from experiment. However, the experimental profiles followed the predicted shape. This indicated that perhaps the boundary layer thickness ratio (concentration to momentum), as chosen by Poreh and

Cermak[28] for the final zone, was somewhat low. Increasing this ratio resulted in lower wall concentrations and improved agreement with experiment.

Wells[72] suggested that uniform injection through a porous wall would be very efficient, since it raises the additive concentration to the drag reducing level in the wall region only. He compared analytically distributed injection with slot injection and found distributed injection to require between 40 and 140 times less additive than slot injection to maintain equivalent drag reduction.

3.4 Flow Past Submerged Bodies-Experimental Studies

In this section previous experimental work concerning flow studies of submerged bodies will be discussed. The studies are limited to homogeneous solutions. Experiments of this sort are performed in towing tanks, in drop tanks, and in situations where the solutions flowed past stationary bodies.

Emerson[73] towed a seven foot plank, two standard models (KC116 and KC119), and an eight foot formica covered plywood pontoon in a towing tank containing PEO WSR-301, with concentration varying from 1¼ to 50 ppm. Although Emerson points out his data are somewhat unreliable because of polymer degradation, he achieved a friction reduction of 50% at a concentration of 50 ppm and a Reynolds number of 1.5×10^6.

Levy and Davis[65] towed a thin three foot long plate in a circular towing tank at speeds from 15 to 45 ft per second, corresponding to Reynolds numbers 3×10^6 to 10^7. The channel was 20 feet wide, had a median radius of 45 ft. and was filled to a depth of 10 ft. The test

plate was curved to fit the relative flow on a 45 foot towing radius. The polymer was PEO WSR-301, and concentrations varied from 1.5 to 100 ppm. Maximum reduction was about 60% at 15 to 20 ppm concentration. They found that at concentrations higher than 20 ppm, the drag reduction was slightly less than maximum. At the highest speeds tested, drag reductions of approximately 60% were obtained for concentrations from 15 to 100 ppm.

Wu[74] conducted a series of measurements of the turbulent drag on a flat plate using homogeneous solutions of Polyox WSR-301, and visual studies concerning diffusion and entrainment of jets with additive solutions flowing in a turbulent stream of pure water. The drag reduction obtained on the plate was generally lower than that for pipe flows. Maximum reduction occurred in the range of 50 to 100 ppm. He confirmed that the additive suppressed turbulent diffusion, and suggested that smaller amounts of additive were needed for ejection than was previously thought. The results indicated that for efficient drag reduction the solution ejected should be dilute, and injection rate should be comparable to the flow within the laminar sublayer with no polymer addition (i.e., the sublayer discharge).

Kowalski[8] tested a flat plate and models of two ships in fresh water and aqueous solutions of up to 50 ppm of Polyox WSR-301. The models were towed at constant speed in a towing tank and the drag was measured by a force block. Reynolds numbers ranged from 7×10^5 to 4×10^6. Drag reductions of the order of 25% were obtained for the ship models, and about 45% for the flat plate. Increasing the concentration above 20 ppm produced only a marginal lowering of resistance.

Merrill et al.[76] tested two bodies in PEO solutions - a flat plate and a scale model of a torpedo. The test apparatus consisted of an open column employing photo-cells to measure terminal velocities of the test models. Test bodies were placed at the bottom of the tank, then accelerated to terminal velocity by a system of counterweights. The models were tested in fresh water and PEO solutions of concentrations up to 100 ppm. The polymer solution led to a substantial increase in the terminal velocity achieved by the flat plate. Up to 20 ppm the terminal velocity of the torpedo also increased with concentration. However as concentration was increased above 20 ppm the terminal velocity decreased. The explanation offered was that the polymer laminarized the boundary layer, promoting early separation, which increased the form drag.

White[77] performed experiments dropping a concrete sphere into a tank containing either water or dilute PEO solutions. The wake pattern was recorded by high speed photography. The sphere was made hydrodynamically smooth, and was dropped from a height such that the average Reynolds number was just below the critical value. Drop tests showed a laminar boundary layer with early separation. The sphere was roughened and the tests repeated. The separation point was moved rearward. When the roughened sphere was dropped into a 60 ppm PEO solution, the separation point was moved forward, increasing the form drag. The drag coefficient was practically the same as that of the smooth sphere.

Lang and Patrick[78] conducted experiments to determine the effect of polymer additives on the drag of cones, disks, spheres, and cylinders. These tests were performed in plain water and Polyox WSR-301 solutions of

200 and 1000 ppm. The spheres showed drag reductions up to 69%. Little or no drag reduction was measured for the bluff-based objects whose boundary layer separation point is independent of the Reynolds number. Also, there was little effect on the drag of the cylinders tested. Wake photographs showed the separation point moved rearward on the spheres that exhibited reduced drag.

Thruston and Jones[79] developed a soluble coating which when applied to the surface of an underwater body resulted in reduction of friction drag. Their test program was carried out using a torpedo-shaped model in a drop tank. Two different nose shapes were used and the coating was applied only to the stagnation region of the nose. Distance-time relationship was measured and the drag calculated from this data. They noted reductions in total drag were about 18% which corresponds to a reduction in friction drag of 30%.

Sarpkaya and Rainey[80] measured drag force, pressure distribution and separation angle on circular cylinders (¼" to 1½") for flow of PEO solutions with concentrations from 1 to 200 ppm. They also measured lift and drag forces on a NACA-0024 hydrofoil model. They found that except for 200 ppm solutions the lift coefficient of the hydrofoil was not significantly changed. For the cylinders PEO altered the mean drag coefficient considerably. In all cases transition occurred earlier than in the pure solvent.

3.5 Experimental Studies with Injection

Love[81] investigated the effects of injecting polymer solutions into the turbulent boundary layer on a flat plate. Solutions were ejected

through slots on each side of the plate near the leading edge. Ejected from the flat plate were pure water, dilute aqueous solutions of sodium carboxymethylcellulose and PEO WSR-301, and suspensions of neutrally buoyant spherical polystyrene particles. The drag of the plate was determined by the wake survey method, using a thirteen tube total head rake and a static pressure probe. The free stream velocities were 9 feet per second and 12 feet per second. He found that water injection caused little change in the plate friction coefficient, that the polystyrene had no effect on the drag of the plate, and that PEO resulted in a maximum drag reduction of 50%.

Wells and Spangler[82] investigated local injection of dilute solutions of drag reducing additives into turbulent shear flow in a pipe. They studied both centerline and pipe wall slot injectors. The following fluids were injected: water and aqueous solutions of guar gum and a copolymer of polyacrylamide and polyacrylic acid. They found that the local pressure gradient could be reduced by the amount comparable to the flow of a uniform concentration when the fluid was injected in the wall region. Conversely, injection into the turbulent core showed no reduction in drag until the fluid diffused into the wall region.

Using PEO WSR-301 and a pipe with circumferential injection slots, Maus and Wilhelm[83] studied the effects of variation of Reynolds number, injection rate, number of injection points, and initial concentration of the injected solution. There were five injection slots located six inches apart, inclined at an angle of 30^{o}. Their investigation showed that, in general, the trends exhibited for premixed flows are also displayed for the case of polymer injection.

Vogel and Patterson[6] investigated the effects of injecting solutions of three linear, high molecular weight polymers into the boundary layer of a three-dimensional streamlined model. Three types of PEO were used: polyox WSR-35, WSR-205, and WRS-301. They ejected the polymer through a nose slot, and varied the concentration of the polymer solutions, the velocity of injection and the tunnel velocity. They ran at speeds from 150 to 650 cm/sec, varied the concentration up to 1000 ppm, and the injection rate up to 30 ml/sec. They found that the PEO WSR-301, having the highest molecular weight, was by far the most effective drag reducer. The drag of the body decreased with increasing polymer concentration, however, there was no drag reduction above 500 ppm. They found that the flow rate of polymer injected into the boundary layer was the controlling factor, and not the injection flow velocity. Since the boundary layer was too thin to probe, velocity measurements were performed in the wake only. These wake studies indicated the turbulence level was affected by polymer injection.

Barone and Hoppmann[84] measured the drag on cylindrical bodies with spherical ends which were suspended coaxially within straight tubes. Dynamometers measured the drag in water and aqueous solutions of PEO coagulant and WSR-35. The models were of three different lengths but of the same diameter. The polymer solutions were introduced into the stream from a 0.8 centimeter diameter slotted tube located transversely in the stream such that a uniform concentration contacted the models. Dye injection studies showed that the polymer solutions mixed homogenously with the stream before contacting the models. The water velocity was varied from 50 to 250 cm/sec. Polymer solution concentration varied from

0.1% to 1.0%. They found that the 1% solution did not disperse as well as the others. Drag reductions of approximately 35% were obtained.

Latto and Shen[85] studied the effect of injecting dilute aqueous polymer solutions into a turbulent boundary layer formed on a flat plate. Using hot film anemonetry, they found that the momentum diffusity was less than that for pure water. It was also observed that the angle and velocity of the injection of a polymer solution can have a pronounced effect on the local skin friction. They found drag reductions as great as 80% compared to no injection conditions.

Wu and Tulin[86] extended previous work[74] to investigate the requirements and techniques for injecting additive solutions into a pure water boundary layer for the most efficient drag reduction. They characterized injection flow rate in terms of the viscous sublayer discharge. This quantity is the flow rate within the laminar sublayer without additive addition. The nominal thickness of the sublayer, σ, is generally defined such that

$$(\sigma u_* / \nu) = 11.6$$

A virtually linear velocity gradient persists within the sublayer and the discharge per width, Qs, can be found as follows:

$$Q_s = \tfrac{1}{2}\,\sigma \frac{\sigma \tau_w}{\nu} = \tfrac{1}{2}\,\nu \left(\frac{\sigma u_*}{\nu}\right)^2 = 67.3\,\nu \qquad (3\text{-}20)$$

This quantity is independent not only of the shear stress but also of the distance along the solid boundary. For a given slot and concentration, drag reduction generally increased with injection at low rates. However, the rate of increase diminished when the injection rate exceeded the

sublayer discharge. The gain in drag reduction with ejection rates greater than the sublayer discharge were nominal. He also noticed that the slot inclination should be small and the width of the opening should be comparable with the thickness of the sublayer. Maximum drag reduction was approximately 55% and occurred between 400 and 1000 ppm. In a further study Wu[87] conducted tests of slots (inclined, vertical, and shielded) and porous type ejectors for introducing polymeric drag reducing additives into aqueous turbulent boundary layers. Slots ejectors were better for dilute solutions, and the porous ejector for concentrated solutions. Compared to the vertical and shielded slots, inclined slots introduced far less mixing between the ejected additive solution and the surrounding water.

Hulsebos[25] investigated the uniform surface injection of PEO WSR-301 into a water boundary layer. He investigated the effect on the velocity profiles in the boundary layer and shear stress, using an integral momentum technique. Maximum drag reduction obtained was 37%. His data indicated that the mass rate of polymer addition was the prime criterion in drag reductions. The polymer additives made the velocity profiles blunter than those of pure water.

3.6 Experimental Studies of Diffusion of Drag Reducing Polymers

Relatively few studies have been done on the diffusion of dilute drag reducing polymers and their effect on boundary layer development. Most investigators have found that diffusion rate is reduced along with the drag. Most diffusion studies in the literature concern injection either from a slot in a flat plate or pipe, or uniformly along a porous surface.

Walters and Wells[88] studied experimentally turbulent diffusion of PEO solution uniformly injected through a porous wall into a fully-developed pipe flow of water. The injection system was comprised of three adjacent independent porous sections. Pressure drop data were obtained while varying mass injection rate for three different velocities (7.5, 13, and 26 ft/sec) and three different polymer concentrations (100, 500 and 1000 ppm). Velocity and concentration profiles were measured immediately downstream of the porous wall sections for a 500 ppm solution at a velocity of 13 ft/sec with constant injection flux. Concentration measurements were based on a fluoroscien tracer,Rhodamine B dye, mixed with the injected fluid. These data were obtained for six different combinations of the porous sections. Their results showed that uniform injection showed more efficient drag reduction than slot injection. They found that the polymer inhibited turbulent diffusion away from the wall, and also noted that the drag reducing effectiveness of the polymer was only in the wall region.

In a further investigation Walters and Wells[89] extended their work to include velocity and diffusion data in the active porous wall section and considered the effect of solution aging. The study was done on PEO solutions of 1000 and 5000 ppm. They evaluated three fluoroscien tracers for concentration measurements and found Uranine B most suited for their setup. Pressure drop, velocity and concentration data were taken at a velocity of 13 ft/sec for two injection flux rates. The "stringiness" of the solution, which is a qualitive indication of the solution's visco-elastic nature, was found to decrease with increasing age. The material tested was aged for both 2 days and 5 days. The former was approximately

the minimum time for complete polymer dispersion in the solvent, while the latter allowed time for a significant change in the solution. Data for the aged solution were taken only for the 5000 ppm. Diffusion coefficients were evaluated from the concentration data using a simplified diffusion equation. They found diffusion was greatly reduced near the wall, resulting in higher wall concentrations than for water injection. The aged solution gave only slightly different pressure drop measurements than the two day old solution. However, the concentration data differed significantly in the active wall section. The aged solution showed a concentration profile more like water than the unaged solution. Downstream from the active section, diffusion appeared to be independent of age. In both investigations they found drag reduction to be a function of polymer mass flux. This conclusion was also reached by Hulsebos[25].

Wetzel and Ripken[24] experimentally studied polymer injection into a developing boundary layer. They used a nine foot wide open channel with a free stream velocity of 18 ft/sec. Aqueous solutions of polyox WSR-301 of from 250 to 2000 ppm were injected from a slot near the origin of the boundary layer. Both velocity and concentration profiles were measured at test stations located 16, 28, and 40 ft. downstream from the injector. Wall shear was calculated from both the momentum equation and semi-logarithmic plots of the velocity profile. Polymer concentrations in the layer were determined by adding a fluorescent material, Rhodamine B dye, to the injected concentrate, and measuring the dye concentration with a fluorometer. Concentration profiles were also determined by a turbidimetric method based on the reaction of PEO with poly(acrylic acid) to product a precipitate. The resulting turbidity, which is pro-

portional to PEO concentration was measured on a colorimeter. Since there was satisfactory agreement between these methods, the authors concluded that the dye and the polymer diffused similarly. Hence, most of their concentration data was analyzed only by the more rapid fluorometeric method. The maximum drag reduction obtained was 35% over the complete 40 foot length. They noted that polymer injection produced a much fuller velocity profile than for water alone. This resulted in reduced displacement and momentum thickness. The ΔB shift of the velocity profiles were lower than those found in pipe flows of homogeneous solutions. At the 16 foot station, the drag reduction was greater for the lower concentration than for the larger. At the downstream locations, more drag reduction was obtained with the larger concentrations. They concluded that this was associated with better mixing. Maximum drag reduction was achieved when the terminal wall concentration was on the order of 30 ppm. Their dye injection showed that near the slot the flow formed a pattern of large wavering parallel streaks. This occurred only for the polymer concentrate. The ΔB shift of the velocity profiles were lower than those found in pipe flows of homogeneous solutions.

Wu[90] measured the diffusion of PEO ejected from a slot into a developing boundary layer. The concentration was measured at one point near the wall close to the trailing edge of a flat plate, for an external velocity of 8 ft/sec. Wu estimated this concentration to be about 85% of the wall concentration for water injection. A laser-phototransistor unit was calibrated by flowing water of varying dye concentrations past the plate, in a circulating water channel. The polymer concentration was then related to the dye concentration. The concentrate contained from

zero to 1000 ppm PEO and was injected at rates up to four times the sublayer discharge. For water ejection, the measured concentration at the test station was about half the value predicted by Poreh and Cermak[28]. The results indicated that PEO supressed diffusion in a turbulent boundary layer.

Tullis and Lindeman[91] measured experimentally drag reductions caused by PEO injection into a developing turbulent boundary layer in a 12 inch hydraulically rough pipe. The injected concentrations varied from 100 to 2400 ppm. Reynolds numbers varied from 6×10^5 to 3×10^6, with velocities up to 46 ft/sec, and the polymer was injected at different rates. The drag reduction was determined on the basis of pressure drop measurements. Velocity and concentration profiles were obtained using a specially fabricated Pitot rake. The rake consisted of eight Pitot tubes mounted in an airfoil. The three tubes nearest the wall were smaller than the other tubes. The concentration profiles were determined by measuring the concentration of a tracer, Rhodamine WT dye, with a fluorometer. Concentration profiles for both water and polymer solution were measured at distance of approximately six diameters downstream from the point of injection, located 3.5 diameters downstream from the entrance. They noted that the wall concentration for polymer was much greater than for water for both injection velocities measured. This was attributed to the viscoelastic nature of the polymer. The lower injection velocity resulted in higher wall concentrations. They also found that for a constant polymer mass injection rate, the drag reduction increased as the injection velocity decreased. However, this dependence was not very strong. Maximum drag reduction based on the friction factor for pure water

was approximately 90%.

3.7 Theoretical Explanations

The details of the interaction between dissolved polymer macromolecules and fluid in turbulent flow are not completely known. Physical models and computational schemes to predict friction reduction have been put forth. Most of the proposed semi-empirical equations require experimental data to evaluate constants. Also these mechanisms are unable to completely describe all the associated anomalities of dilute polymer flow.

3.7.1 Wall Effects

Early theories were based on wall effects. Oldroyd[92], trying to explain Tom's[1] data, proposed the existence of a thin laminar layer at the wall when the main stream is turbulent. This thin layer is behaving abnormally due to the presence of the wall. Shaver and Merrill[3] offered an explanation based on shear thinning at the wall. This viscosity gradient would leave the sublayer unchanged and inhibit diffusion of vortices from the wall, hence decreasing the vortex formation rate and lowering turbulent intensity. Hoyt[2] cites experimental measurements which refute these viscosity lowering theories.

Davis and Ponter[93] and El'perin and Smolskii[94] suggested that the presence of adsorbed polymer molecules at an interface influenced the nature of flow. To explain drag-reduction after polymer solution was displaced by the base solvent, these authors proposed that an adsorbed layer on the wall remained after the bulk of the polymer solution was flushed from the system. Little[95] measured the adsorption of PEO on glass beads and postulated a quasi-BET model to explain high values of

Meyer's fluid property parameter (ΔB) at low polymer concentrations. In further work, Little[96], using dyed CMC solutions, noted that the solution diffused slowly into the fluid (water) contained in the pressure tap connections. He found that the prolonged drag reduction after the polymer solution was swept out by solvent corresponded to the slow diffusion of entrapped solution into the flowing solvent.

Hoyt[2] concludes that it seems impossible that either shear thinning at the wall, or adsorbed or attached layers at the wall, or any other indication of peculiar particle attraction to surfaces, has any bearing on the friction-reduction effect.

3.7.2 Viscoelastic Fluids

Metzner and Park[42] point out that the turbulent flow characteristics of purely viscous non-Newtonian fluids are generally similar to those of Newtonian fluids. However, viscoelastic polymeric solutions contrast considerably with Newtonian fluids, and turbulent viscoelastic characteristics may be brought out in solutions in the ppm range. Although the friction coefficient of a viscous non-Newtonian fluid may be somewhat lower than Newtonian, viscoelastic fluids account for the large decreases in friction encountered. The authors further demonstrate that viscoelastic fluids show the effect of tube diameter and can account for increased stability and supressed turbulence. They suggest viscoelasticity as the relevant additional fluid property which causes turbulent friction reduction. Lumley[30] also concluded viscoelasticity to be essential for drag reduction.

The Maxwell fluid is a superposition of the Hookean solid and the Newtonian liquid. Patterson and Zakin[97] assumed a linear Maxwell model

to approximate the viscoelastic response of the polymer solution under shear. Neglecting changes in turbulent intensity and assuming a crude approximation for the relationship between Lagrangian and Eulerian energy spectra, they developed simple equations to predict drag reduction. However, for a given system, preliminary experimental measurements are necessary, including velocities and turbulence intensities for the pure solvent. For the polymer-solvent pairs studied, there was an order of magnitude agreement with experiment.

Elata and Poreh[98] developed the mean momentum transfer equations for two dimensional shear flow for a Rivlin-Ericksen fluid of complexity-2. After various assumptions they arrived at a simple equation for shear stress, showing Reynolds stresses causing an increase in shear and a cross vorticity term which reduced shear. A knowledge of experimentally determined "cross viscosities" and flow structure are required for their model; no comparison with experiment is offered.

Boggs[99] derived the viscoelastic equivalent of the Navier Stokes equations by substituting a more complex relation to account for normal stresses. He developed an approximate method of solving their equations in terms of the Navier Stokes equation. The constitutive equation contained constants which depend on solvent viscosity, polymer concentration and molecular structure. He concluded that viscoelasticity was destablizing in laminar flow; hence transition would occur sooner. Earlier transition was also suggested by Lockett[100], while Black[101] indicated more stable flow. Boggs also proposed that stagnation pressure would violate Bernoulli's principle, and that turbulent skin friction was dependent on the ratio of elastic to viscous forces.

Despite deviations from experiment and the necessity of empirical constants, the second order fluid appears to be a promising model for the behaviour of friction-reducing polymer solutions. Calculations based on these models form a good approximation. Whether viscoelasticity is the primary cause of drag reduction is open to question. Most theories put forth assume that viscoelastic properties account for the friction reduction. However, work with aged solutions, which have lesser viscoelastic properties, indicates the aged solution was as effective a drag reducer as fresh solution[89,102].

3.7.3 Macromolecular/Turbulence Interaction

The absence of anomalous effects in laminar flow and experimental evidence of the onset phenomena point to some sort of interaction between macromolecules and the turbulent flow structure.

Lumley[103] proposed a mechanism for drag reduction based on molecular entanglement. He bases a simple molecular model on the assumption that spring forces tend to return molecular units to their original location when displaced. When such a molecule is placed in shear flow, elongation results. Because his calculations of the extent of elongation did not suffice in accounting for the observed effect, Lumley advanced the idea that an entangled cluster of molecules would distort similar to a single molecule. These entanglements grow to approximately the size of the sublayer, extract energy, and resist the formation of streamwise vortices. In a later paper, Lumley[30] points out an error in his elongation calculation. However, the entanglement theory is still a possibility. Ellis *et al.*[102] based on their experiments with aged PEO and Separan solutions, suggest entanglement of polymer molecules could be one of the

important mechanisms involved in drag reduction. From experiments at concentrations less than 0.03 ppm Paterson and Abernathy[104] concluded that friction would be reduced in the limits of infinite dilution and that the phenomenon was due to the interaction of individual polymer molecules with the surrounding solvent.

Models of turbulence dissipation by individual interactions between macromolecules and turbulent vortices have been proposed. Basically, these theories involve some mechanism whereby turbulent energy is absorbed by the polymer molecules, and eventually dissipated. For example, Peterlin[105] postulates that the random coiled macromolecule deforms such that one end lies in a microvortex and the other one is outside it. This strains that molecular chain, which expands, absorbing the energy of the vortex. The tensile force is then transmitted along the stretched chain to the other end of the molecule, which is in an unperturbed region of the flow. Tulin[106] pictures the molecule becoming extended and stiffened, thus absorbing turbulent energy, which is eventually dissipated as elastic waves that decay due to viscosity. Gordon[107] suggests that turbulent drag reduction in dilute polymer solutions results from the resistance of these solutions to dispersion or breakup. Millward[108] explains the mechanism of drag reduction in terms of a branching process involving energy transfer. Upon contact with a small eddy, a molecule acquires circulation and absorbs energy, causing it to uncoil. Upon leaving the high shear region the molecule recovers its coiled state and the excess energy is dissipated as heat.

Other authors suggest that drag reduction is the result of decreased turbulence production rather than some scheme of dissipating

turbulent energy. Gadd[109,110] suggests that viscoelastic effects counter vortex motion and minimize turbulent mixing and eddy generation. Johnson and Barch[111] concluded that polymer additives decrease small scale turbulence production, which decreases the dissipation of turbulence energy, hence lowering skin friction. Walsh[112] used the Rouse model for a polymer molecule in solution. This model predicts that the molecule will store energy as a function of the local strain rate. Thus enery is transported from the highly strained wall region to the essentially unstrained core of the pipe flow. Small disturbances at the edge of the sublayer ultimately become responsible for the Reynolds stresses. A decrease in turbulent momentum transport results because the polymer molecules alter the energy balance at the sublayer edge and allow viscous dissipation to destroy the resulting less energetic disturbances. By decreasing the number of disturbances per unit area and time, polymer molecules ultimately change the structure of turbulence. Combining the equations of motion with the Rouse model, Walsh developed a scheme to predict drag reduction. Hoyt[2] claims Walsh's theory is the most comprehensive theory advanced to date and is a valuable contribution to understanding friction reduction. Walsh's theory presumes friction reduction is a wall effect and does not account for turbulence damping in free jets.

Black[113] proposed a theory of wall turbulence whereby shear flow consists of an organized non-turbulent motion and a random small-scale turbulent motion. He defined the former as primary motion and the latter, secondary. Black postulates that an instability starts at the wall, grows and eventually breaks down, creating a horseshoe vortex. Thus turbulent shear flow is pictured as a sheet of horseshoe vortices, which are even-

tually dissipated by the action of viscosity. Considering the effect of polymer additives, Black[101] proposes the macromolecules fundamentally alter the structure of wall turbulence by increasing the stability of the sublayer flow. He suggests that macromolecules either modify the process of vortex stretching or reduce the intensity of turbulence. Hoyt[2] suggests that pursuing the ideas of Black may assist considerably in understanding the drag reducing phenomenon.

CHAPTER IV

EXPERIMENTAL APPARATUS AND PROCEDURES

4.1 Experimental Apparatus

4.1.1 Water Tunnel

The investigation was conducted in the water funnel of the School of Chemical Engineering, Georgia Institute of Technology. The equipment was built by Hulsebos[25] for a previous investigation and was modified for this study - Figure 1. The apparatus was a single-pass, continuous-flow, low-speed water tunnel consisting of an inlet section, a test section, and an exit duct, all constructed of 1/4 inch aluminum plate. Water entered the apparatus through a 3 inch polyvinyl chloride pipe from a 500 gallon stainless steel overhead tank. This tank received water from a main line and discharged a major portion through the test section. The remainder of the water flowed through an overflow line to another 500 gallon tank. In this manner, a constant head was maintained on the test apparatus. The water leaving the exit duct was discharged through a globe valve to a 3 inch polyvinyl chloride pipe which emptied into a drain approximately 20 feet below the apparatus.

The eight foot long inlet section of the apparatus diverged from a 2.9 x 2.9 in. cross section to an area 6 x 12 inches in cross section. The maximum angle between the diverging walls was less than seven degrees, to prevent separation of the flow.

The test section had internal dimensions of seven inches high by twelve inches wide, and was eight feet long. The test plate was attached to an insert (8' x 1' x ½" aluminum plate) and the test plate assembly

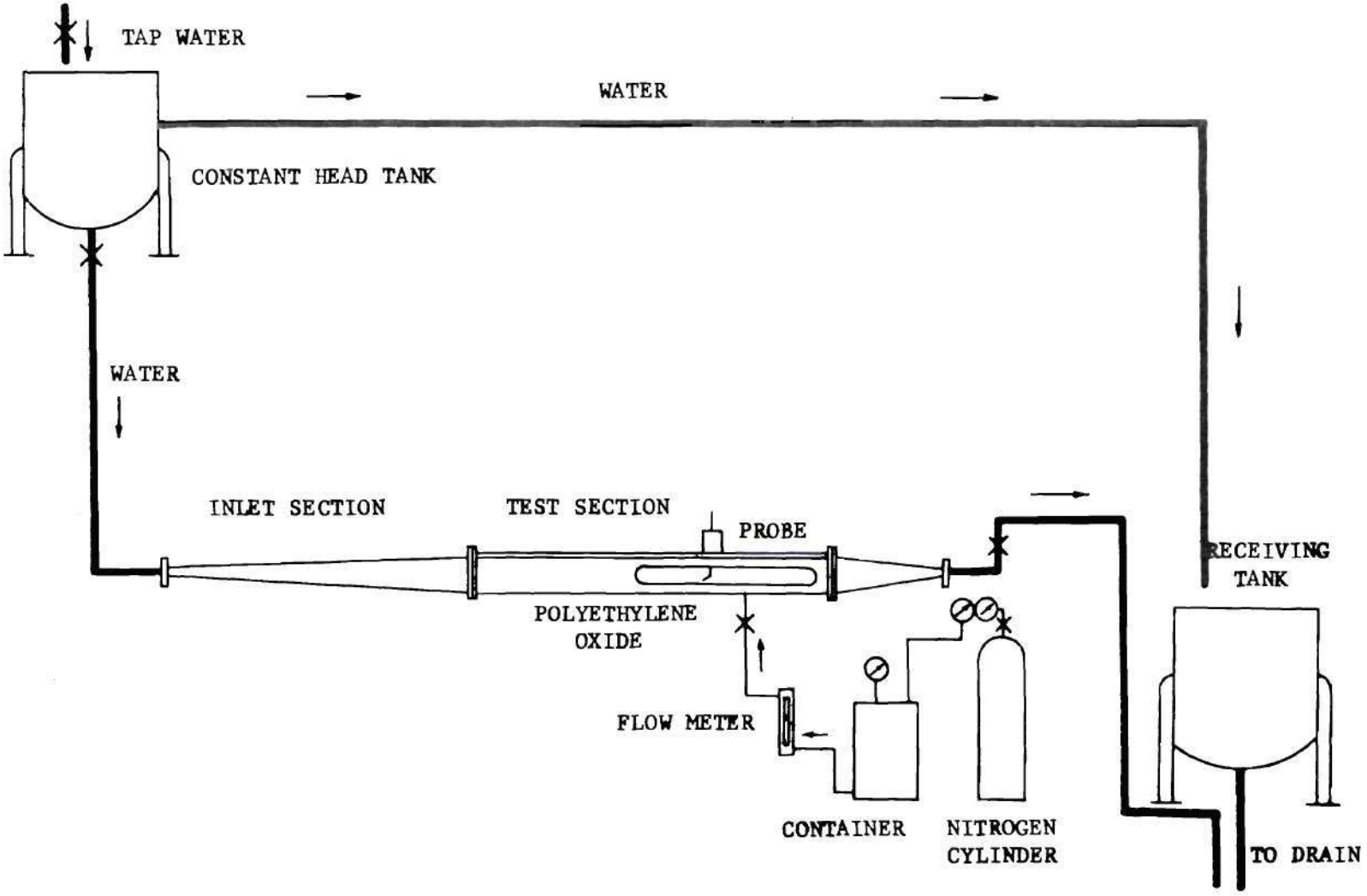

Figure 1. Schematic Layout of the Experimental Apparatus.

was placed on the channel floor - Figure 2. Aluminum strips, 1/4" thick and 1" wide were attached on top of the first half. These were placed around the periphery of the insert and were butted against a ¼" aluminum plate which was attached to the last half ot the insert. Over all this was placed a 1/4" rigid polyethylene plate (the test plate) 96" x 12". The insert plus accessories comprised the test assembly and reduced the test section to a 12" x 6" section. The first half of the test assembly served as a reservoir for the injected fluid. In lieu of a slot, which created structural and experimental problems, two rows of holes, 1/2" apart, were drilled in the test plate. These holes, 0.089" in diameter (#43 drill), were drilled on 1/4" centers, at an angle of 15^{o} with the horizontal. The mean distance of the holes from the beginning of the test section was 45 inches.

With a water supply limited to approximately 250 gallons per minute (gpm), it was necessary to increase the flow of water in the channel to attain a wall shear sufficiently large to exhibit the Toms' effect. This also resulted in more accurate velocity measurements. The bulk flow rate of the main stream was increased by installing a section of rigid styrofoam backed with a sheet of aluminum in the top of the test section. This insert was 3 inches thick, 12 inches wide, and 96 inches long. At the end of the diverging duct a styrofoam insert, elliptical in shape was attached to the top. This reduced the exit area of the diverging duct such that it equalled the modified area of the test section. Appropriate holes were provided to allow passage of the velocity probe into the channel. This gave a test section approximately 12 by 3 inches, or a 4:1 aspect ratio. This is considered the minimum aspect ratio for which edge effects may be neglected.

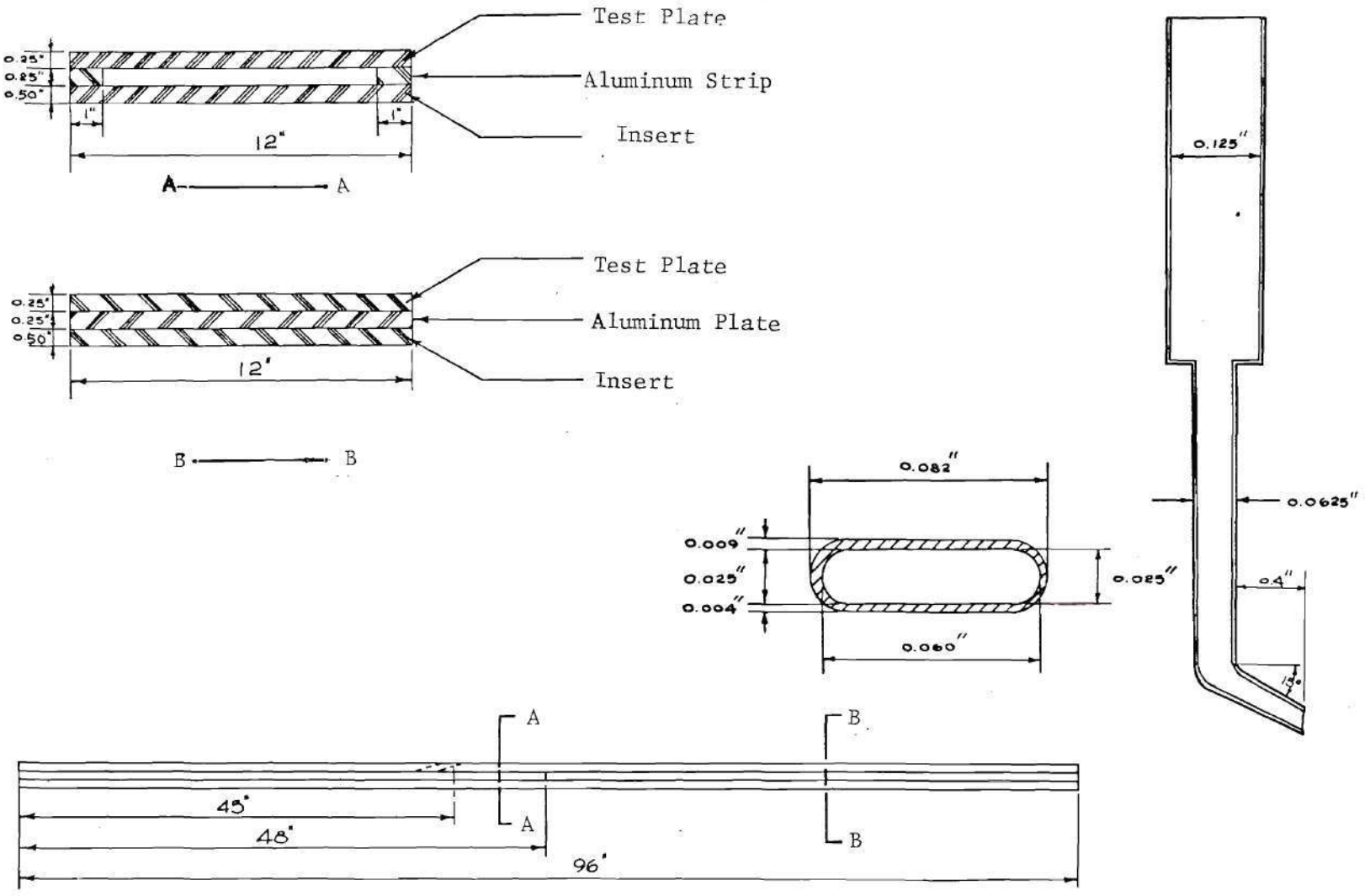

Figure 2. Detail of Test Plate Assembly and Pitot Probe

A honeycomb located 19" downstream from the test section inlet broke up any large vortices. The honeycomb was two inches long and had hexagonal holes; the edges of the hexagon were 1/8".

The plenum between the test plate and the 3/8" aluminum insert was connected to a 40 liter aluminum container through a quarter inch line. The ejected fluid was metered by a rotameter. For low injection rates a Fisher and Porter flowmeter, Model 10A4136 ND LK equipped with a 2L-150 tube and glass float, was used. For high injection rates a Brooks model 1231 with a R-8M-25-2 tube and an 8-RV-14 float was used. With increasing concentration the floats of both rotameters fluctuated more, giving less precise readings. The Fisher & Porter flowmeter was considerably more unstable.

The container, equipped with a relief valve, was pressurized by nitrogen to pump the drag-reducing solution into the boundary layer on the bottom surface. The test section contained two horizontal windows of plexiglass to enable initial adjustment of the probe.

The test section flow was dumped into a 20 inch-long duct which converged from a 6 x 12 inch cross-sectional area to an area with a cross section of 2.9 x 2.9 inches. The water discharged from this section through a 3 inch polyvinyl chloride pipe into a drain twenty feet below the elevation of the test section. A globe valve was placed in this discharge line to maintain a positive test section pressure.

Boundary-layer measurements were made with the probe assembly shown in Figure 3. This assembly was supported by an aluminum track, 4½ inches wide by 96 inches long, which was attached to the top plate of the test section. This track contained eight ports located 6 inches

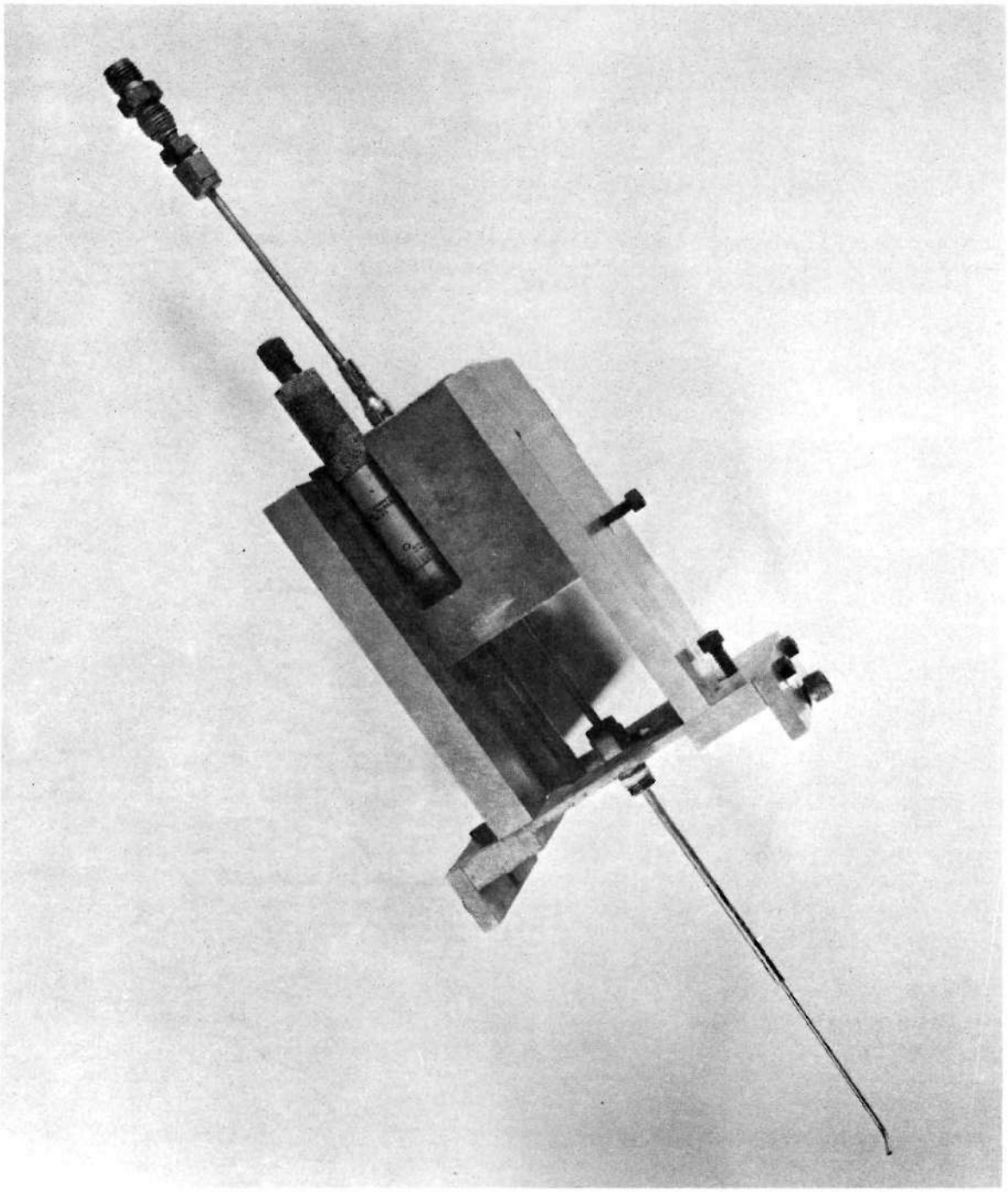

Figure 3. Pitot Probe Assembly

apart, starting at a distance of 48 inches from the test section inlet. Boundary-layer measurements were made by probing through these ports. O-ring seals around the probe prevented water leakage from the test chamber. To measure vertical distances a micrometer drive was employed to raise or lower a slide to which the probe was attached.

The probe itself was constructed from 1/8" stainless steel tubing. Its tip was fabricated from 1/16" diameter stainless steel hypodermic tubing and telescoped into the bottom end of the larger tube. The probe tip had a rectangular opening 0.060-inch wide and was 0.025 inches high. The end of the probe was sanded so that the edge of the tip was vertical, and would be perpendicular to the flow. Probe details are shown in Figure 2. This probe was used to conduct the measurements described later in this work. The probe was connected to the differential-pressure cell during velocity measurements, or was left open to collect samples for concentration measurements.

4.1.2 Differential-Pressure Cell

To measure the relatively low differential pressures involved in this study, a Foxboro type 15A Differential-Pressure Cell Transmitter with a range of from 0 to 2.4 inches of water was employed. Air required to operate the cell was supplied through an air filter and a regulator, which was adjusted to provide air at a pressure of 20 psi. The high pre-pressure capsule of the differential-pressure cell was connected to the velocity probe, and the low-pressure side to one of several static taps in the side wall of the channel. A crossover valve enabled equal pressures to be applied to both capsules of the cell. This is necessary to obtain the zero reading, or balance pressure. The output of the cell was

transmitted to a mercury manometer.

4.1.3 Spectrophotometer

Concentration analyses of samples taken from the channel were determined colormeterically from the intensity of a tracer (Rhodamine B dye), which was added to the injected concentrate. The spectrophotometer used for these analyses was a Bausch & Lomb Spectronic 20. Either of two curved cuvettes may be used. The larger (1") was selected because it gave better resolution at low tracer intensities. For a typical concentration profile, most of the data were in this range. Samples too concentrated to be measured properly were diluted with water using pipettes.

4.2 The Drag-Reducing Agent Selected

Poly (ethylene oxide), Polyox WRS-301, manufactured by Union Carbide Chemicals Company was selected for this investigation. This chemical is the most effective drag-reducing agent presently known, is relatively inexpensive, is available in commercial quantities, and is the most common drag reducing agent used in research.

PEO is one of the high-molecular-weight polymers of ethylene oxide $H-(O-CH_2-CH_2)_n-O-H$. The lower members of the series, which may be liquids, waxy solids, or greasy solids, are known as poly (oxyethylene) glycols. The physical state depends on the molecular weight which varies from about 200 to 10000. At the high molecular weight end of the series, the polymers are called poly (ethylene oxide), with molecular weights up to several million. Polyox resins, from Union Carbide, are manufactured in nine grades -- Table 1. The WSR variety have very high thickening power in aequous solutions; the WSR N produce less stringy solutions, and their viscosity is lower than WSR aequous solutions.

Table 1. Grades of Polyox Water-Soluble Resins*

Grade	Approximate Molecular Weight	Viscosity Range, cps, 25% C	
		5% Solution	1% Solution
POLYOX WSR N-10	100,000	10-20	--
POLYOX WSR N-80	200,000	55-95	--
POLYOX WSR N-750	300,000	550-900	--
POLYOX WSR N-3000	400,000	2250-3350	--
POLYOX WSR-205	600,000	4100-8000	--
POLYOX WSR-1105	900,000	8100-16000	--
POLYOX WSR-301	4,000,000	--	1500-3500
POLYOX Coagulant	5,000,000	--	5000-8000
POLYOX FRA	> 6,000,000	--	> 8000

All aqueous solutions of polyethylene oxide, even though dilute, show polymer-solvent interaction. At concentrations of the order of one percent, the solutions are stringy and are classed rheologically as pseudoplastic, i.e., the viscosity decreases in a reversible manner with increasing shear rate. Solutions over 5 percent in concentration are elastic gels which show a yield point.

Solutions of polyethylene oxide in water are characterized by a parameter called the intrinsic viscosity, $[\eta]$, which is defined as:

$$[\eta] = \lim_{C \to 0} \frac{\mu - \mu_o}{C\mu_o} \qquad (4\text{-}1)$$

It has been shown that a relationship exists between average molecular

*Data taken from reference 114

weight of the polymer in solution and its intrinsic viscosity:

$$[\eta] = KM^a \qquad (4\text{-}2)$$

where $[\eta]$ is expressed in units of dl/gm. The constants K and a are temperature dependent -- Table 2.

Table 2. Constants for the Intrinsic Viscosity-Molecular Weight Relationship for Poly(ethylene Oxide) and Water.*

Temperature C^o	Approximate mol-wt range	$K \times 10^5$	a
25	2×10^2-8×10^3	156.0	0.5
30	10^4 - 10^7	12.5	0.78
35	10^4 - 10^7	6.4	0.82
40	10^4 - 10^7	6.9	0.81

Most solution properties are dependent on temperature and concentration. Shear rate in the preparation of PEO solutions can, in some instances, be more pronounced than the effect of temperature and concentration on solution viscosity.Shear rate also affects the molecular weight in solution.

Polymers of ethylene oxide are used in a great variety of agricultural, commercial, household, and industrial applications. Poly(oxyethylene) glycols are generally used in the pure or highly concentrated form. The high-molecular-weight poly-(ethylene oxides) are used as thermoplastic resins and film formers, or they are diluted and used as thickeners, protective colloids, and sizing agents.

*Data taken from reference 115

4.3 Experimental Parameters

In the experimental investigation, runs were made without mass addition, with water addition, and with polymer injections at various injection rates and concentrations. Polymer solutions of 500, 1000, and 2000 ppm were injected into the boundary layer at rates of 250, 350, 500 and 1000 cc/min. In these runs, velocity and concentration profiles were obtained at each of four stations located at 48, 54, 60 and 66 inches from the inlet of the test section. This corresponds to 3, 9, 15, and 21 inches downstream from the injection source respectively. The system was operated at the maximum capacity of 240 gallons of water per minute for all runs.

The injected concentrations were chosen so that at the minimum concentrations there would be adequate polymer to cause drag reduction at station 4. The maximum concentration was chosen such that at lower injection rates, the wall concentrations would be in the range of maximum drag reduction over most of the test section.

The injection rates were selected to correspond to a fraction of the sublayer discharge. The sublayer discharge is defined as the flow rate through the sublayer, with no polymer addition:

$$Q_s = 67.3 \nu \text{ ft}^3/\text{ft sec}$$

Based on a kinematic viscosity of water at 20°C of 1.08×10^{-5} ft^2/sec and an injector width of 9.75 inches, Q_s is approximately 1 liter/min. Thus, the maximum injection (1 liter/min) corresponded to the sublayer discharge at 20°C. The other injection rates corresponded to 25, 35, and 50 percent of the sublayer discharge.

4.4 Procedures

4.4.1 Solution Preparation

Polyethylene oxide is more susceptible to mechanical degradation and aging than are most drag reducing polymers. Although intrinsic viscosity is commonly used to characterize degradation, Stratta indicated that this parameter can only indicate wholesale degradation. The effect of mechanical degradation was minimized by a consistent technique of solution preparation. Aging was minimized by using about 2.5% by volume isopropyl alcohol in making the solution (this suggestion was made by Dr. J. J. Stratta in a private communication).

PEO was prepared following a procedure similar to that recommended by Union Carbide[114]. The solid PEO was slurried in isopropanol with a high speed agitator, yielding suspension of small PEO particles. No mechanical degradation occurs unless the PEO is dissolved[114]. About half the final volume of water (90 L) was stirred by an agitator until a large vortex was formed. At this point the agitator was removed and the isopropanol-PEO slurry added to the water. The vortex disperses the PEO particles. Gentle manual agitation of the suspension was continued for about an hour, so that no large agglomerations were formed. The slurry beaker was filled with water to dissolve the PEO remaining. After a day, the solution was transferred to a second container, along with the solution from the slurry beaker. The original slurry vessel was rinsed thoroughly to flush out the few jelly like agglomerates of PEO which adhered to the walls. This rinse was added to the final container, which was then topped up to volume. The solution sat one more day to allow the PEO to completely dissolve. Walters and Wells[89] also found that two days was

approximately the minimum time for the polymer to fully disperse in the solvent; their concentrations were 1000 and 5000 ppm.

The nature of PEO solutions was such that the rotameters had to be calibrated for each concentration. This calibration was done immediately before an experimental run, so that the solution temperature, degree of aging, and viscoelasticity were the same as the injected concentrate.

4.4.2 Velocity Measurements

In the runs without injection, velocity measurements were started almost immediately after the gate valve in the main line had been opened and the sensing lines and Foxboro Differential-Pressure Cell Transmitter were flushed to purge trapped air. The static pressure was picked up from a 1/32 inch static tap in the wall of the test section, adjacent to the dynamic probe. The difference between the static and dynamic pressure with the water at standstill was zero, regardless of the probe's vertical position. With the main stream in motion, the difference between the static and probe pressures was directly due to the dynamic head. Measurements were started at bottom. The probe was carefully lowered until the probe tip touched the bottom. The probe was then raised(approximately .002 inches) to take up backlash and probe bending until a noticeable velocity change occurred. At this location the mid-point of the Pitot tube was 0.016 inches from the surface. A vertical traverse of the boundary layer was made until the differential pressure became constant.

For the injection runs the channel water flow was first established and then the storage container was pressurized to approximately 40 psi. The flow rate of PEO was then adjusted to the desired value. Fluctuations

in the rotameter floats (approximately $\pm$ 2%) caused the only difficulty in maintaining the injection rates constant for the duration of the run. The system reached equilibrium approximately ten minutes after injection was commenced.

4.4.3 Concentration Measurements

To obtain concentrations of PEO in the boundary layer, samples of approximately 25 mls were withdrawn through the probe. The sampling period was based on isokinetic sampling at the velocity of pure water at the probe center. In this technique, samples are withdrawn into the probe tip at the local flow rate. Exact isokinetic sampling is not experimentally possible, since there is some inaccuracy in velocity measurements due to viscoelasticity of the polymer and to velocity gradients across the probe near the wall. A preliminary test, varing sampling time, indicated that the sample time is not critical.

Rhodamine B dye was added to the injected concentrate at 150 ppm. This high tracer concentration was necessary to obtain good data at the farthest station from the source. Near the source (Station 1) it was necessary to dilute the samples taken near the wall.

Strictly speaking, it is the dye concentration, not PEO, which is measured. (Originally it was planned to compare dye concentration measurements to chemical analyses. To this end, a chemical analysis for PEO was developed, based on the chemical oxygen demand analysis performed by water chemists.) However, Wetzel and Ripken[24] compared concentration data obtained from a tracer dye to chemical analysis based on turbidity. They concluded that their dye, Rhodamine B, and PEO diffused at the same rate in turbulent flow. This assumption is, therefore, made in the present study.

Preliminary experiments indicated that the dye lost color intensity with time. Since the sample containers became somewhat tinted, it was thought the intensity decreased because dye was adsorbed on the container walls. Therefore, it was essential to analyze the samples immediately after they were taken. Studies[116,117] indicate that the accuracy of chemical analyses of ppm range quantities is questionable when the samples are stored for any length of time. This is due to adsorption of particles on container walls. A drawback to the polargraphic technique used by Hulsebos[25] is the necessity to store the samples before analysis.

The probe tip was carefully located at the surface before injection was commenced. Injection was started, and the withdrawal rate adjusted. Equilibrium was attained when the color intensity of a sample taken from the wall region became time independent. This took approximately five minutes after each change in injection rates. The time from the start of injection to steady state was a function of the injection rate. At the lowest rates this took about ten minutes.

Transmittancy was measured on the spectrophotometer as samples were withdrawn. Samples were taken only at those locations for which the transmittancy was greater than 90%. Samples were also taken from the 40 liter feed tank during the run. From these a calibration curve was constructed for each run by diluting to known concentration ratios and measuring the transmittancy. Using the experimentally measured transmittancy the ratio of the sample concentration to the injected concentration was read from the standard curve. This analysis was felt to be more reliable than the overall reproducability of the system and sampling technique.

CHAPTER V

DATA REDUCTION

The purpose of this study was to investigate how the concentration of injected solution and injection rate affected the wall shear, polymer concentration at the wall, and the development of both the momentum and concentration boundary layers. Because of the differences involved in obtaining and interpreting the data, velocity and concentration measurements are treated separately.

Velocity profiles were obtained at four axial locations. The velocities were computed from the measured differences between the total and static pressures (i.e. the dynamic head).

Concentration analyses were obtained in the form of spectrophotometric data. Using known dilution ratios, a calibration curve of percent transmittancy versus concentration of dye added to the injected concentrate was prepared. Concentration analyses were determined from this calibration curve.

5.1 Velocity Data

Velocity data were used to evaluate the following boundary layer parameters: boundary layer thickness (δ), momentum thickness (θ), form factor (H), displacement thickness (δ_1), and wall shear (τ_w). These parameters are useful in evaluating the effect of polymer injections on the momentum boundary layer.

The wall shear may be calculated from velocity profiles in four

different ways: from the law of the wall, from the law of the wake, from the velocity profile in the sublayer, and by using the momentum equation. Displacement thickness and momentum thickness were calculated from the velocity profile using numerical integration (Equations 2-6 and 2-7).

The boundary layer thickness (δ) is somewhat arbitrary in its definition. Many investigators take δ as the vertical distance from the surface, y, where the velocity is some fraction of the free stream velocity (usually this is 99 or 99.5%). In this work, δ was taken as the thickness at which the velocity equals 99% of free stream. A second boundary layer thickness, δ_∞, was defined as the distance where the velocity reaches the free stream value. The outermost four points in the profile, not including U, were fitted to the following equation using a least squares technique:

$$U = a + b \ln y \tag{5-1}$$

This resulting equation was extrapolated to determine the value of y for the free stream velocity, hence, δ_∞, and solved for 0.99 U to get δ. The same technique was used to determine δ and δ_∞ for all runs, with and without polymer injection.

A least squares fit is preferable to interpolation between data points to find δ, since interpolation is more sensitive to error in one data point. Equation (5-1) appeared to best represent the velocity profile in the outer portion of the boundary layer. A linear form was found unsuitable. Polynomial equations of the following form were also tried:

$$U = a + by^{\frac{1}{n}} + cy^{\frac{2}{n}} \tag{5-2}$$

The boundary layer parameters were fitted to polynomial expressions in the axial distance (x) by the least squares method. Two approaches were taken. First, the values from several surveys at each axial location (station) were averaged and the averages were used for the fitting. In this case no values were discarded. The second approach used all individual values at all stations to obtain a fit. Data points were discarded below the 99% confidence level. That is, data points which differed by more than a specified number of "standard deviations" from the mean for the station were thrown out. The criterion for amount of allowable discrepency varied according to the number of data points and number of regression variables (in this case, maximum power of x). The maximum number of "standard deviations" (usually three) was then found[118]. Averaging removes the randomness in the boundary layer parameter. However, axial distance (x) is a fixed quantity. Therefore, fitting boundary layer parameters versus axial distance is not a true regression analysis since there is no deviation in location of the axial distance. Because of errors encountered in velocity measurements of dilute polymer solutions, the other analyses required special handling for polymer injection runs.

5.1.1 No Injection

The law of the wall (Equation 2-12) was used to determine the wall shear. A semi-logarithmic plot of velocity (u) versus vertical distance (y) produces a straight line in the region where the law of the wall is valid, and the friction velocity, u_*, is found from the slope. It is generally assumed that the law of the wall is valid from values of $y_+ = 26$ up to 15 percent of the boundary layer thickness. An examination of the data presented in Coles[19] seems to indicate that the law of the wall

extends somewhat beyond this 15 percent. Clauser[16] shows that the range of validity of the law of the wall is greater in channels and pipes than in flat plate boundary layers. For each station, a least squares fit was performed for all velocity profiles up to about 30 or 40 percent of the boundary layer thickness. To establish the region where this relation was valid, the largest values of y were omitted from the fit until the last point dropped did not signficantly affect the value of u_*.

It was judged that at stations 1 and 2 the law of the wall was valid up to about 0.2 inches; for stations 3 and 4, up to about 0.3 inches. The effective lower limit for y in these fits was 0.03 inches, although in some cases this gives a y_+ less than 26. These limits were used for subsequent data analyses. For each velocity profile, the shear stress was found from the slope of a linear least squares fit of u vs ln y. The slope was assumed to be $2.5u_*$, where 2.5 is the reciprocal of the von Karman constant. Having determined u_*, B was determined from the law of the wall equation. Since there are only four or five data values available in each profile, a relatively small error in one point would affect the slope considerably. In cases where this happened, the erroneous point was discarded if the omission caused a deviation in u_* of greater than 10%. The wall shear (τ_w) was determined from a least squares fit of the remaining points.

The momentum equation (Equation 2-5) was also used to evaluate wall shear. The momentum equation is rewritten:

$$\frac{\tau_w}{\rho U^2} = \frac{d\theta}{dx} + (H + 2)\frac{\theta}{U}\frac{dU}{dx} \qquad (5\text{-}3)$$

The parameters θ, δ_1, and H were evaluated at all four stations from the velocity profiles using numerical integration of Equations 2-6 and 2-7. The gradients in U and θ are then calculated and substituted into Equation (5-3) to obtain the shear stress. For better results this procedure was repeated experimentally three or four times and a least squares technique used to fit θ, H, and U as functions of x (axial distance). The best fits were of the form:

$$H(x) = a + bx \tag{5-4}$$

$$U(x) \text{ and } \theta(x) = a + bx + cx^2 \tag{5-5}$$

Least squares techniques were used to fit both the parameters H and θ, and the velocity U. Values of wall shear, τ_w, can be determined at all points along the test section using these relations.

Shear stress can also be calculated from the velocity defect law, given an equilibrium profile. The simplified wake equation (2-25) did not give consistent values of u_*. That is, for the flow configuration studied, the simple relation given by Equation 2-25 proved a poor approximation for the velocity profile in the wake region of the boundary layer. The wake relations of Coles (Equation 2-18) required prior knowledge of u_* to determine δ, hence was unsuitable for directly determining wall shear in this study.

Because the velocity gradient is linear in the laminar sublayer, the friction velocity can be determined from the slope of the velocity profile:

$$u = \frac{u_*^2}{\nu} y \tag{5-6}$$

Since the sublayer was very thin (about the same size as the Pitot tube) this method could not be used.

5.1.2 Polymer Injection

As has been indicated earlier, Pitot tube measurements in flows of polymer solutions are susceptable to errors because of the presence of large normal stresses. Various authors have attempted to calibrate Pitot tubes. However, the magnitude of the normal stress contribution is dependent on flow conditions as well as concentration. Hence, calibrations of Pitot tubes are very difficult. Two investigations in the literature differed in their conclusion as to the effect of probe Reynolds number on the error. Wetzel and Tsai[61] indicated that the percent error is independent of the velocity. Frumen et al.[62] disagreed. In an effort to develop a scheme for correcting our data, the results of both investigators were examined very thoroughly. The results of Wetzel and Tsai were presented in dimensionless form and it was impossible to work back to the original measurements. They stated that the ratio $\Delta U/U_{true}$ was independent of velocity. Frumen, Sulmont and Loiseau[62] concluded that percent error was Reynolds number (based on solvent viscosity) dependent. In order to reconstruct their raw data it was noted that the error in their measurements was dependent on only concentration and Pitot tube dimensions. That is to say, the absolute error, in feet per second, was independent of the velocity. To obtain accurate velocities close to the wall, corrections to the data would be necessary.

The momentum equation and the law of the wall were found to be unsuitable in evaluating the wall shear for the injection runs. The

momentum equation cannot be used since near the wall (where the errors are greatest), values of u(U-u) are at their maximum, and a small relative error in this region significantly effects the value of θ. Hence the momentum equation was unsuitable without adequate velocity corrections. The law of the wall was unsuitable because there is considerable polymer throughout its region of applicability. Since taking the slope of the velocity profile was involved, the technique was open to significant error. Because of these difficulties it was necessary to utilize a method based on velocity measurements which were outside the polymer plume to obtain the wall shear.

The concept of velocity defect was discussed earlier (Sections 2.2 and 2.1.3). It is generally assumed that for a given flow situation (e.g. pipe flow, channel flow, or flat plate flow) the functional relation between the velocity defect, $(U-u)/u_*$, and the ratio y/δ (or y/R for pipe flow) remains the same for dilute polymer solution flows as for pure solvent flow. The experiments of Virk[36] for pipe flow show this assumption to be valid for all values of y/R. Results by Goren and Norbury[37] show the range of validity to be for $y/R > 0.3$. Results by Wetzel and Ripken[24] for open channel flow show no deviation in velocity defect when plotted versus the parameter $yu_*/U\delta_1$.

The velocity defects were plotted versus y/δ for all four stations for the no injection runs. This plot was assumed to be valid for the injection runs. Then from the velocity measurements in the outer region of the layer and the velocity defect determined from the chart for a given value of y/δ, the friction velocity, u_*, and hence τ_w could be determined. In determining u_* the values in this region were merely averaged. Values

of u_* which differed by more than 10% of the average were discarded in the averaging procedure.

5.2 Concentration Data

The concentration measurements were used to evaluate the effect of polymer injection on the concentration plume and wall concentration. Walters and Wells[89] have used the turbulent mass diffusivity, E_D, to evaluate the effect of polymer on turbulent diffusion. Generally in computing E_D velocity profiles are required. However their flow geometry and injection rates (adjacent to and downstream from a porous wall) enabled them to neglect the terms involving local velocity. For this investigation, these terms might not be negligible. Poreh and Cermak outlined a method of calculating E_D by assuming a 1/nth velocity profile. Since our profile was not reasonably represented by a 1/nth profile and the measured local velocities were inaccurate, turbulent mass diffusivities were not calculated.

From experimental measurements of C/C_i vs vertical distance (y) a plot of log (C/C_i) vs y was generated. The wall concentration was determined by smoothing the data and extrapolating the curve back to $y = 0$. This technique was subjective. The possibility of least squares fitting of data was discarded because of insufficient amounts of data and the irregularity of the resulting profile. Having found the wall concentration, λ, the value of y where the concentration is one half of the wall concentration, was determined from the plot. The relative rate parameter, β, was determined from the rate of growth of both the concentration and the momentum boundary layers. A plot of λ versus x and least squares fits of λ and δ versus x were used to evaluate the parameter, β.

The least squares method used was the "average value" method described in Section 5.1. Again, this technique was extremely subjective because it involved taking slopes. However it was necessary to determine β to compare results with that of other investigators, and to determine the various zones of concentration boundary layer development. The values of C_w/C_i and λ were used then as a basis for comparing the injection rates and concentrations.

CHAPTER VI

DISCUSSION OF RESULTS

6.1 Preliminary Considerations

In all test runs reported in this investigation, the bulk flow rate of liquid through the test section was constant at a Re/ft of approximately 2.4×10^5. A globe valve was provided at the channel discharge to maintain the system above atmospheric pressure, and for adjustment of the flow rate in case of changes caused by different operating temperatures. No adjustments were necessary due to PEO addition because the only resistance significantly affected by the polymer addition, the channel floor, contributed little to the overall head loss for the system. However, temperature changes required adjustment of the globe valve. In the experiments of this investigation, measurements were made of mean velocity and concentration profiles in turbulent flow. There are errors inherent in measurements of these quantities.

There is an error in the probe position. With the micrometer drive used in this investigation and the technique used to locate the bottom position, the error in the probe location could be as much as 0.002 inch; normally the error would be approximately .001 inch. At low probe Reynolds numbers (the Reynolds number based on probe thickness) the viscous effects in the fluid affect the measured stagnation pressure. The lowest probe Reynolds number in this investigation was approximately 300. According to an investigation performed by MacMillan[119] the Pitot tube measurement at this Reynolds number should be within .5% of the true

value. At higher velocities this effect becomes less significant.

There is some error due the effective displacement of the center of the probe. A total pressure probe placed in a fluid with a transverse velocity gradient experiences a displacement of the effective center of total pressure from the geometric center. At the initial point closest to the wall, the displacement for the probe used caused a 2% error in the pressure measurement. For all other measurements the error was negligible. These calculations were performed following a method outlined by Knudsen and Katz[120].

Shaw[121], investigating the influence of hole dimensions on static pressure measurements, concluded that the observed static pressure was always greater than the true static pressure. In the present investigation, the diameter of the static taps was 0.03 inches, and the effect was therefore believed to be negligible according to Shaw's results.

It has been shown by various authors that dilute solutions of polyethylene oxide are viscoelastic. This property causes errors in the total pressure measurement using a dynamic probe. The simple Bernoulli expression used in calculating velocities from differential-pressure measurements should not be used without correction. However, no good correction scheme exists. Since in some cases errors in the measured local mean velocities were considerable, all the velocity data are listed in Appendix A so that the reader may have the raw data at his disposal. Near the wall ($y < 0.4$ in) the relative error was greatest. In fact, in many instances negative velocities were measured. Concentration experiments revealed dye patterns which indicated the flow was not negative. Hence, in those cases the error due to viscoelastic effects was greater

than 100%. A summary of runs showing injection rate and injection concentration, and water viscosity is given in Table 3 (Appendix C).

Concentration samples should be withdrawn at the local flow rate. Because of inaccuracy in the velocity measurements, this was not possible in this investigation. However, preliminary tests indicated the sampling time was not extremely critical. Concentration data are presented in Appendix B.

6.2 Analysis of Velocity Data-No Polymer Addition

6.2.1 Boundary Layer Parameters, θ, δ_1, δ, and δ_∞

The momentum thickness (θ) and the displacement thickness (δ_1) were evaluated by numerical integration of the velocity profiles, according to Equations (2-6)and (2-7):

$$\theta = \int_o^\infty \frac{u}{U}\left(1 - \frac{u}{U}\right) dy \qquad (2\text{-}6)$$

$$\delta_1 = \int_o^\infty \left(1 - \frac{u}{U}\right) dy \qquad (2\text{-}7)$$

The boundary layer thicknesses, δ and δ_∞ were determined from a linear least squares fit of u vs ln (y) in the outer region of the layer. The results are in Tables 4, 5, and 6 respectively. Runs 1-4 were conducted at 48°F, runs 5-7 at 57°F and runs 8-10 at 65°F. Any effect of water temperature on these parameters appears to be less than deviations due to experimental error. The ratio $H(=\delta_1/\theta)$ was constant, approximately 1.44 at all stations. There was no change in H with temperature.

Boundary layer thickness (δ) data are displayed in figure 4. Since the slope $d\delta/dx$ was needed in evaluating concentration data, a fitted

relation for $\delta(x)$ was developed. First, the technique using individual observations was used, and least squares fits were obtained for δ vs x and δ vs $x^{0.8}$. The highest power term considered was x^2 (or $x^{1.6}$). Second, fits of δ_{ave} vs x and $x^{0.8}$ were tried, with the highest power term considered was x^2 (or $x^{1.6}$). The technique using individual observations resulted in poor fits for all cases considered. Better results were obtained using δ_{ave} vs x. The best fit was a linear fit of δ_{ave} vs $x^{0.8}$; this result is also shown on Figure 4. The ratio of δ_∞/δ averaged 1.08.

6.2.2 Wall Shear Stress

Wall shear was determined from the momentum equation using both least squares techniques outlined earlier, and from the slope of the law of the wall equation. The results of these analyses are presented in Table 7 along with a value for shear stress computed from the Ludweig-Tillman Equation (2-9). In using the momentum equation, a measured axial pressure drop (dp/dx) was used to calculate dU/dx, in lieu of the slope of a fitted equation; this makes the results less sensitive to error in slope calculation. In the least squares technique whereby individual observations were fitted vs x (method C), the best fit for θ (x) was Equation (5-5). θ was averaged at each station (Method D), the best fit was:

$$\theta(x) = a + bx^{0.8} \qquad (6\text{-}1)$$

An examination of the results in Table 7 shows no significant axial variation in shear stress; also all methods give essentially the same result. Other authors (e.g. Wetzel and Ripken[28]) feel that determining

local shear stress is more accurate using the slope of the velocity profile rather than the momentum equation, because the momentum equation reflects three-dimensional effects. The close agreement between the law of the wall result and the momentum balance shows that the flow is two-dimensional. Hence, Method A (the law of the wall) was chosen for further data analysis. Values of u_* and B were calculated for each profile, from the law of the wall. These results are tabulated in Table 8. These individual u_* values were used to compute u/u_* and yu_*/ν for each run. Figures 5 through 8 show the non-dimensional velocity profiles. There was considerable deviation in values of B. The average was 5.4, maximum 9.2 and minimum 4.1. Most of the results ranged between 4.5 and 6.0.

The boundary layer parameters Δ and G, defined by Equations 2-23 and 2-24, respectively, were evaluated using the u_* values determined from the least squares fit of the velocity profile to the law of the wall. The results are shown in Table 9. Clauser[16] indicates that for constant pressure layers G should be 6.8 and Δ/δ 3.6. For this work the overall average of G was 6.68. The ratio of Δ/δ varied from 3.91 to 4.16. This ratio is greater than that suggested by Clauser.

Velocity defect data are presented in Figure 9. The curve shown is an estimation of the best values. Figure 10 was taken from Clauser[16] and shows velocity defect results for three pressure gradient parameters: the zero pressure gradient layer (G = 6.8) and two cases of adverse pressure gradient flows (G = 10.1 and 19.3). Representative values, chosen from the curve in Figure 9 and with the absissa adjusted to y/δ_∞ from y/δ, are shown on Figure 10. The present results agree well with the curves proposed by Clauser for zero pressure gradient flows.

6.2.3 Free Stream Velocity

Figure 11 shows a plot of the free stream velocity versus axial distance from the channel inlet. All the data from the pure water runs are shown. The curve shown is an estimation and not a fitted relation.

6.3 Analysis of Velocity Data-With Polymer Addition

6.3.1 Boundary Layer Parameters θ, δ_1, δ and δ_∞

There was considerable error in the velocity measurements taken near the wall for all cases of polymer injection. The momentum thickness, θ, and displacement thickness, δ_1, were not evaluated because there was no suitable correction for the velocities.

The boundary layer thickness data are presented in Tables 10, 11 and 12. The averages at each station were fitted to a curve of the form:

$$\delta(x) = 2 + bx^{0.8} \tag{6-2}$$

and are shown in Figure 12 through 14. An examination of these plots shows that for all cases of polymer injection there was a decreased rate of growth in the boundary layer. Table 13 is a summary of the reduction in boundary layer growth. This reduction is over a 21 inch portion of the test section which is the axial distance of the farthest station (station 4, x = 66) from the point of injection (x = 45):

$$\%\,\delta_{red} \quad \frac{\delta^p_{66} - \delta^o_{45}}{\delta^o_{66} - \delta^o_{45}} \times 100\% \tag{6-3}$$

For all polymer concentrations the growth rate of the boundary layer was retarded more with increased injection rates.

6.3.2 Wall Shear Stress

Due to the errors in the velocity profiles caused by the viscoelasticity of the PEO, it was impossible to evaluate the wall shear using the momentum equation or the law of the wall. The velocity defect chart, Figure 9, was used to evaluate the wall shear from the velocity data in the outer regions of the boundary layer.

Assuming that the curve presented in Figure 9 was correct in representing the velocity defect for polymer flows, (see 5.1.2) velocity data outside the concentration plume were used to evaluate wall shear. In determining u_* the values in this region were merely averaged. Values of u_* which differed by more than 10% from the mean were discarded. The wall shear calculated using this technique was compared to wall shear for the corresponding "no injection" case. The results of this analysis are presented in Tables 14, 15 and 16.

An examination of these results shows that in some cases there was drag reduction at the two stations nearest the source. However at the latter stations (3 and 4) only in isolated cases is any reduction in drag evidenced. In fact, drag increases are shown. In cases where there was a drag reduction indicated, it was not of the magnitude found by other investigators. That is to say, in only one case was there drag reduction greater than 30%. Most of the drag reductions were between about 10% and 20%. This is lower than results of other investigators.

As was mentioned previously (3.1.3 and 5.1.2) the pipe flow results of Virk[36] show close adherence to a single defect law, with the radius of his pipe approximately the same size as the boundary layer thickness in this investigation. An examination of his results shows approximately

the same maximum deviation from the suggested curve as can be seen in Figure 9. For a given y/δ, maximum error for $(U-u)/u_*$ is approximately $\pm$ 0.25 in the range $y/\delta > 0.3$. This accounts partially for the spread in the results shown in Tables 14 through 16. The results of the boundary layer thickness determination (Tables 10-12) show most results lie within $\pm$ .05" of the average δ. Because δ averages about .85" for the investigation, a fairly high percent error is reflected in y/δ. This also contributes to the lack of precision in the results in Tables 14 through 16. Although there is considerable variation among individual computations, the ratio τ_w^P/τ_w^o is consistently greater than 1.0.

There was quite a dramatic reduction in the growth in the boundary layer. Since the rate of boundary layer growth is somewhat indicative of the magnitude of wall shear, perhaps the velocity defect law is not applicable to flow situations where polymer solutions are injected downstream from the boundary layer origin, with the test section near the injection source. The idea of reduced boundary layer growth and increased drag are not consistent.

6.4 Analysis of Concentration Data

Concentration data were analyzed similar to the manner of Poreh and Cermak[28]. The wall concentration, C_w, and characteristic plume height, λ, were determined by smoothing the data and extrapolation back to the wall, as was described in Section 5.2. Figure 15 is a typical concentration profile and an example of the determination of the wall concentration and plume height. The growth rate parameters for the momentum boundary layer, L_δ, and the concentration boundary layer, L_λ, were determined in order to develop the relative rate parameter, β. The

growth rate parameter for the momentum boundary layer for each injection concentration and rate was determined from a least squares fit of the data to the following function (Figures 12 to 14):

$$\delta = a + bx^{0.8} \tag{6-2}$$

Concentration boundary layer thickness data are in Table 17. Since there was no apparent effect of injection rate on λ for a given injection concentration, λ averaged at each station reflects the mean of all injection rates. The growth parameter for the pure water concentration boundary layer was determined by subjectively drawing a curve through the points and taking the slopes at each station accordingly. For the cases of polymer injection, the plume heights, λ, were fitted versus distance from channel inlet according to a following relation:

$$\ln \lambda = a + bx \tag{6-4}$$

This form of equation was chosen to represent $\lambda(x)$ since plots of λ vs x on semi-logarithmic co-ordinates appeared to approximate straight lines. Tables 18 and 19 contain the results of these analyses for determining the growth rate parameters. The results of these fits for boundary layers and a comparison with the pure water layer are shown in Figures 12 through 14. The plume height λ and the corresponding fitted equations are shown in figure 16. Table 20 contains a summary of C_w data.

6.4.1 Injection of Pure Water

The results of the concentration data for the pure water injection are shown in Figures 17 through 20 and are compared with the curves

suggested by Morkovin[29] and Poreh and Cermak[28] for the intermediate zone of diffusion. The relative rate parameter, β, for water injection and the ratio of λ/δ are given in Table 21. According to Poreh and Cermak the intermediate zone lies in the ranges $0.15 < \lambda/\delta < 0.36$ and $0.08 < \beta < 0.38$. These criteria indicate that stations 2,3, and perhaps station 4 should be in the intermediate zone, and station 1 is in the initial zone. Although there is some scatter in the data, the results here show good agreement with the suggested curves of Morkovin[29] and Poreh and Cermak[28] for the intermediate zone at stations 2, 3, 4. At station 1 there appears to be considerable deviation from the suggested curve. Figure 21 shows the curve of Poreh and Cermak for the intermediate zone and the suggested equations of Morkovin for the intermediate and final zones. Mental extrapolation of the directional displacement of concentration profiles from the intermediate to the final zones indicates that the trend of the deviation at station 1 is expected.

6.4.2 Injection of PEO Solutions

The non-dimensional concentration profiles for polymer solution injection are shown in Figures 22 through 24; on each of these displays all the test stations are shown. The relative rate parameter, β, and the ratio, τ/δ, are given in Tables 22 through 24. In all cases except for the injection of the 2000 ppm solution the plume height was independent of the injection rate, and even for the 2000 ppm case the amount of variation was within experimental limits. Wall concentrations (C_w/C_i) are given in Table 20.

An examination of Table 20 shows that for a given injection concentration (C_i) and station, wall concentration increased with injection

rate. For constant injection rate and concentration (except 2000 ppm at 1000 cc/min), the wall concentration decreased with distance from the source. Both these results are to be expected. The normalized wall concentration (C_w/C_i) increased with increasing C_i for a given injection rate and station, except for some of the 2000 ppm cases. This increase of (C_w/C_i) with increasing C_i indicates that the turbulent diffusion process is supressed. (The dye pattern for the 2000 ppm injections showed wavering streaks near the source; this effect was not as pronounced for the less dilute concentrations. Perhaps these streaks caused errors in the 2000 ppm determinations giving low results in some instances. Wetzel and Ripken[28] also noticed streaking of PEO solutions near the slot.) The growth rate of the concentration boundary layer (Figure 16) is also reduced by increasing polymer concentration - a result of reduced turbulent diffusion. Reduced turbulent diffusion was also noticed by other investigators[88,89,90,91].

The concentration profiles for injection of 500 ppm solutions are shown in Figure 22. Also shown are the curves of Morkovin[29] and Poreh and Cermak[28] for the intermediate zone of diffusion. Close examination reveals that only station 4 appears to be in the intermediate zone; the other stations appear to the left just like station 1 of the water injection case. The growth of the concentration layer, λ, appears to be exponential in this zone, (Figure 16). However, the concentration layer thickness at station 4 has almost reached that of the water layer. One would expect that this rate of growth would not continue but would level off to the water rate of growth. The relative rate parameter, β, indicates that station 4 should be in the initial zone. However, because the ratio, λ/δ,

indicates that the diffusion has reached the intermediate zone, the concentration profile at station 4 is a reasonable result.

From Figures 23 and 24 all the data for 1000 ppm and 2000 ppm injection deviate considerably from the intermediate zone curves of Morkovin[29] and Poreh and Cermak[28] and appear to be in the initial zone. The relative rate parameter, β, (Table 23 and 24) indicates that the diffusion process should be in the intermediate zone. However, the ratio, λ/δ (except for station 4 of the 1000 ppm injection) indicates that diffusion should be in the initial zone. Overall the data indicate that the initial zone has been stretched out and the growth rate of the concentration boundary layer, $d\lambda/dx$, is retarded by increased polymer concentration. (Figure 16). The relative rate parameter, β, alone can not characterize the diffusion process in the initial zone with polymer addition. The results show that PEO retards the rate of diffusion hence $d\lambda/dx$ decreases, $L\lambda$ and hence β increases. However, the non-dimensionalized concentration profiles indicate the initial zone or turbulent diffusion.

CHAPTER VII

CONCLUSIONS AND RECOMMENDATIONS

7.1 Conclusions

From the experiments conducted in this investigation, the following was concluded:

1. Poly(ethylene oxide) caused the "initial zone" of turbulent diffusion to be extended. For injection of water into the boundary layer the initial zone lasted approximately to the first measuring station, three inches from the source. For injection of PEO solutions, the initial zone lasted approximately 15 inches for 500 ppm. For injections of 1000 and 2000 ppm solutions, all 21 inches of the test section was in the initial zone. At the time of this writing, this investigation reports the only experimental data for the "initial zone" of turbulent diffusion.

2. The structure of the wake section of the boundary layer did not appear to follow the same velocity defect law as did the pure water boundary layer. The assumption of the same velocity defect relationship resulted in predicting drag increase. However, experimentally, there was considerable reduction in boundary layer growth. Since boundary layer growth rate is indicative of the magnitude of skin friction, these results are contradictory.

3. The normalized wall concentration (C_w/C_i) increased with increasing injected concentration, for a given injection rate and axial distance from the source. Thus, slot injection appears to be more

efficient at higher injection concentration. This trend does not hold for some of the 2000 ppm solution injections, perhaps due to the formation of streaks at this high concentration.

4. The rate of growth of both the boundary layer and concentration plume were slowed by the addition of Poly(ethylene oxide) to the boundary layer. For a given injection concentration, the growth rate of the concentration characteristic plume height was independent of injection rate. In the "initial zone" of turbulent diffusion, the characteristic plume height, λ, grew exponentially with respect to axial distance downstream from the source.

7.2 Recommendations for Further Study

On the basis of this study the following further work is recommended:

1. A comprehensive study should be undertaken to develop a reliable correction scheme for velocity probes in viscoelastic flows.

2. The effect of poly (ethylene oxide) on the outer portion of the boundary layer should be studied experimentally under conditions other than the one used for this investigation. For example, performing the study at greater distances downstream from the source; examining the effect in a true boundary layer situation, rather than channel flow; and considering the flow situation where the injection point and boundary layer origin coincide.

3. There is a need for an analytical solution to characterize concentration profiles in the initial zone.

4. A thorough study of the effect of polymer on boundary layer separation should be undertaken. One possibility is using the entrainment equation of Head[14] in combination with the momentum equation to calculate

the separation point on an underwater body. Head's concept might be the best starting point since it is not Reynolds number dependent.

APPENDIX A

EXPERIMENTAL VELOCITY DATA

Appendix A lists the experimental velocity data. The velocities are in ft/sec. The vertical distance from the test plate, y is in inches. Stations 1, 2, 3 and 4 correspond to 48.0, 54.0, 60.0 and 66.0 inches from the channel inlet, respectively.

RUN 01 NO INJECTION

Y	STN. 1	STN. 2	STN. 3	STN. 4
.0000	.000	.000	.000	.000
.0165	1.150	1.115	1.172	1.079
.0200	1.217	1.184	1.217	1.150
.0300	1.445	1.417	1.427	1.436
.0500	1.568	1.610	1.601	1.542
.1000	1.744	1.766	1.774	1.728
.2000	1.978	1.978	1.965	1.917
.3000	2.157	2.139	2.107	2.076
.4000	2.276	2.270	2.223	2.193
.5000	2.417	2.406	2.345	2.282
.6000	2.503	2.477	2.444	2.395
.7000	2.601	2.550	2.529	2.487
.8000	2.632	2.601	2.601	2.555
.9000	2.632	2.652	2.642	2.607
1.0000		2.652	2.672	2.657
1.1000			2.677	2.686
1.2000				2.686

RUN 02 NO INJECTION

Y	STN. 1	STN. 2	STN. 3	STN. 4
.0000	.000	.000	.000	.000
.0165	1.161	1.115	1.138	1.091
.0200	1.249	1.206	1.184	1.150
.0300	1.454	1.408	1.427	1.380
.0500	1.610	1.576	1.576	1.560
.1000	1.781	1.766	1.751	1.736
.2000	1.991	1.958	1.924	1.938
.3000	2.175	2.126	2.082	2.072
.4000	2.294	2.276	2.229	2.187
.5000	2.406	2.384	2.334	2.305
.6000	2.508	2.498	2.439	2.395
.7000	2.561	2.571	2.535	2.508
.8000	2.591	2.622	2.581	2.566
.9000	2.622	2.642	2.622	2.632
1.0000	2.627	2.652	2.647	2.652
1.1000		2.652	2.672	2.682
1.2000			2.672	2.682

RUN 03 NO INJECTION

Y	STN. 1	STN. 2	STN. 3	STN. 4
.0000	.000	.000	.000	.000
.0165	1.161	1.138	1.184	1.115
.0200	1.249	1.184	1.249	1.206
.0300	1.417	1.454	1.417	1.427
.0500	1.585	1.576	1.593	1.593
.1000	1.766	1.766	1.744	1.766
.2000	1.971	1.965	1.951	1.938
.3000	2.169	2.107	2.101	2.069
.4000	2.305	2.247	2.223	2.187
.5000	2.417	2.373	2.351	2.294
.6000	2.487	2.492	2.428	2.406
.7000	2.561	2.561	2.529	2.487
.8000	2.591	2.591	2.581	2.561
.9000	2.622	2.622	2.624	2.612
1.0000	2.627	2.642	2.652	2.657
1.1000		2.652	2.672	2.691
1.2000		2.647	2.672	2.691
1.3000				

RUN 04 NO INJECTION

Y	STN. 1	STN. 2	STN. 3	STN. 4
.0000	.000	.000	.000	.000
.0165	1.161	1.138	1.138	1.066
.0200	1.217	1.184	1.228	1.161
.0300	1.445	1.454	1.436	1.417
.0500	1.610	1.610	1.593	1.576
.1000	1.766	1.766	1.751	1.736
.2000	1.998	1.985	1.944	1.917
.3000	2.163	2.114	2.089	2.076
.4000	2.305	2.259	2.223	2.187
.5000	2.417	2.395	2.351	2.305
.6000	2.508	2.487	2.444	2.428
.7000	2.571	2.566	2.540	2.492
.8000	2.601	2.612	2.591	2.571
.9000	2.622	2.632	2.632	2.612
1.0000	2.622	2.642	2.657	2.652
1.1000		2.642	2.667	2.662
1.2000			2.667	2.672
1.3000				2.672

RUN 05 NO INJECTION

Y	STN. 1	STN. 2	STN. 3	STN. 4
.0000	.000	.000	.000	.000
.0165	1.206	1.206	1.115	1.115
.0200	1.301	1.249	1.184	1.184
.0300	1.481	1.508	1.417	1.399
.0500	1.626	1.658	1.585	1.576
.1000	1.789	1.811	1.759	1.744
.2000	2.018	2.011	1.958	1.931
.3000	2.181	2.187	2.101	2.050
.4000	2.322	2.317	2.235	2.223
.5000	2.433	2.428	2.373	2.328
.6000	2.524	2.508	2.466	2.444
.7000	2.586	2.596	2.550	2.540
.8000	2.607	2.632	2.601	2.601
.9000	2.627	2.662	2.647	2.642
1.0000	2.627	2.662	2.662	2.672
1.1000			2.672	2.691
1.2000			2.672	2.701
1.3000				2.701

RUN 006 NO INJECTION

Y	STN. 1	STN. 2	STN. 3	STN. 4
.0000	.000	.000	.000	.000
.0165	1.028	1.091	1.172	1.172
.0200	1.150	1.184	1.301	1.238
.0300	1.490	1.445	1.472	1.436
.0400	1.534	1.525	1.568	1.534
.0500	1.601	1.593	1.601	1.601
.1000	1.781	1.781	1.759	1.759
.2000	2.011	1.985	1.971	1.958
.3000	2.151	2.120	2.120	2.069
.4000	2.276	2.259	2.241	2.187
.5000	2.412	2.390	2.356	2.299
.6000	2.514	2.492	2.471	2.401
.7000	2.561	2.566	2.540	2.514
.8000	2.596	2.622	2.637	2.576
.9000	2.617	2.647	2.647	2.627
1.0000	2.622	2.657	2.677	2.657
1.1000	2.622	2.657	2.677	2.677
1.2000				2.677

RUN 007 NO INJECTION

Y	STN. 1	STN. 2	STN. 3	STN. 4
.0000	.000	.000	.000	.000
.0165	1.150	1.195	1.066	1.054
.0200	1.238	1.259	1.150	1.172
.0300	1.463	1.481	1.427	1.389
.0400	1.525	1.568	1.517	1.481
.0500	1.601	1.610	1.568	1.568
.1000	1.759	1.774	1.759	1.736
.2000	2.011	1.991	1.978	1.924
.3000	2.132	2.132	2.107	2.076
.4000	2.253	2.276	2.241	2.193
.5000	2.401	2.390	2.379	2.311
.6000	2.471	2.492	2.460	2.412
.7000	2.555	2.576	2.524	2.482
.8000	2.601	2.622	2.607	2.545
.9000	2.617	2.637	2.647	2.617
1.0000	2.617	2.657	2.667	2.637
1.1000		2.657	2.677	2.677
1.2000			2.677	2.686
1.3000				2.686

RUN 008 NO INJECTION

Y	STN. 1	STN. 2	STN. 3	STN. 4
.0000	.000	.000	.000	.000
.0165	1.195	1.217	1.217	1.150
.0200	1.280	1.280	1.280	1.249
.0300	1.463	1.490	1.454	1.472
.0400	1.551	1.551	1.499	1.534
.0500	1.601	1.626	1.585	1.601
.1000	1.736	1.811	1.781	1.721
.2000	1.991	1.991	1.938	1.924
.3000	2.145	2.169	2.082	2.069
.4000	2.288	2.288	2.217	2.206
.5000	2.401	2.401	2.322	2.299
.6000	2.482	2.482	2.433	2.401
.7000	2.566	2.576	2.503	2.471
.8000	2.596	2.617	2.586	2.566
.9000	2.617	2.647	2.627	2.596
1.0000	2.617	2.647	2.647	2.627
1.1000			2.657	2.667
1.2000			2.657	2.672
1.3000				2.672

RUN 009 NO INJECTION

Y	STN. 1	STN. 2	STN. 3	STN. 4
.0000	.000	.000	.000	.000
.0165	1.206	1.217	1.217	1.150
.0200	1.270	1.360	1.280	1.249
.0300	1.499	1.517	1.499	1.472
.0400	1.576	1.576	1.568	1.534
.0500	1.634	1.626	1.610	1.601
.1000	1.766	1.721	1.781	1.721
.2000	2.018	1.965	1.938	1.924
.3000	2.145	2.120	2.082	2.069
.4000	2.270	2.265	2.200	2.206
.5000	2.384	2.356	2.334	2.299
.6000	2.482	2.471	2.423	2.401
.7000	2.535	2.535	2.524	2.471
.8000	2.566	2.586	2.566	2.566
.9000	2.596	2.627	2.627	2.596
1.0000	2.617	2.637	2.647	2.627
1.1000	2.617	2.637	2.657	2.667
1.2000			2.657	2.672
1.3000				2.672
1.4000				
1.5000				

RUN 010 NO INJECTION

Y	STN. 1	STN. 2	STN. 3	STN. 4
.0000	.000	.000	.000	.000
.0165	1.172	1.217	1.195	1.079
.0200	1.217	1.259	1.259	1.217
.0300	1.445	1.454	1.454	1.389
.0400	1.517	1.525	1.525	1.499
.0500	1.585	1.576	1.576	1.568
.0750	1.682	1.690	1.650	1.634
.1000	1.766	1.721	1.721	1.698
.1500	1.868	1.882	1.854	1.811
.2000	1.951	1.965	1.924	1.896
.3000	2.107	2.082	2.082	2.031
.4000	2.241	2.253	2.193	2.163
.5000	2.367	2.367	2.311	2.276
.6000	2.460	2.460	2.417	2.379
.7000	2.524	2.535	2.492	2.460
.8000	2.566	2.586	2.555	2.524
.9000	2.607	2.617	2.622	2.596
1.0000	2.607	2.637	2.632	2.637
1.1000		2.637	2.647	2.647
1.2000			2.647	2.667
1.3000				2.667

Y	RUN 101 STN. 1	500 PPM STN. 2	250 CC/MIN STN. 3	STN. 4
.0000	.000	.000	.000	.000
.0165	1.002	.948	1.079	1.002
.0200	1.054	1.002	1.103	1.054
.0300	1.360	1.321	1.351	1.341
.0400	1.472	1.436	1.472	1.445
.0500	1.568	1.585	1.551	1.585
.1000	1.721	1.781	1.751	1.796
.2000	1.991	1.991	1.938	1.978
.3000	2.095	2.169	2.095	2.095
.4000	2.253	2.282	2.206	2.217
.5000	2.390	2.390	2.322	2.334
.6000	2.471	2.482	2.423	2.412
.7000	2.535	2.545	2.492	2.471
.8000	2.576	2.581	2.566	2.566
.9000	2.596	2.627	2.617	2.617
1.0000	2.617	2.637	2.637	2.667
1.1000	2.617	2.637	2.642	2.677
1.2000				2.677

Y	RUN 102 STN. 1	500 PPM STN. 2	250 CC/MIN STN. 3	STN. 4
.0000	.000	.000	.000	.000
.0165	1.028	.920	1.002	.920
.0200	1.172	1.079	1.066	.948
.0300	1.370	1.351	1.360	1.301
.0400	1.499	1.453	1.508	1.427
.0500	1.568	1.593	1.534	1.542
.1000	1.781	1.766	1.781	1.781
.2000	1.991	1.991	1.965	1.978
.3000	2.145	2.145	2.107	2.120
.4000	2.299	2.322	2.206	2.217
.5000	2.417	2.401	2.345	2.345
.6000	2.503	2.503	2.428	2.428
.7000	2.576	2.566	2.482	2.508
.8000	2.607	2.627	2.555	2.566
.9000	2.637	2.637	2.637	2.617
1.0000	2.637	2.647	2.647	2.662
1.1000		2.647	2.657	2.667
1.2000			2.657	2.667

Y	RUN 111 STN. 1	500 PPM STN. 2	350 CC/MIN STN. 3	STN. 4
.0000	.000	.000	.000	.000
.0165	.920	.891	1.002	.876
.0200	1.126	.948	1.126	.976
.0300	1.370	1.238	1.238	1.259
.0400	1.445	1.427	1.408	1.364
.0500	1.534	1.534	1.517	1.534
.1000	1.736	1.736	1.766	1.751
.2000	1.971	1.991	1.991	1.965
.3000	2.132	2.145	2.107	2.107
.4000	2.253	2.265	2.229	2.229
.5000	2.379	2.401	2.345	2.345
.6000	2.450	2.503	2.439	2.412
.7000	2.535	2.586	2.535	2.482
.8000	2.586	2.617	2.586	2.566
.9000	2.607	2.637	2.637	2.617
1.0000	2.617	2.647	2.657	2.657
1.1000	2.617	2.647	2.657	2.667
1.2000				2.667

Y	RUN 112 STN. 1	500 PPM STN. 2	350 CC/MIN STN. 3	STN. 4
.0000	.000	.000	.000	.000
.0165	.976	.920	.976	.860
.0200	1.002	1.002	1.028	.829
.0300	1.280	1.217	1.301	1.126
.0400	1.445	1.408	1.481	1.427
.0500	1.534	1.568	1.568	1.517
.1000	1.736	1.766	1.766	1.751
.2000	1.882	2.005	1.978	1.965
.3000	2.120	2.145	2.107	2.120
.4000	2.288	2.288	2.241	2.229
.5000	2.423	2.367	2.345	2.334
.6000	2.514	2.492	2.428	2.428
.7000	2.586	2.555	2.503	2.503
.8000	2.607	2.617	2.586	2.576
.9000	2.637	2.637	2.607	2.627
1.0000	2.637	2.657	2.647	2.657
1.1000		2.657	2.667	2.667
1.2000			2.667	2.667

Y	RUN 113 STN. 1	500 PPM STN. 2	350 CC/MIN STN. 3	STN. 4
.0000	.000	.000	.000	.000
.0165	.920	.797	.905	.860
.0200	1.002	.920	1.015	1.002
.0300	1.301	1.238	1.301	1.301
.0400	1.472	1.417	1.454	1.463
.0500	1.534	1.517	1.560	1.551
.1000	1.766	1.825	1.760	1.766
.2000	2.018	2.018	1.978	1.991
.3000	2.181	2.181	2.151	2.120
.4000	2.334	2.334	2.282	2.253
.5000	2.450	2.428	2.384	2.356
.6000	2.535	2.545	2.466	2.433
.7000	2.607	2.617	2.550	2.524
.8000	2.647	2.657	2.632	2.586
.9000	2.647	2.667	2.672	2.657
1.0000		2.667	2.682	2.696
1.1000			2.682	2.696

Y	RUN 121 STN. 1	500 PPM STN. 2	500 CC/MIN STN. 3	STN. 4
.0000	.000	.000	.000	.000
.0165	.876	.797	1.028	.763
.0200	1.079	.920	1.103	.920
.0300	1.301	1.217	1.280	1.217
.0400	1.389	1.341	1.389	1.380
.0500	1.481	1.427	1.517	1.481
.1000	1.705	1.721	1.766	1.736
.2000	1.978	2.005	1.951	1.965
.3000	2.120	2.169	2.132	2.095
.4000	2.241	2.299	2.241	2.223
.5000	2.401	2.401	2.367	2.322
.6000	2.482	2.492	2.482	2.417
.7000	2.555	2.545	2.545	2.503
.8000	2.596	2.637	2.586	2.555
.9000	2.627	2.642	2.647	2.627
1.0000	2.627	2.642	2.657	2.667
1.1000			2.657	2.667

Y	RUN 122 STN. 1	500 PPM STN. 2	500 CC/MIN STN. 3	STN. 4
.0000	.000	.000	.000	.000
.0165	.920	.829	.934	.829
.0200	.891	.891	.970	.763
.0300	1.238	1.126	1.259	1.126
.0400	1.380	1.321	1.406	1.341
.0500	1.499	1.499	1.499	1.408
.1000	1.796	1.736	1.721	1.674
.2000	2.005	1.978	1.965	1.978
.3000	2.169	2.120	2.120	2.095
.4000	2.288	2.276	2.229	2.217
.5000	2.428	2.401	2.356	2.334
.6000	2.514	2.492	2.460	2.417
.7000	2.586	2.576	2.535	2.514
.8000	2.617	2.617	2.586	2.576
.9000	2.637	2.637	2.627	2.637
1.0000	2.647	2.637	2.667	2.667
1.1000	2.647		2.667	2.667

Y	RUN 123 STN. 1	500 PPM STN. 2	500 CC/MIN STN. 3	STN. 4
.0000	.000	.000	.000	.000
.0165	.829	.727	.829	.608
.0200	1.002	.829	.962	.690
.0300	1.280	1.150	1.259	.891
.0400	1.436	1.301	1.408	1.079
.0500	1.525	1.445	1.517	1.427
.1000	1.751	1.736	1.728	1.721
.2000	2.031	2.005	1.978	1.965
.3000	2.193	2.161	2.157	2.107
.4000	2.334	2.311	2.288	2.265
.5000	2.444	2.439	2.401	2.367
.6000	2.545	2.535	2.492	2.460
.7000	2.586	2.627	2.581	2.535
.8000	2.637	2.657	2.637	2.607
.9000	2.637	2.667	2.682	2.667
1.0000		2.667	2.686	2.696
1.1000			2.686	2.696

Y	RUN 131 STN. 1	500 PPM STN. 2	1000 CC/MIN STN. 3	STN. 4
.0000	.000	.000	.000	.000
.0165	.829	.763	1.054	.829
.0200	.920	.860	1.054	.860
.0300	1.126	1.150	1.217	1.150
.0400	1.301	1.280	1.389	1.399
.0500	1.436	1.490	1.481	1.445
.1000	1.658	1.721	1.721	1.658
.2000	1.938	1.951	1.938	1.910
.3000	2.120	2.107	2.095	2.095
.4000	2.265	2.276	2.229	2.217
.5000	2.401	2.390	2.367	2.322
.6000	2.492	2.492	2.450	2.439
.7000	2.555	2.576	2.535	2.514
.8000	2.607	2.637	2.607	2.576
.9000	2.617	2.637	2.647	2.637
1.0000	2.617		2.657	2.667
1.1000			2.657	2.667

Y	RUN 132 STN. 1	500 PPM STN. 2	1000 CC/MIN STN. 3	STN. 4
.0000	.000	.000	.000	.000
.0165	.727	.829	.727	.763
.0200	.763	.891	.690	.727
.0300	.829	1.079	1.259	1.150
.0400	1.280	1.321	1.408	1.360
.0500	1.380	1.427	1.463	1.389
.1000	1.650	1.728	1.721	1.658
.2000	1.965	1.965	1.924	1.924
.3000	2.132	2.132	2.107	2.095
.4000	2.276	2.276	2.217	2.217
.5000	2.428	2.417	2.345	2.345
.6000	2.503	2.462	2.450	2.428
.7000	2.596	2.566	2.524	2.503
.8000	2.617	2.627	2.586	2.586
.9000	2.627	2.637	2.647	2.647
1.0000	2.627	2.637	2.657	2.667
1.1000			2.657	2.667

Y	RUN 201 1000 PPM 250 CC/MIN STN. 1	STN. 2	STN. 3	STN. 4
.0000	.000	.000	.000	.000
.0165	.891	.727	.797	.727
.0200	.948	.763	.860	.650
.0300	1.280	1.103	1.120	1.079
.0400	1.389	1.321	1.280	1.238
.0500	1.481	1.463	1.465	1.341
.1000	1.690	1.736	1.721	1.642
.2000	1.934	1.965	1.936	1.938
.3000	2.107	2.145	2.082	2.095
.4000	2.253	2.265	2.229	2.206
.5000	2.390	2.379	2.345	2.311
.6000	2.439	2.471	2.428	2.412
.7000	2.524	2.545	2.492	2.471
.8000	2.566	2.576	2.576	2.545
.9000	2.607	2.596	2.617	2.591
1.0000	2.607	2.637	2.637	2.637
1.1000		2.637	2.657	2.647
1.2000			2.657	2.647
1.3000				
1.4000				

Y	RUN 202 1000 PPM 250 CC/MIN STN. 1	STN. 2	STN. 3	STN. 4
.0000	.000	.000	.000	.000
.0165	.891	.563	.690	.608
.0200	1.002	.514	.690	.282
.0300	1.280	.797	1.028	.860
.0400	1.427	1.079	1.217	1.126
.0500	1.481	1.408	1.351	1.321
.0750	1.601	1.551	1.517	1.472
.1000	1.705	1.721	1.736	1.634
.1500	1.811	1.868	1.840	1.766
.2000	1.938	1.978	1.938	1.924
.3000	2.120	2.132	2.107	2.044
.4000	2.241	2.253	2.311	2.181
.5000	2.345	2.390	2.334	2.299
.6000	2.460	2.482	2.412	2.367
.7000	2.514	2.555	2.492	2.460
.8000	2.596	2.586	2.576	2.535
.9000	2.607	2.607	2.617	2.607
1.0000	2.612	2.637	2.647	2.627
1.1000		2.637	2.647	2.667
1.2000				2.667

Y	RUN 211 1000 PPM 350 CC/MIN STN. 1	STN. 2	STN. 3	STN. 4
.0000	.000	.000	.000	.000
.0165	.752	.608	.701	.650
.0200	.891	.727	.745	.563
.0300	1.238	1.103	1.002	.948
.0400	1.360	1.280	1.238	1.172
.0500	1.481	1.399	1.427	1.321
.1000	1.791	1.690	1.656	1.682
.2000	1.991	1.951	1.938	1.910
.3000	2.132	2.157	2.120	2.069
.4000	2.276	2.276	2.247	2.193
.5000	2.401	2.367	2.345	2.322
.6000	2.492	2.471	2.450	2.417
.7000	2.555	2.555	2.514	2.482
.8000	2.596	2.586	2.576	2.545
.9000	2.617	2.627	2.622	2.607
1.0000	2.617	2.647	2.647	2.647
1.1000		2.647	2.667	2.657
1.2000			2.667	2.657

Y	RUN 212 1000 PPM 350 CC/MIN STN. 1	STN. 2	STN. 3	STN. 4
.0000	.000	.000	.000	.000
.0165	1.103	.398	.398	.364
.0200	1.217	.514	.430	.325
.0300	1.341	.860	.608	.539
.0400	1.436	1.103	.829	.650
.0500	1.525	1.280	1.079	.920
.1000	1.744	1.650	1.585	1.463
.2000	2.005	1.938	1.938	1.896
.3000	2.193	2.145	2.132	2.069
.4000	2.322	2.276	2.241	2.217
.5000	2.417	2.401	2.367	2.311
.6000	2.492	2.503	2.460	2.423
.7000	2.576	2.576	2.535	2.492
.8000	2.596	2.617	2.617	2.566
.9000	2.617	2.647	2.657	2.617
1.0000	2.617	2.647	2.686	2.667
1.1000			2.686	2.677
1.2000				2.677

Y	RUN 213 1000 PPM 3500 CC/MIN STN. 1	STN. 2	STN. 3	STN. 4
.0000	.000	.000	.000	.000
.0165	.563	.192	.430	.325
.0200	1.002	.460	.514	.563
.0300	1.217	.905	.650	.650
.0400	1.408	1.150	.920	.797
.0500	1.499	1.380	1.079	.976
.1000	1.759	1.698	1.568	1.551
.2000	2.005	1.971	1.951	1.882
.3000	2.157	2.132	2.107	2.069
.4000	2.334	2.288	2.241	2.217
.5000	2.412	2.395	2.367	2.334
.6000	2.514	2.514	2.460	2.417
.7000	2.576	2.576	2.535	2.514
.8000	2.617	2.617	2.607	2.596
.9000	2.627	2.647	2.657	2.627
1.0000	2.627	2.647	2.677	2.647
1.1000			2.677	2.686
1.2000				2.686

Y	RUN 214 1000 PPM 350 CC/MIN STN. 1	STN. 2	STN. 3	STN. 4
.0000	.000	.000	.000	.000
.0165	.514	.364	.364	.325
.0200	.860	.230	.650	.460
.0300	1.259	.797	.650	.650
.0400	1.389	1.054	.976	.891
.0500	1.481	1.301	1.103	1.028
.1000	1.759	1.705	1.560	1.601
.2000	2.018	1.978	1.910	1.917
.3000	2.193	2.145	2.120	2.095
.4000	2.334	2.322	2.241	2.235
.5000	2.428	2.417	2.356	2.334
.6000	2.535	2.524	2.466	2.450
.7000	2.596	2.596	2.545	2.514
.8000	2.627	2.647	2.607	2.576
.9000	2.627	2.657	2.657	2.627
1.0000		2.657	2.677	2.677
1.1000			2.677	2.686
1.2000				2.686

Y	RUN 215 1000 PPM 350 CC/MIN STN. 1	STN. 2	STN. 3	STN. 4
.0000	.000	.000	.000	.000
.0165	.514	-.364	-.398	.325
.0200	.727	.325	.230	.460
.0300	1.217	.891	.690	.650
.0400	1.321	1.172	1.002	.891
.0500	1.445	1.341	1.172	1.028
.1000	1.713	1.674	1.618	1.601
.2000	1.958	1.978	1.938	1.917
.3000	2.145	2.132	2.120	2.095
.4000	2.288	2.265	2.265	2.235
.5000	2.390	2.423	2.379	2.334
.6000	2.482	2.471	2.471	2.450
.7000	2.566	2.566	2.555	2.514
.8000	2.607	2.607	2.617	2.576
.9000	2.617	2.637	2.657	2.627
1.0000	2.622	2.647	2.677	2.677
1.1000		2.647	2.677	2.686
1.2000				2.686
1.3000				
1.4000				

Y	RUN 216 1000 PPM 350 CC/MIN STN. 1	STN. 2	STN. 3	STN. 4
.0000	.000	.000	.000	.000
.0165	.727	.514	.608	.163
.0200	.948	.563	.514	.230
.0300	1.259	.797	.920	.797
.0400	1.370	1.079	1.079	1.002
.0500	1.445	1.259	1.238	1.238
.0750	1.601	1.534	1.454	1.463
.1000	1.721	1.721	1.618	1.551
.1500	1.854	1.825	1.803	1.721
.2000	1.951	1.938	1.924	1.896
.3000	2.120	2.120	2.107	2.069
.4000	2.241	2.265	2.217	2.217
.5000	2.345	2.401	2.345	2.322
.6000	2.460	2.482	2.428	2.401
.7000	2.535	2.545	2.524	2.482
.8000	2.576	2.586	2.576	2.545
.9000	2.617	2.637	2.617	2.607
1.0000	2.617	2.642	2.647	2.637
1.1000		2.642	2.657	2.657
1.2000			2.647	2.657

Y	RUN 221 STN. 1	1000 PPM STN. 2	500 CC/MIN STN. 3	STN. 4
.0000	.000	.000	.000	.000
.0165	.529	.364	.709	.642
.0200	.763	.608	.650	.308
.0300	1.172	.891	.920	.763
.0400	1.360	1.150	1.054	.976
.0500	1.408	1.321	1.301	1.238
.1000	1.705	1.674	1.642	1.551
.2000	1.978	1.951	1.924	1.896
.3000	2.169	2.169	2.095	2.095
.4000	2.276	2.288	2.241	2.193
.5000	2.401	2.412	2.356	2.322
.6000	2.482	2.482	2.428	2.401
.7000	2.571	2.561	2.524	2.482
.8000	2.596	2.617	2.566	2.555
.9000	2.627	2.637	2.637	2.596
1.0000	2.627	2.647	2.652	2.647
1.1000		2.647	2.667	2.649
1.2000			2.667	2.649
1.3000				
1.4000				

Y	RUN 222 STN. 1	1000 PPM STN. 2	500 CC/MIN STN. 3	STN. 4
.0000	.000	.000	.000	.000
.0165	.398	-.364	.398	-.563
.0200	.797	-.230	.514	-.563
.0300	1.150	.608	.829	.514
.0400	1.301	.948	1.054	.948
.0500	1.427	1.150	1.217	1.103
.0750	1.568	1.461	1.499	1.311
.1000	1.674	1.601	1.658	1.534
.1500	1.854	1.811	1.811	1.690
.2000	1.965	1.951	1.910	1.854
.3000	2.120	2.145	2.120	2.095
.4000	2.276	2.265	2.241	2.206
.5000	2.379	2.379	2.345	2.322
.6000	2.471	2.482	2.428	2.401
.7000	2.545	2.555	2.514	2.492
.8000	2.586	2.607	2.566	2.535
.9000	2.607	2.637	2.627	2.607
1.0000	2.607	2.647	2.657	2.647
1.1000		2.647	2.657	2.657
1.2000				2.657

Y	RUN 231 STN. 1	1000 PPM STN. 2	1000 CC/MIN STN. 3	STN. 4
.0000	.000	.000	.000	.000
.0165	-.325	.163	.642	.192
.0200	.262	.230	.662	.192
.0300	.989	.763	.829	.727
.0400	1.138	1.150	1.054	1.054
.0500	1.351	1.259	1.259	1.172
.1000	1.642	1.634	1.585	1.517
.2000	1.951	1.924	1.882	1.825
.3000	2.120	2.151	2.095	2.031
.4000	2.276	2.294	2.217	2.193
.5000	2.401	2.390	2.356	2.299
.6000	2.503	2.487	2.439	2.417
.7000	2.576	2.566	2.514	2.492
.8000	2.617	2.627	2.576	2.566
.9000	2.647	2.642	2.637	2.627
1.0000	2.647	2.647	2.667	2.637
1.1000		2.647	2.667	2.647
1.2000				2.657
1.3000				
1.4000				

Y	RUN 232 STN. 1	1000 PPM STN. 2	1000CC/MIN STN. 3	STN. 4
.0000	.000	.000	.000	.000
.0165	-.876	-.642	.192	-.325
.0200	-.230	-.498	.230	-.690
.0300	.920	.262	.650	.262
.0400	1.150	.727	.860	.642
.0500	1.259	1.054	1.054	.948
.0750	1.463	1.399	1.341	1.150
.1000	1.642	1.534	1.481	1.351
.1500	1.825	1.781	1.766	1.593
.2000	1.965	1.910	1.868	1.751
.3000	2.107	2.120	2.057	2.031
.4000	2.253	2.241	2.206	2.169
.5000	2.390	2.367	2.322	2.288
.6000	2.482	2.492	2.428	2.390
.7000	2.555	2.555	2.514	2.482
.8000	2.586	2.607	2.586	2.566
.9000	2.617	2.647	2.637	2.622
1.0000	2.617	2.647	2.657	2.647
1.1000			2.667	2.667
1.2000			2.667	2.667

RUN 301 2000 PPM 250 CC/MIN

Y	STN. 1	STN. 2	STN. 3	STN. 4
.0000	.000	.000	.000	.000
.0165	.488	.364	.460	.460
.0200	.745	.398	.460	.514
.0300	1.041	.745	.608	.763
.0500	1.351	1.259	1.126	1.028
.1000	1.721	1.634	1.568	1.490
.2000	2.011	1.944	1.896	1.803
.3000	2.193	2.120	2.076	2.018
.4000	2.339	2.253	2.235	2.181
.5000	2.439	2.384	2.362	2.299
.6000	2.519	2.498	2.466	2.423
.7000	2.601	2.576	2.555	2.503
.8000	2.617	2.637	2.596	2.586
.9000	2.622	2.657	2.652	2.632
1.0000	2.622	2.657	2.672	2.667
1.1000			2.672	2.686
1.2000				2.686

RUN 302 2000 PPM 250 CC/MIN

Y	STN. 1	STN. 2	STN. 3	STN. 4
.0000	.000	.000	.000	.000
.0165	.430	.325	.364	.488
.0200	.745	.418	.488	.630
.0300	1.041	.780	.813	.745
.0500	1.370	1.228	1.206	1.238
.1000	1.721	1.642	1.517	1.534
.2000	1.991	1.951	1.882	1.840
.3000	2.163	2.114	2.082	2.057
.4000	2.282	2.270	2.229	2.193
.5000	2.417	2.395	2.339	2.317
.6000	2.519	2.503	2.450	2.428
.7000	2.576	2.566	2.535	2.524
.8000	2.622	2.622	2.601	2.571
.9000	2.632	2.652	2.642	2.642
1.0000	2.632	2.652	2.662	2.672
1.1000			2.662	2.682
1.2000				2.682

RUN 303 2000 PPM 250 CC/MIN

Y	STN. 1	STN. 2	STN. 3	STN. 4
.0000	.000	.000	.000	.000
.0165	.398	.325	.460	-.514
.0200	.539	.504	.514	-.325
.0300	1.041	.813	.670	.670
.0500	1.351	1.161	1.066	1.115
.1000	1.713	1.610	1.525	1.472
.2000	1.991	1.938	1.875	1.854
.3000	2.151	2.101	2.076	2.050
.4000	2.294	2.270	2.235	2.200
.5000	2.417	2.417	2.351	2.317
.6000	2.498	2.492	2.450	2.406
.7000	2.581	2.571	2.529	2.498
.8000	2.612	2.617	2.601	2.581
.9000	2.632	2.642	2.652	2.622
1.0000	2.632	2.652	2.662	2.662
1.1000		2.652	2.672	2.682
1.2000			2.672	2.686
1.3000				

RUN 304 2000 PPM 250 CC/MIN

Y	STN. 1	STN. 2	STN. 3	STN. 4
.0000	.000	.000	.000	.000
.0165	.608	.398	.398	-.364
.0200	.845	.573	.460	-.325
.0300	1.206	.905	.745	.670
.0400	1.351	1.091	1.028	1.041
.0500	1.463	1.184	1.138	1.184
.1000	1.736	1.634	1.601	1.560
.2000	2.024	1.944	1.910	1.825
.3000	2.187	2.101	2.089	2.031
.4000	2.328	2.276	2.211	2.187
.5000	2.428	2.406	2.339	2.317
.6000	2.529	2.498	2.450	2.439
.7000	2.571	2.576	2.540	2.508
.8000	2.612	2.622	2.601	2.591
.9000	2.622	2.642	2.642	2.622
1.0000	2.622	2.642	2.662	2.662
1.1000			2.662	2.672
1.2000				2.682

RUN 305 2000 PPM 250 CC/MIN

Y	STN. 1	STN. 2	STN. 3	STN. 4
.0000	.000	.000	.000	.000
.0165	.514	.230	.262	-.586
.0200	.891	.103	.103	-.586
.0300	1.206	.608	.563	.163
.0400	1.351	.948	.948	.745
.0500	1.445	1.331	1.172	1.066
.0750	1.634	1.542	1.465	1.311
.1000	1.736	1.642	1.601	1.463
.1500	1.910	1.796	1.796	1.751
.2000	2.005	1.978	1.924	1.868
.3000	2.169	2.132	2.082	2.082
.4000	2.282	2.276	2.206	2.217
.5000	2.395	2.412	2.322	2.311
.6000	2.482	2.514	2.417	2.390
.7000	2.545	2.576	2.492	2.482
.8000	2.596	2.607	2.576	2.586
.9000	2.607	2.647	2.607	2.617
1.0000	2.627	2.647	2.637	2.657
1.1000	2.627		2.667	2.677
1.2000			2.667	2.677

RUN 311 2000 PPM 350 CC/MIN

Y	STN. 1	STN. 2	STN. 3	STN. 4
.0000	.000	.000	.000	.000
.0165	.582	-.797	-.563	.241
.0200	.709	-.763	-.563	.325
.0300	1.041	.460	.282	.690
.0500	1.351	1.079	.962	1.028
.1000	1.713	1.593	1.399	1.490
.2000	1.991	1.917	1.889	1.818
.3000	2.175	2.082	2.076	2.031
.4000	2.305	2.276	2.247	2.193
.5000	2.433	2.412	2.362	2.345
.6000	2.519	2.503	2.466	2.433
.7000	2.581	2.596	2.545	2.514
.8000	2.627	2.627	2.617	2.576
.9000	2.627	2.637	2.657	2.637
1.0000		2.637	2.677	2.677
1.1000			2.677	2.677
1.2000				
1.3000				
1.4000				
1.5000				

RUN 312 2000 PPM 350 CC/MIN

Y	STN. 1	STN. 2	STN. 3	STN. 4
.0000	.000	.000	.000	.000
.0165	.325	.325	.325	.460
.0200	.514	.325	.430	.488
.0300	.989	.745	.709	.745
.0500	1.331	1.091	1.091	.962
.1000	1.705	1.610	1.499	1.445
.2000	1.991	1.951	1.882	1.825
.3000	2.163	2.145	2.095	2.018
.4000	2.294	2.282	2.229	2.163
.5000	2.428	2.406	2.350	2.305
.6000	2.540	2.514	2.450	2.428
.7000	2.581	2.591	2.555	2.508
.8000	2.617	2.642	2.622	2.581
.9000	2.622	2.657	2.652	2.642
1.0000	2.632	2.657	2.662	2.662
1.1000			2.667	2.677
1.2000				2.677
1.3000				

RUN 313 2000 PPM 350 CC/MIN

Y	STN. 1	STN. 2	STN. 3	STN. 4
.0000	.000	.000	.000	.000
.0165	-.230	-.650	.262	-.514
.0200	.325	-.539	.364	-.514
.0300	.962	.488	.488	.514
.0400	1.161	.934	.727	.845
.0500	1.311	1.161	.989	1.015
.1000	1.698	1.542	1.436	1.436
.2000	2.005	1.869	1.882	1.796
.3000	2.175	2.114	2.076	2.024
.4000	2.305	2.270	2.211	2.200
.5000	2.428	2.364	2.362	2.317
.6000	2.508	2.492	2.460	2.428
.7000	2.591	2.571	2.540	2.519
.8000	2.622	2.612	2.612	2.591
.9000	2.622	2.652	2.657	2.632
1.0000		2.652	2.662	2.662
1.1000			2.672	2.672
1.2000			2.667	2.672

Y	RUN 314 STN. 1	2000 PPM STN. 2	350 CC/MIN STN. 3	STN. 4
.0000	.000	.000	.000	.000
.0165	.514	-.763	-.539	-.488
.0200	.876	-.780	-.488	.163
.0300	1.161	.563	.539	.586
.0400	1.351	.962	.763	.920
.0500	1.463	1.184	.988	1.079
.1000	1.766	1.593	1.417	1.499
.2000	2.037	1.944	1.790	1.796
.3000	2.200	2.114	2.037	2.018
.4000	2.351	2.282	2.211	2.206
.5000	2.439	2.406	2.339	2.322
.6000	2.540	2.508	2.450	2.406
.7000	2.591	2.591	2.550	2.514
.8000	2.622	2.622	2.607	2.586
.9000	2.627	2.647	2.632	2.642
1.0000	2.627	2.647	2.642	2.667
1.1000			2.662	2.677
1.2000			2.662	2.677
1.3000				
1.4000				

Y	RUN 315 STN. 1	2000 PPM STN. 2	350 CC/MIN STN. 3	STN. 4
.0000	.000	.000	.000	.000
.0165	.488	-.325	-.563	-.608
.0200	.891	.398	-.563	-.727
.0300	1.195	1.002	.398	.230
.0400	1.341	1.217	.860	.608
.0500	1.417	1.351	1.079	1.015
.0750	1.610	1.568	1.408	1.291
.1000	1.728	1.642	1.601	1.463
.1500	1.889	1.811	1.766	1.713
.2000	2.011	1.951	1.896	1.903
.3000	2.163	2.169	2.069	2.082
.4000	2.299	2.288	2.217	2.206
.5000	2.423	2.401	2.334	2.322
.6000	2.487	2.492	2.428	2.406
.7000	2.571	2.566	2.503	2.492
.8000	2.601	2.637	2.555	2.555
.9000	2.622	2.647	2.607	2.617
1.0000	2.622	2.647	2.647	2.657
1.1000			2.662	2.667
1.2000			2.662	2.667

Y	RUN 321 STN. 1	2000 PPM STN. 2	500 CC/MIN STN. 3	STN. 4
.0000	.000	.000	.000	.000
.0165	.230	-.586	-.727	-.727
.0200	.650	-.539	-.676	-.586
.0300	1.150	.364	.230	.230
.0400	1.280	.670	.709	.709
.0500	1.427	.690	.905	1.066
.1000	1.728	1.517	1.472	1.399
.2000	2.018	1.931	1.889	1.818
.3000	2.193	2.101	2.089	2.089
.4000	2.334	2.270	2.223	2.223
.5000	2.455	2.384	2.376	2.339
.6000	2.535	2.498	2.460	2.450
.7000	2.596	2.601	2.540	2.529
.8000	2.617	2.632	2.601	2.581
.9000	2.617	2.652	2.652	2.632
1.0000		2.652	2.662	2.662
1.1000			2.662	2.682
1.2000				2.682

Y	RUN 322 STN. 1	2000 PPM STN. 2	500 CC/MIN STN. 3	STN. 4
.0000	.000	.000	.000	.000
.0165	-.325	-.763	-.797	-.780
.0200	.325	-.650	-.650	-.727
.0300	1.015	.398	-.163	-.460
.0400	1.217	.891	.563	.608
.0500	1.360	1.015	.727	1.079
.1000	1.690	1.585	1.408	1.534
.2000	1.991	1.924	1.868	1.854
.3000	2.145	2.107	2.057	2.018
.4000	2.311	2.276	2.229	2.175
.5000	2.423	2.401	2.334	2.322
.6000	2.503	2.540	2.444	2.412
.7000	2.576	2.576	2.535	2.514
.8000	2.607	2.627	2.596	2.566
.9000	2.607	2.647	2.622	2.627
1.0000		2.647	2.667	2.667
1.1000			2.667	2.677
1.2000				2.677

Y	RUN 323 STN. 1	2000 PPM STN. 2	500 CC/MIN STN. 3	STN. 4
.0000	.000	.000	.000	.000
.0165	.163	-.650	-.514	-.460
.0200	.650	-.563	-.398	-.230
.0300	1.054	.650	.430	.709
.0400	1.195	.934	.829	.948
.0500	1.321	1.161	.891	1.103
.1000	1.642	1.642	1.517	1.481
.2000	1.965	1.896	1.854	1.825
.3000	2.169	2.120	2.082	2.044
.4000	2.322	2.299	2.229	2.217
.5000	2.439	2.412	2.345	2.345
.6000	2.535	2.498	2.439	2.428
.7000	2.586	2.561	2.535	2.514
.8000	2.596	2.617	2.617	2.596
.9000	2.622	2.637	2.647	2.637
1.0000	2.622	2.642	2.647	2.677
1.1000		2.642		2.677
1.2000				
1.3000				

Y	RUN 324 STN. 1	2000 PPM STN. 2	500 CC/MIN STN. 3	STN. 4
.0000	.000	.000	.000	.000
.0165	.364	-.727	-.690	-.563
.0200	.860	-.514	-.608	-.763
.0300	1.126	.829	-.163	-.514
.0400	1.360	1.079	.727	.488
.0500	1.436	1.217	1.028	.745
.0750	1.593	1.389	1.301	1.126
.1000	1.713	1.585	1.534	1.463
.1500	1.917	1.751	1.721	1.698
.2000	2.024	1.924	1.896	1.840
.3000	2.175	2.120	2.057	2.095
.4000	2.299	2.265	2.206	2.206
.5000	2.423	2.417	2.345	2.345
.6000	2.519	2.503	2.417	2.428
.7000	2.581	2.576	2.514	2.492
.8000	2.612	2.607	2.576	2.576
.9000	2.622	2.647	2.627	2.637
1.0000	2.622	2.647	2.657	2.667
1.1000			2.657	2.667

Y	RUN 331 STN. 1	2000 PPM STN. 2	1000 CC/MIN STN. 3	STN. 4
.0000	.000	.000	.000	.000
.0165	-.488	-.813	-.934	-.860
.0200	-.325	-.745	-.845	-.797
.0300	.797	-.539	-.488	-.460
.0400	1.054	.488	.460	.539
.0500	1.206	.876	.670	.727
.1000	1.634	1.436	1.331	1.079
.2000	1.991	1.903	1.811	1.698
.3000	2.181	2.089	2.037	2.044
.4000	2.334	2.294	2.187	2.181
.5000	2.455	2.423	2.320	2.345
.6000	2.535	2.519	2.444	2.444
.7000	2.586	2.581	2.540	2.535
.8000	2.607	2.642	2.591	2.596
.9000	2.607	2.642	2.662	2.657
1.0000			2.662	2.677
1.1000				2.677

Y	RUN 332 STN. 1	2000 PPM STN. 2	1000 CC/MIN STN. 3	STN. 4
.0000	.000	.000	.000	.000
.0165	-.364	-.829	-.845	-.860
.0200	-.460	-.727	-.797	-.763
.0300	.398	-.460	-.460	-.563
.0400	.690	.460	.398	.325
.0500	1.015	.860	.563	.563
.1000	1.389	1.481	1.321	1.280
.2000	1.991	1.882	1.751	1.728
.3000	2.169	2.095	2.005	2.024
.4000	2.299	2.229	2.193	2.169
.5000	2.428	2.406	2.345	2.265
.6000	2.514	2.524	2.455	2.401
.7000	2.535	2.576	2.492	2.492
.8000	2.561	2.627	2.601	2.586
.9000	2.576	2.657	2.647	2.657
1.0000	2.576	2.657	2.662	2.677
1.1000			2.662	2.677

Y	RUN 333 STN. 1	2000 PPM STN. 2	1000 CC/MIN STN. 3	STN. 4
.0000	.000	.000	.000	.000
.0165	.163	-.727	-.876	-.650
.0200	.341	-.650	-.845	-.325
.0300	.650	-.325	-.563	.488
.0400	.797	.690	.325	.727
.0500	1.028	.829	.650	.962
.1000	1.534	1.517	1.351	1.389
.2000	1.978	1.854	1.825	1.736
.3000	2.157	2.069	2.057	1.965
.4000	2.311	2.265	2.206	2.157
.5000	2.439	2.390	2.334	2.322
.6000	2.555	2.514	2.428	2.439
.7000	2.607	2.586	2.535	2.535
.8000	2.617	2.627	2.607	2.607
.9000	2.617	2.637	2.647	2.657
1.0000		2.647	2.647	2.677
1.1000		2.647		2.677
1.2000				
1.3000				

Y	RUN 334 STN. 1	2000 PPM STN. 2	1000CC/MIN STN. 3	STN. 4
.0000	.000	.000	.000	.000
.0165	-.876	-.563	-.563	-.670
.0200	.282	-.325	-.460	-.920
.0300	.691	.690	.448	-.860
.0400	1.150	1.150	.727	-.398
.0500	1.280	1.301	1.079	.460
.0750	1.490	1.445	1.380	.934
.1000	1.626	1.674	1.534	1.270
.1500	1.861	1.825	1.705	1.568
.2000	1.998	1.938	1.896	1.796
.3000	2.181	2.132	2.069	1.991
.4000	2.299	2.299	2.229	2.163
.5000	2.401	2.412	2.345	2.305
.6000	2.487	2.514	2.450	2.417
.7000	2.561	2.566	2.524	2.503
.8000	2.601	2.637	2.586	2.586
.9000	2.612	2.667	2.657	2.637
1.0000	2.612	2.667	2.657	2.667
1.1000				2.667

APPENDIX B

EXPERIMENTAL CONCENTRATION DATA

Appendix B lists the experimental concentration data. Concentrations listed are the ratio of local concentration divided by .001 times the injected concentration (1000 C/C_i). Injection rates are given in cc/min (CCM). The vertical distance from the test plate, y, is in inches. Values listed for y = .000 are not experimental quantities but result from extrapolation. Stations 1, 2, 3 and 4 correspond to 48.0, 54.0, 60.0 and 66.0 inches from the channel inlet, respectively.

FLUID INJECTED--WATER

	STATION 1				STATION 2			
Y	250 CCM	350 CCM	500 CCM	1000 CCM	250 CCM	350 CCM	500 CCM	1000 CCM
.0000	14.50	22.00	37.00	55.00	3.50	6.80	11.80	18.80
.0165	12.80	16.90	30.60	43.80	3.00	6.50	11.30	17.70
.0200	12.00	17.60	29.70	44.00	3.50	6.80	11.20	18.30
.0300	9.80	15.00	24.80	39.60	3.40	6.70	11.00	17.00
.0400	8.35	13.60	21.20	35.10	3.50	6.60	10.80	17.00
.0500	7.40	12.70	22.50	32.40	3.50	6.60	10.60	16.20
.0750	6.00	8.60	16.90	26.10	3.50	6.20	10.00	16.00
.1000	4.00	6.90	12.30	17.10	3.10	5.90	9.80	15.00
.1500	2.20	3.20	5.60	8.90	2.50	5.20	8.40	12.80
.2000	.87	1.30	3.50	3.20	2.20	4.60	6.90	10.90
.2500	.22	.28	.98	1.20	1.47	3.40	5.40	8.40
.3000					1.20	2.50	4.30	6.60
.3500					.82	1.75	2.90	5.40
.4000					.33	1.47	2.20	3.36

	STATION 3				STATION 4			
Y	250 CCM	350 CCM	500 CCM	1000 CCM	250 CCM	350 CCM	500 CCM	1000 CCM
.0000	2.20	4.40	6.60	10.50	1.50	3.10	5.00	8.40
.0165	2.15	4.30	6.50	10.20	1.50	3.00	5.00	8.20
.0200	2.12	4.20	6.50	10.00	1.50	3.00	4.90	8.20
.0300	2.10	4.20	6.40	10.00	1.50	3.00	4.90	8.10
.0400	2.10	4.10	6.40	10.00	1.48	2.90	4.90	8.00
.0500	2.00	4.00	6.20	9.90	1.45	2.90	4.80	7.90
.0750	2.00	3.90	6.20	9.60	1.42	2.80	4.70	7.60
.1000	1.90	3.80	5.90	9.40	1.40	2.70	4.60	7.40
.1500	1.75	3.50	5.60	8.80	1.35	2.60	4.40	7.10
.2000	1.60	3.20	5.20	8.10	1.30	2.40	4.30	6.70
.2500	1.50	2.80	4.60	7.30	1.20	2.30	4.00	6.40
.3000	1.30	2.50	4.00	6.40	1.10	2.10	3.70	5.80
.3500	1.20	2.10	3.40	5.40	1.00	1.90	3.30	5.20
.4000	1.00	1.80	2.80	4.40	.93	1.70	2.90	4.50
.5000	.76	1.20	1.80	2.70	.69	1.25	2.10	3.10
.6000	.53	.80	1.20	1.60	.50	.78	1.20	1.80

FLUID INJECTED--WATER

	STATION 1				STATION 2			
Y	250 CCM	350 CCM	500 CCM	1000 CCM	250 CCM	350 CCM	500 CCM	1000 CCM
.0000	15.50	25.00	37.00	68.00	3.40	6.10	10.20	18.00
.0165	10.90	21.40	32.00	56.40	3.22	6.00	10.00	17.90
.0200	11.70	20.60	30.40	56.40	3.34	6.00	10.20	16.90
.0300	10.90	17.60	28.80	49.80	3.06	5.70	9.60	15.80
.0400	9.80	16.00	24.80	45.50	3.06	5.80	9.30	16.00
.0500	9.00	14.50	22.20	40.70	3.10	5.70	9.00	13.40
.0750	6.40	11.00	16.80	31.10	3.22	5.40	8.80	15.50
.1000	4.80	8.30	12.70	22.80	3.06	5.10	8.00	14.30
.1500	2.16	3.80	5.80	11.20	2.74	4.20	6.70	12.70
.2000	.78	1.28	2.40	4.50	2.02	3.50	5.40	10.60
.2500	.20	.48	.90	1.36	1.66	2.80	4.40	8.80
.3000					1.16	2.20	3.10	6.90
.3500					.78	1.60	2.50	5.60
.4000					.31	1.04	1.60	3.75

FLUID INJECTED--PEO, CI= 500 PPM

	STATION 1				STATION 2			
Y	250 CCM	350 CCM	500 CCM	1000 CCM	250 CCM	350 CCM	500 CCM	1000 CCM
.0000	40.00	66.00	90.00	140.00	15.00	22.50	33.00	56.00
.0165	27.00	40.00	60.00	100.00	12.30	18.90	27.90	40.00
.0200	24.30	37.40	52.00	93.00	11.30	19.80	26.10	41.60
.0300	19.20	28.40	42.00	75.60	11.40	17.10	23.10	36.40
.0400	14.20	21.20	30.80	55.80	9.80	14.50	21.00	33.60
.0500	11.00	14.80	23.60	45.00	8.70	13.40	19.20	29.30
.0750	7.80	9.10	13.80	30.90	6.80	10.80	14.40	24.60
.1000	4.85	5.70	8.90	18.60	5.30	8.00	11.70	21.30
.1500	1.35	2.00	3.60	7.10	4.05	5.65	7.90	14.50
.2000	.47	.76	1.30	2.90	2.70	3.59	5.15	10.00
.2500					1.80	2.60	3.40	6.40
.3000					1.25	1.70	2.40	4.50
.3500					.84	1.10	1.50	2.90
.4000					.57	.84	.97	2.05
.5000					.27	.32	.45	.89

	STATION 3				STATION 4			
Y	250 CCM	350 CCM	500 CCM	1000 CCM	250 CCM	350 CCM	500 CCM	1000 CCM
.0000	7.20	12.00	15.00	24.00	2.50	3.90	5.70	9.60
.0165	6.49	10.00	13.70	20.85	2.49	3.90	5.50	9.50
.0200	6.30	10.00	13.00	19.35	2.50	3.95	5.65	9.50
.0300	5.40	9.35	12.60	18.30	2.49	3.90	5.55	9.50
.0400	5.30	8.35	11.70	18.00	2.35	3.90	5.55	9.00
.0500	5.00	7.60	11.40	17.50	2.35	3.85	5.40	9.10
.0750	4.70	7.00	10.00	16.60	2.25	3.85	5.20	9.00
.1000	4.30	6.55	9.00	15.00	2.35	3.85	5.10	8.80
.1500	3.80	5.65	7.80	13.00	2.28	3.70	4.80	8.30
.2000	3.10	4.70	6.45	10.70	2.10	3.30	4.40	8.10
.2500	2.65	3.75	5.00	9.00	1.90	3.10	4.00	7.50
.3000	2.15	2.80	4.20	7.60	1.70	2.60	3.80	6.80
.3500	1.60	2.20	3.30	6.00	1.50	2.40	3.20	6.00
.4000	1.23	1.70	2.65	4.60	1.35	2.15	2.69	5.20
.5000	.69	.90	1.55	2.75	1.00	1.53	1.97	3.70
.6000	.37	.46	.71	1.25	.60	.96	1.29	2.29

FLUID INJECTED--PEO, CI=1000 PPM

	STATION 1				STATION 2			
Y	250 CCM	350 CCM	500 CCM	1000 CCM	250 CCM	350 CCM	500 CCM	1000 CCM
.0000	76.00	115.00	200.00	250.00	27.50	46.00	66.00	115.00
.0165	48.50	68.50	184.00	152.20	20.00	35.00	51.50	76.00
.0200	39.50	65.00	121.00	149.60	18.20	33.00	48.30	57.50
.0300	30.50	42.75	106.20	126.50	15.00	24.80	42.00	68.00
.0400	17.25	30.00	74.25	100.10	13.00	20.10	33.30	63.00
.0500	13.50	21.75	35.50	62.00	10.60	19.20	30.90	39.50
.0750	8.60	11.50	20.75	39.50	7.90	11.80	21.00	32.10
.1000	4.85	6.10	11.30	22.50	6.30	8.35	14.70	20.00
.1500	1.35	1.90	3.75	6.00	3.80	5.25	8.90	12.50
.2000	.30	.61	3.65	1.80	2.39	3.15	5.10	8.00
.2500					1.43	2.00	3.40	5.00
.3000					.85	1.17	1.95	3.30

	STATION 3				STATION 4			
Y	250 CCM	350 CCM	500 CCM	1000 CCM	250 CCM	350 CCM	500 CCM	1000 CCM
.0000	16.40	29.00	36.00	60.00	6.20	10.20	12.00	17.00
.0165	14.70	24.30	30.50	45.50	5.80	9.15	10.55	14.75
.0200	13.30	23.10	28.80	48.00	5.70	9.30	10.20	15.00
.0300	11.30	19.50	25.20	40.00	5.65	8.40	10.00	14.75
.0400	10.50	16.05	21.00	42.00	5.30	8.10	9.90	13.50
.0500	9.40	15.30	20.70	33.50	5.00	7.40	9.30	12.90
.0750	7.70	12.30	16.60	25.80	4.45	6.70	8.40	12.60
.1000	6.30	10.30	13.20	22.50	4.35	6.00	8.00	11.40
.1500	4.95	7.25	9.40	16.00	3.95	5.00	7.60	10.80
.2000	3.95	5.35	6.90	12.00	3.40	4.10	6.30	9.60
.2500	2.70	3.90	5.00	8.90	3.05	3.70	5.70	9.00
.3000	2.15	2.89	3.85	6.30	2.50	3.25	4.80	7.60
.3500	1.60	2.00	2.70	5.00	2.10	2.70	4.00	6.60
.4000	1.17	1.47	1.95	3.30	1.70	2.21	3.30	5.50
.5000	.65	.80	.94	1.60	1.13	1.53	2.20	3.70
.6000					.62	1.00	1.30	2.30

FLUID INJECTED--PEO, CI=2000 PPM

	STATION 1				STATION 2			
Y	250 CCM	350 CCM	500 CCM	1000 CCM	250 CCM	350 CCM	500 CCM	1000 CCM
.0000	33.00	37.00	180.00	400.00	20.00	32.00	160.00	400.00
.0165	9.40	16.20	82.40	200.00	14.20	19.20	81.60	164.00
.0200	13.20	16.40	140.80	171.00	13.20	20.80	138.00	166.50
.0300	7.90	15.40	70.40	117.00	12.00	17.20	70.40	117.00
.0400	5.20	11.20	22.40	77.40	9.30	13.20	22.60	77.00
.0500	4.80	8.80	13.50	51.30	8.00	12.00	13.80	51.30
.0750	3.90	5.00	6.20	26.80	6.40	9.10	6.10	27.30
.1000	2.40	2.90	3.30	15.30	4.40	6.20	3.40	15.50
.1500	.78	.90	1.28	3.30	3.00	3.60	1.30	3.40
.2000					1.52	2.00	.38	.80

	STATION 3				STATION 4			
Y	250 CCM	350 CCM	500 CCM	1000 CCM	250 CCM	350 CCM	500 CCM	1000 CCM
.0000	11.50	18.00	58.00	105.00	4.50	8.50	38.00	62.00
.0165	8.60	13.20	39.90	74.00	3.70	6.00	29.40	45.00
.0200	9.00	14.00	36.00	80.00	4.00	6.60	27.00	49.50
.0300	8.60	12.40	25.50	66.50	3.80	6.60	20.90	42.00
.0400	7.30	10.60	20.90	52.50	3.50	5.80	17.70	36.50
.0500	6.90	9.60	17.70	39.00	3.40	5.50	14.70	31.80
.0750	5.50	8.20	12.00	28.40	3.20	5.00	10.70	23.40
.1000	5.00	6.60	10.00	19.60	2.80	4.40	8.00	17.00
.1500	3.20	4.40	6.10	12.00	2.20	3.70	5.50	11.80
.2000	2.30	3.60	4.10	8.20	1.90	3.00	4.20	7.30
.2500	1.60	2.50	2.90	5.00	1.60	2.50	3.10	5.30
.3000	1.12	1.64	1.90	4.00	1.20	2.10	2.50	4.10
.3500	.80	1.20	1.40	3.00	1.00	1.60	1.60	3.20

FLUID INJECTED--PEO, CI=2000 PPM

	STATION 1				STATION 2			
Y	250 CCM	350 CCM	500 CCM	1000 CCM	250 CCM	350 CCM	500 CCM	1000 CC
.0000	22.00	58.00	180.00	400.00	16.00	26.00	160.00	400.00
.0165	12.60	22.20	82.40	200.00	11.10	16.40	81.60	164.00
.0200	10.50	31.60	140.80	171.00	11.10	16.80	138.00	166.50
.0300	15.20	21.60	70.40	117.00	9.40	15.60	70.40	117.00
.0400	9.20	16.80	22.40	77.40	8.00	11.60	22.60	77.00
.0500	5.80	11.60	13.50	51.30	7.50	10.40	13.80	51.30
.0750	4.60	7.10	6.20	26.80	5.20	7.20	6.10	27.30
.1000	2.80	4.30	3.30	15.30	3.80	5.00	3.40	15.50
.1500	.86	1.06	1.28	3.30	2.30	2.30	1.30	3.40
.2000					1.40	2.00	.38	.80

	STATION 3				STATION 4			
Y	250 CCM	350 CCM	500 CCM	1000 CCM	250 CCM	350 CCM	500 CCM	1000 CC
.0000	10.50	21.00	29.00	48.00	5.40	9.50	32.00	38.00
.0165	7.60	17.70	18.00	37.20	4.30	8.00	18.60	30.00
.0200	9.60	15.60	18.40	32.10	5.00	7.70	18.30	30.00
.0300	8.60	14.20	15.40	29.40	4.40	7.40	17.80	27.00
.0400	7.00	13.20	13.00	25.80	4.20	6.40	17.00	25.20
.0500	7.40	12.00	12.40	22.20	4.10	5.80	15.00	25.00
.0750	5.50	8.90	8.40	16.80	3.70	5.20	11.20	20.00
.1000	4.60	7.40	6.70	15.40	3.60	4.60	9.20	16.00
.1500	3.30	5.00	4.90	10.00	2.70	3.90	7.20	12.80
.2000	2.20	3.40	3.00	8.00	2.30	3.40	5.30	10.70
.2500	1.60	2.60	2.30	5.20	1.90	2.70	4.60	8.00
.3000	1.10	1.80	1.72	3.60	1.60	2.00	3.40	6.50
.3500	.80	1.10	1.15	2.80	1.10	1.60	2.80	4.20

APPENDIX C

RESULTS

This appendix contains the results of calculations performed on both concentration and velocity data.

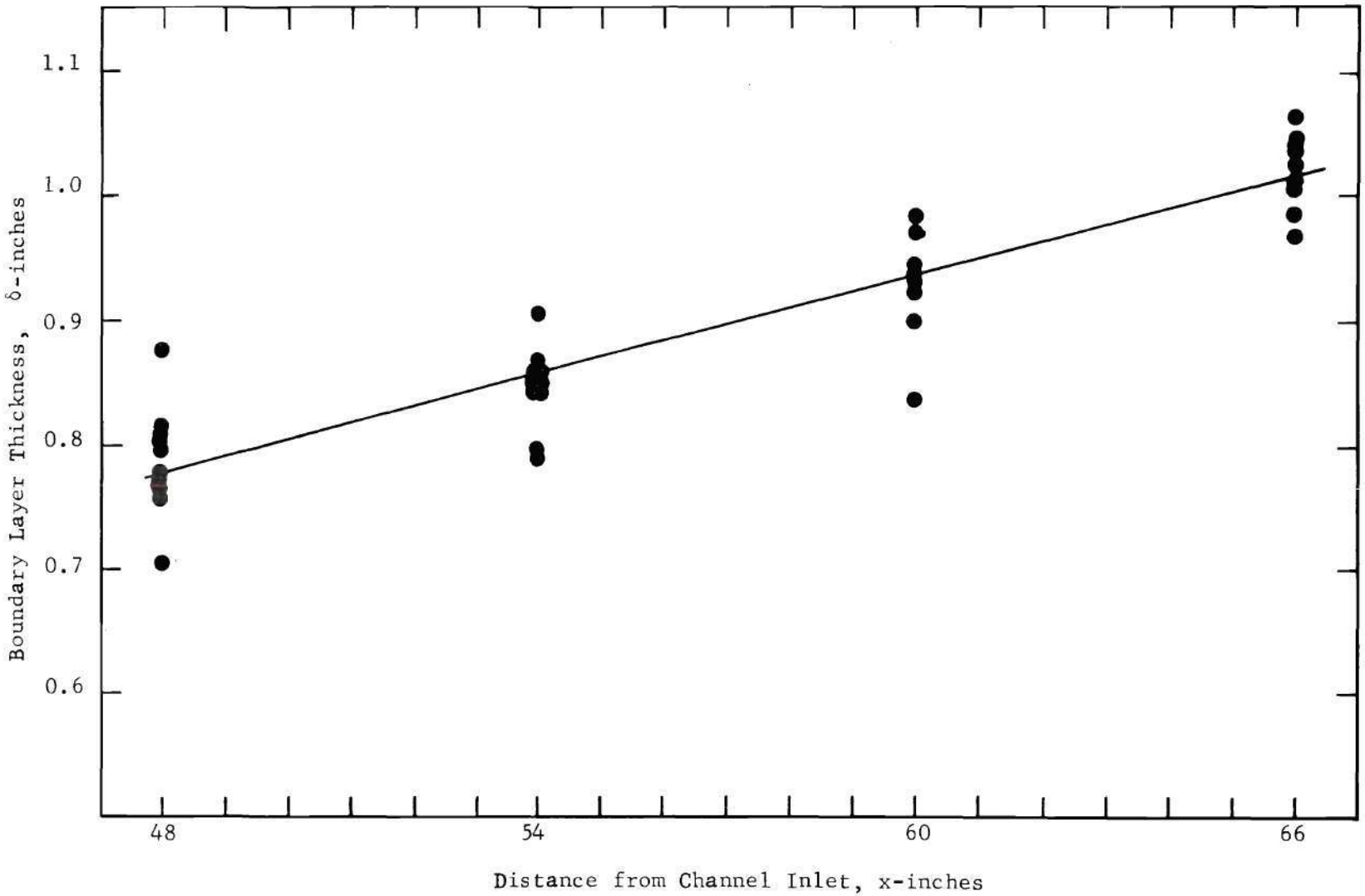

Figure 4. Boundary Layer Thickness, No Polymer Injection

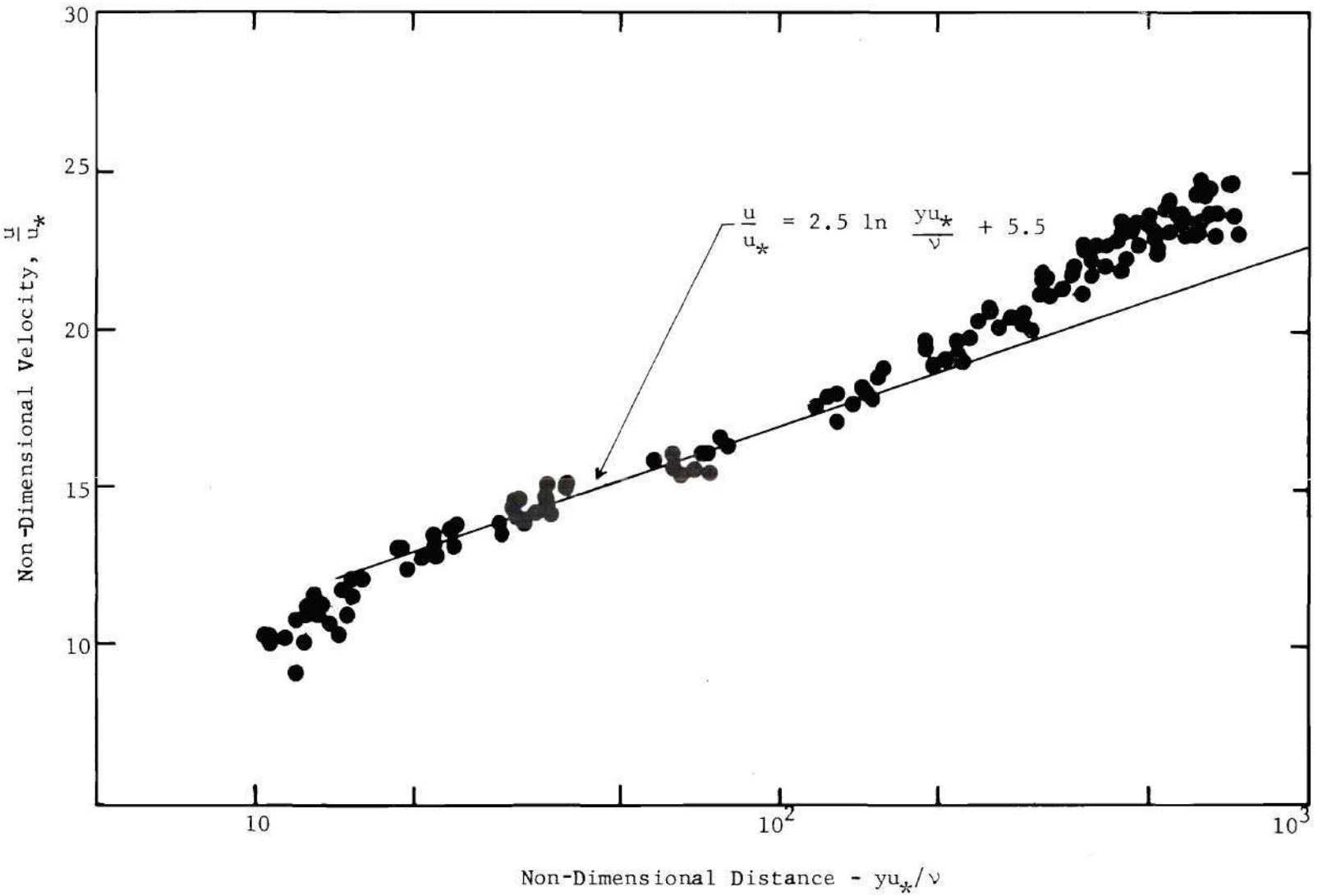

Figure 5. Non-Dimensional Velocity Profile; Station 1, No Polymer Injection

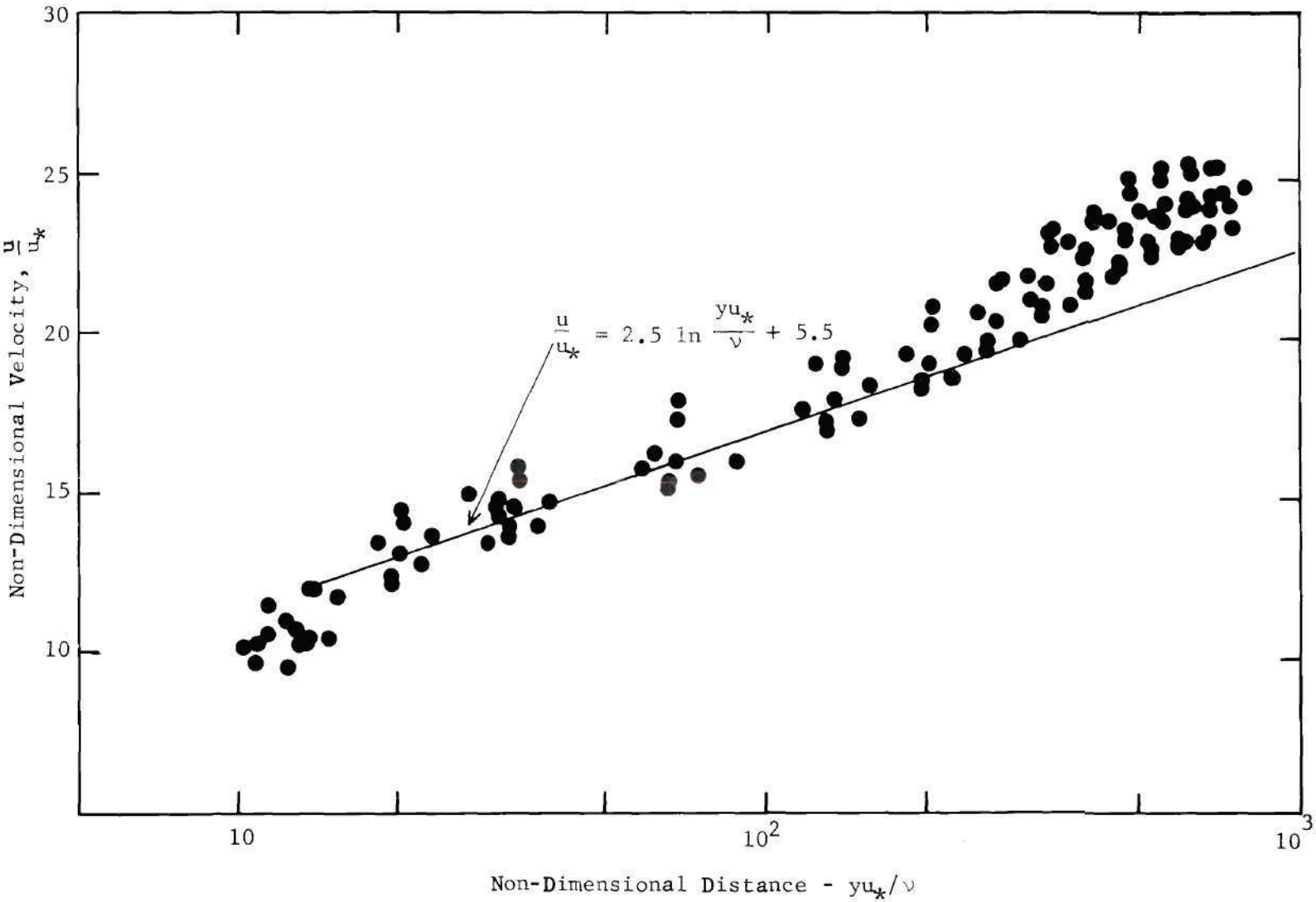

Figure 6. Non-Dimensional Velocity Profile, Station 2, No Polymer Injection

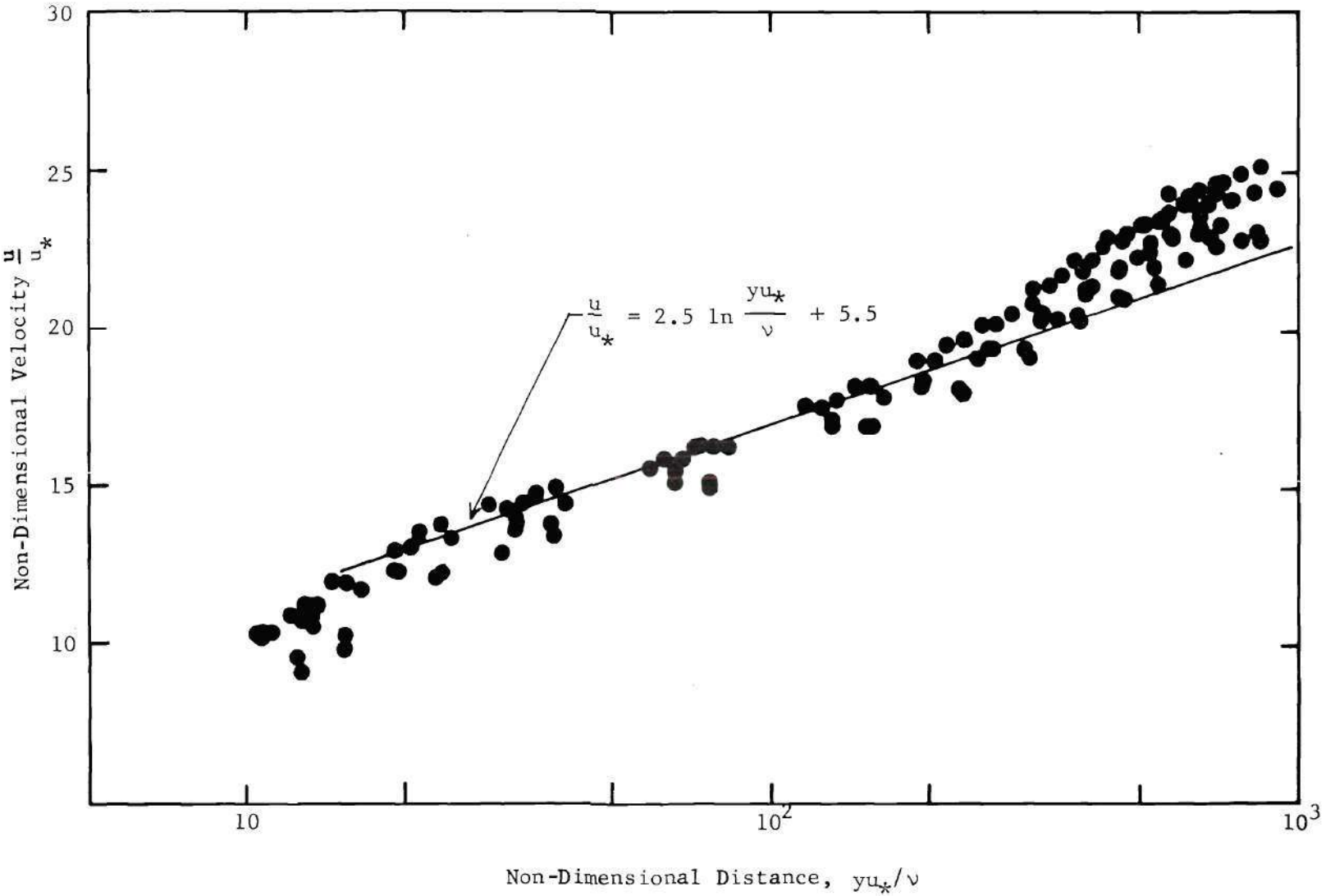

Figure 7. Non-Dimensional Velocity Profile, Station 3, No Polymer Injection

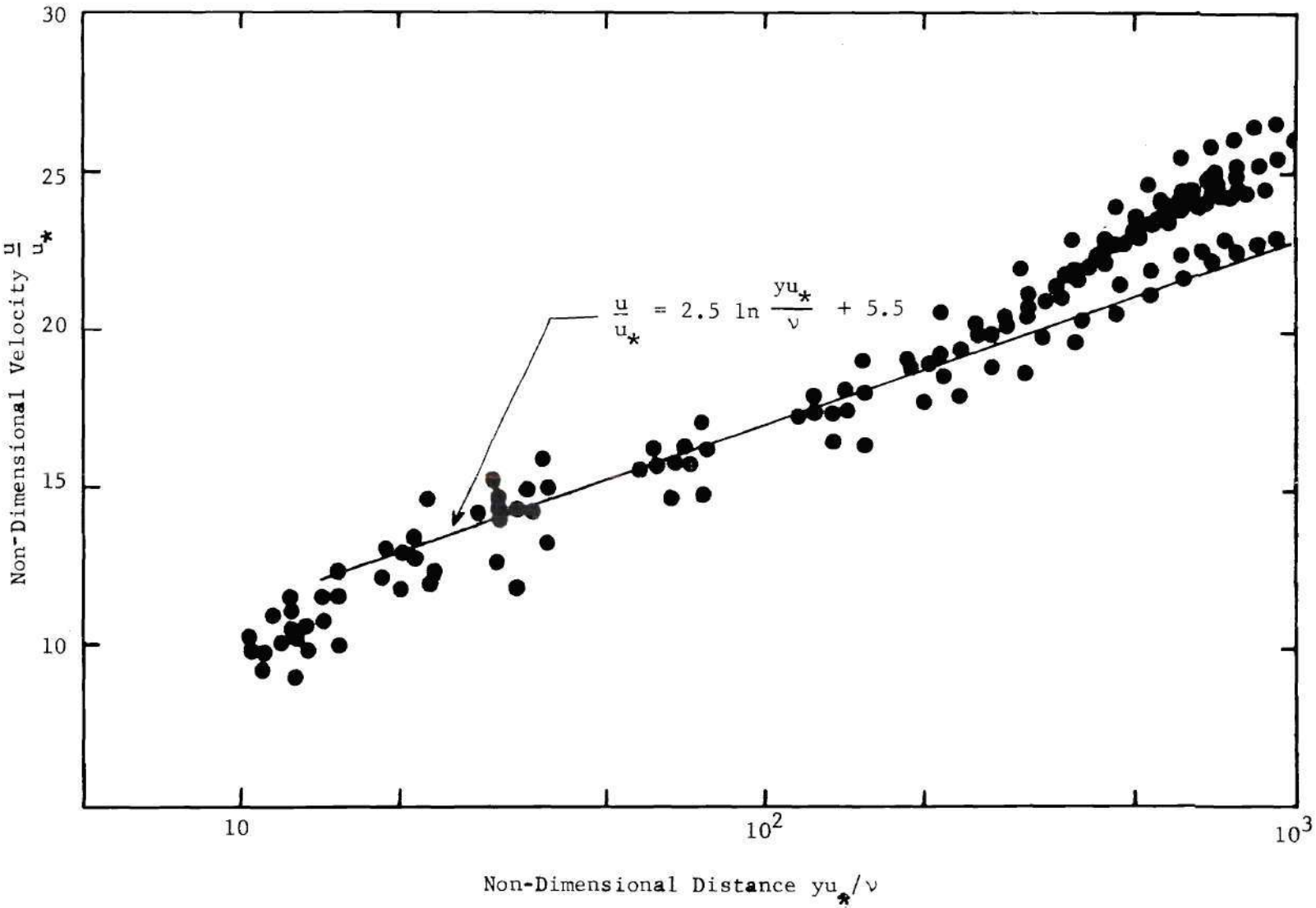

Figure 8. Non-Dimensional Velocity Profile, Station 4, No Polymer Injection

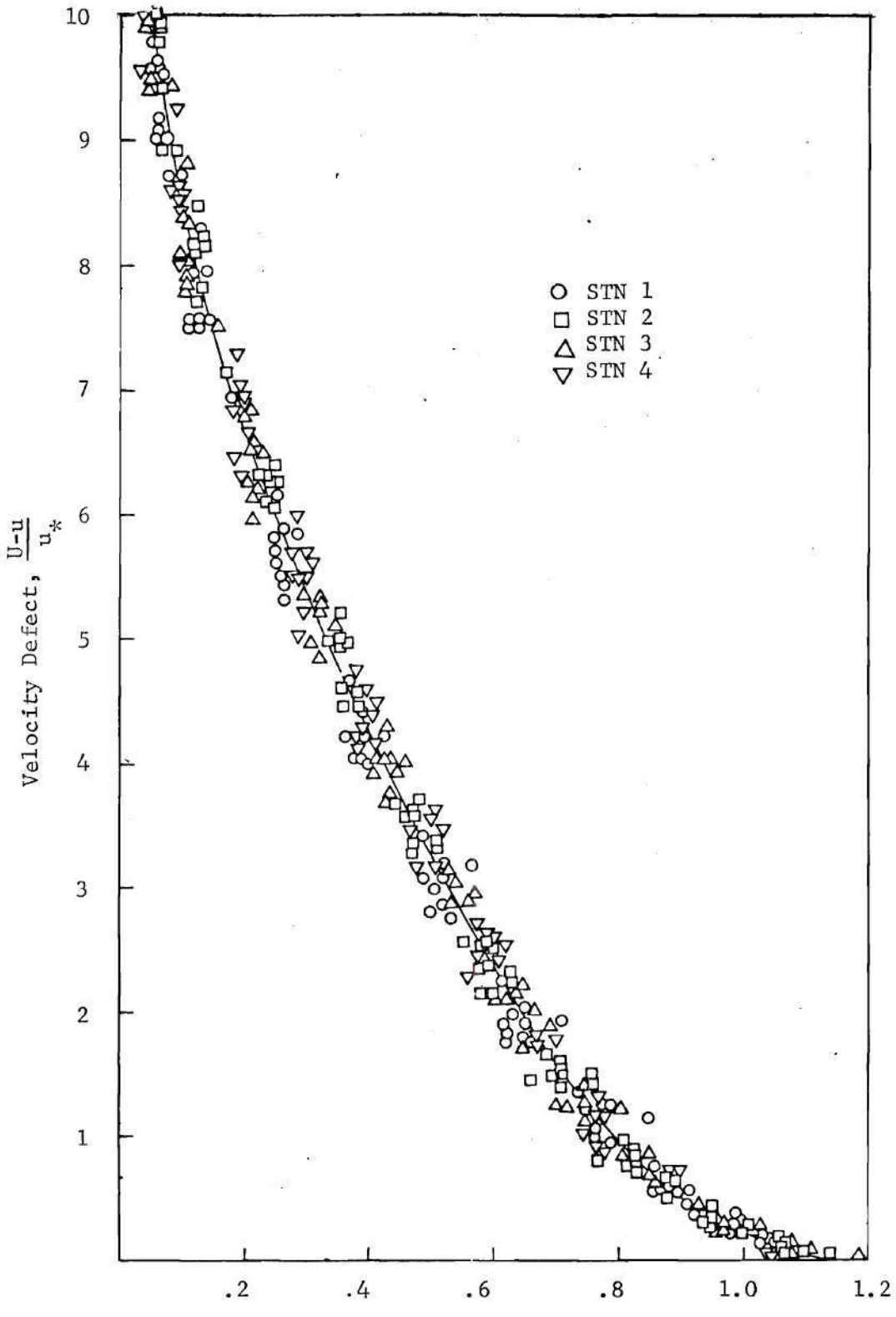

Figure 9. Velocity Defect Law, No Polymer Injection

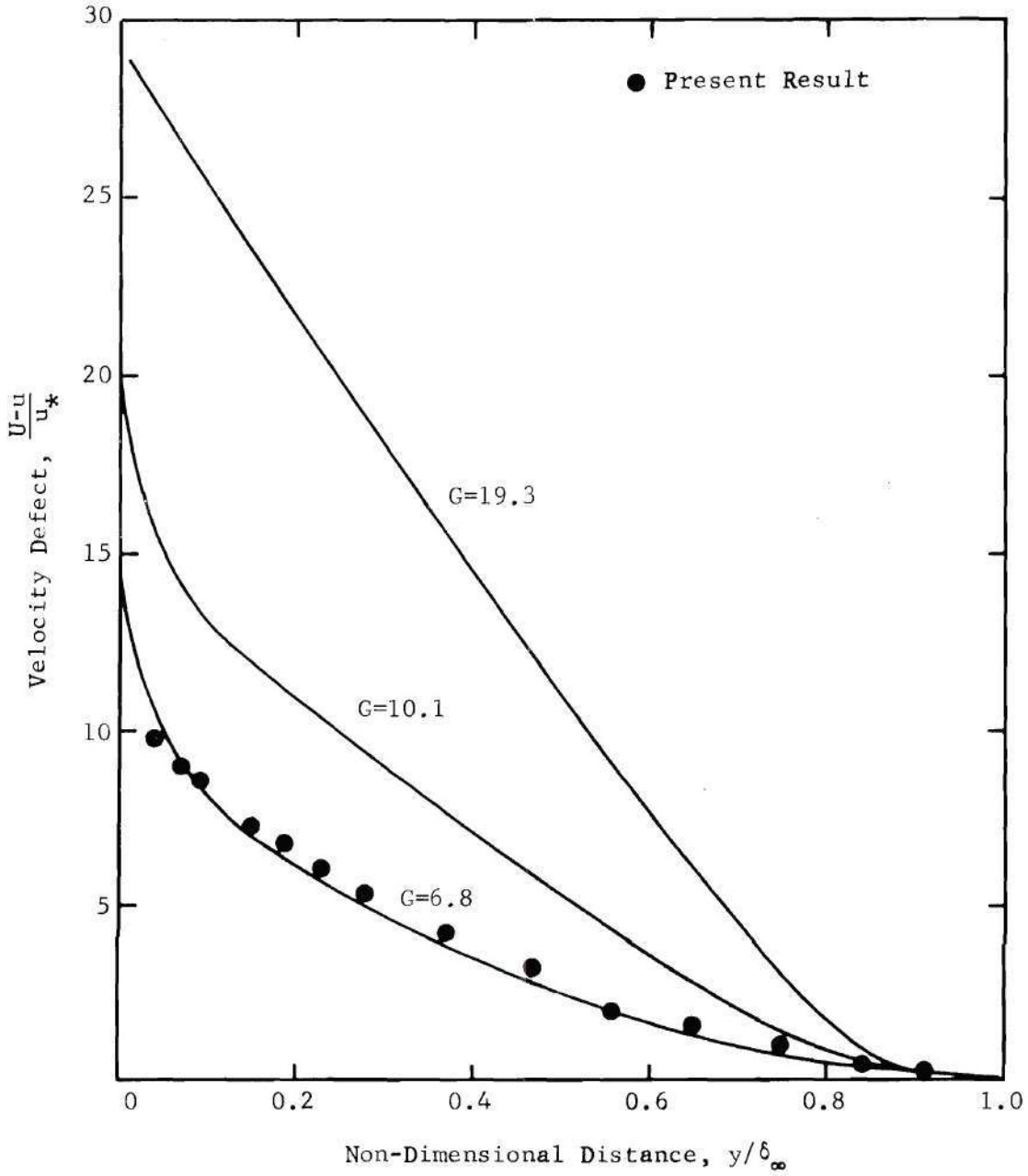

Figure 10. Universal Turbulent Boundary Layer Profiles for Equilibrium Pressure Gradients.

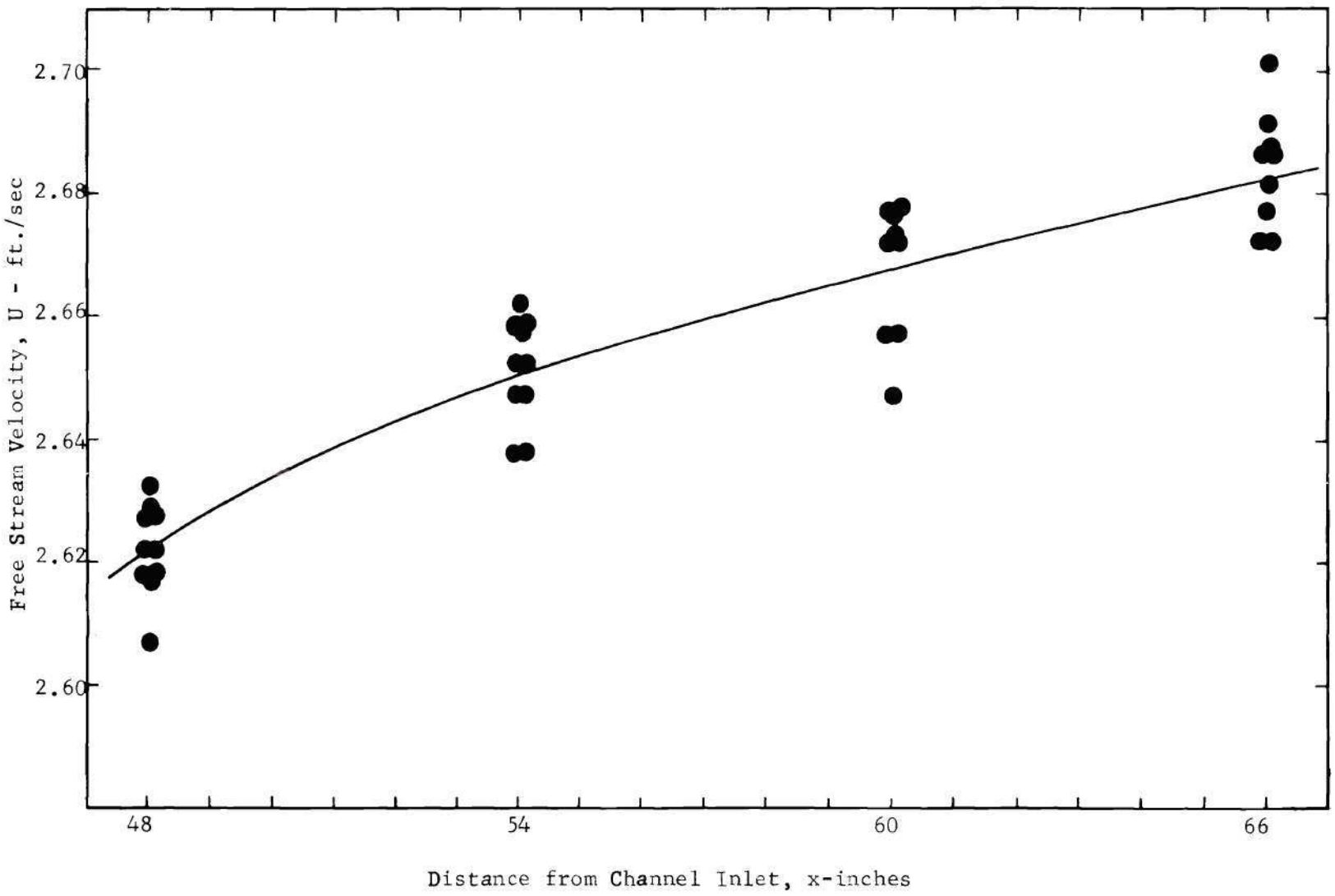

Figure 11. Free Stream Velocity, No Polymer Injection

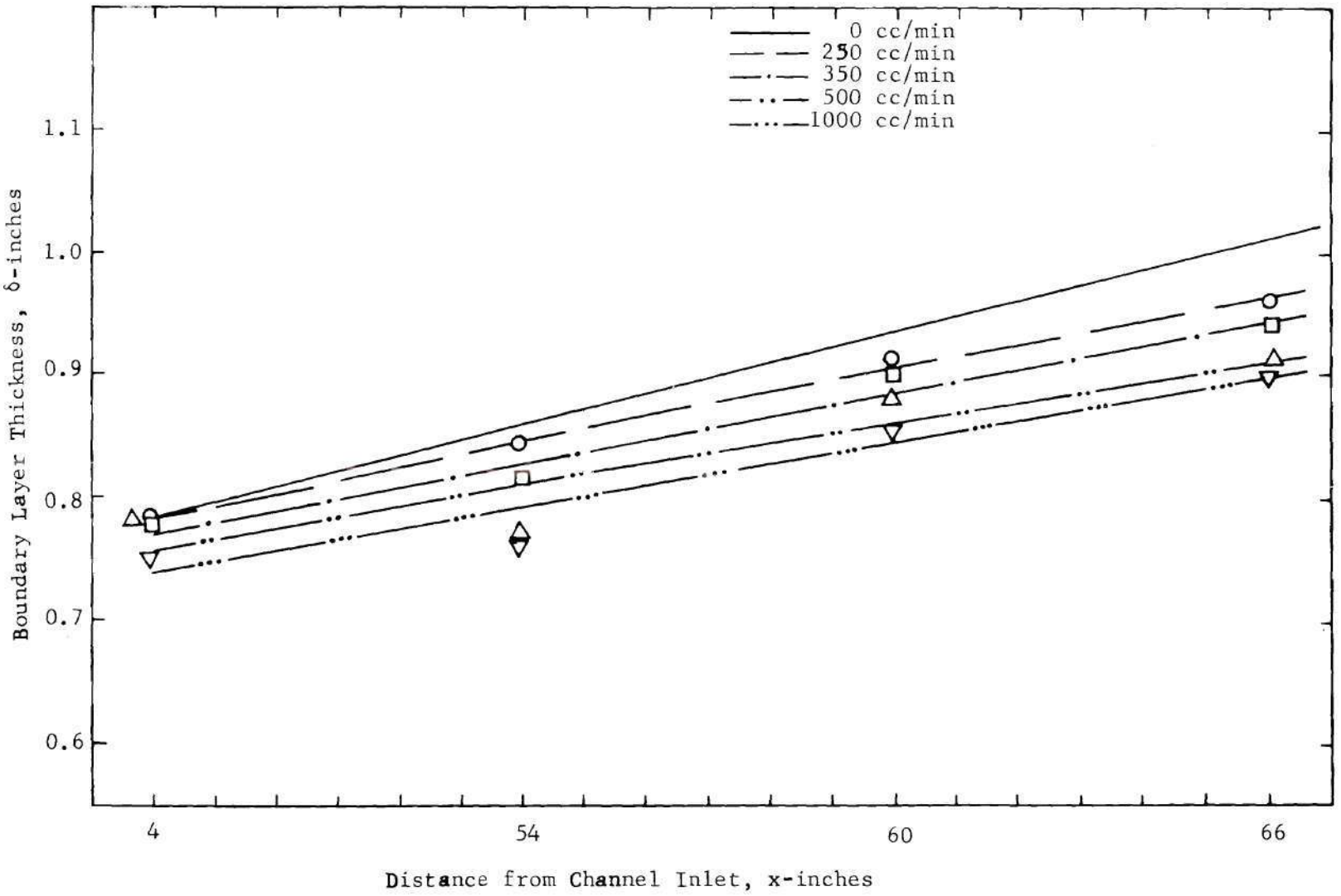

Figure 12. Boundary Layer Thickness, Injected Solution 500 ppm PEO

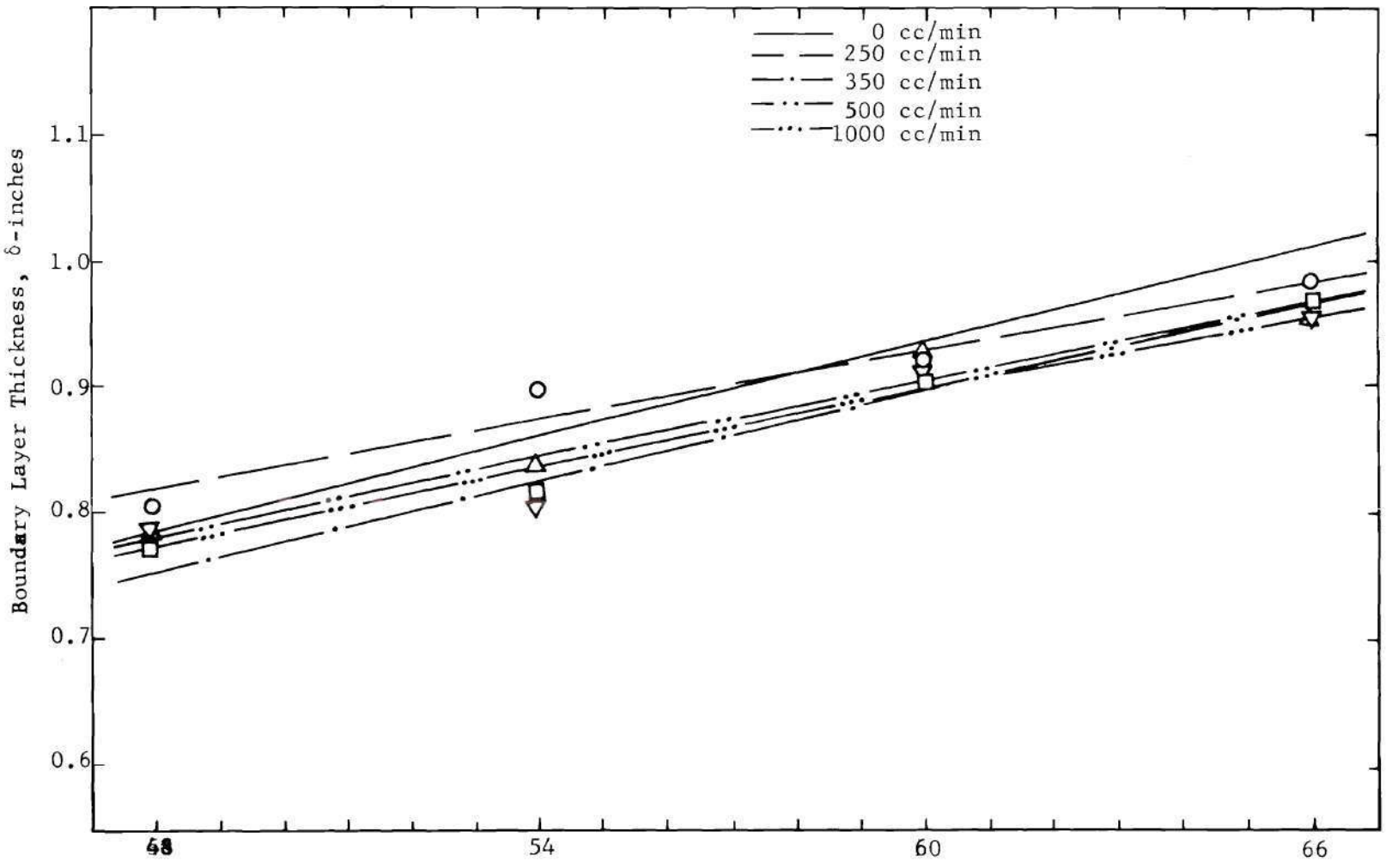

Figure 13. Boundary Layer Thickness, Injected Solution 1000 ppm PEO

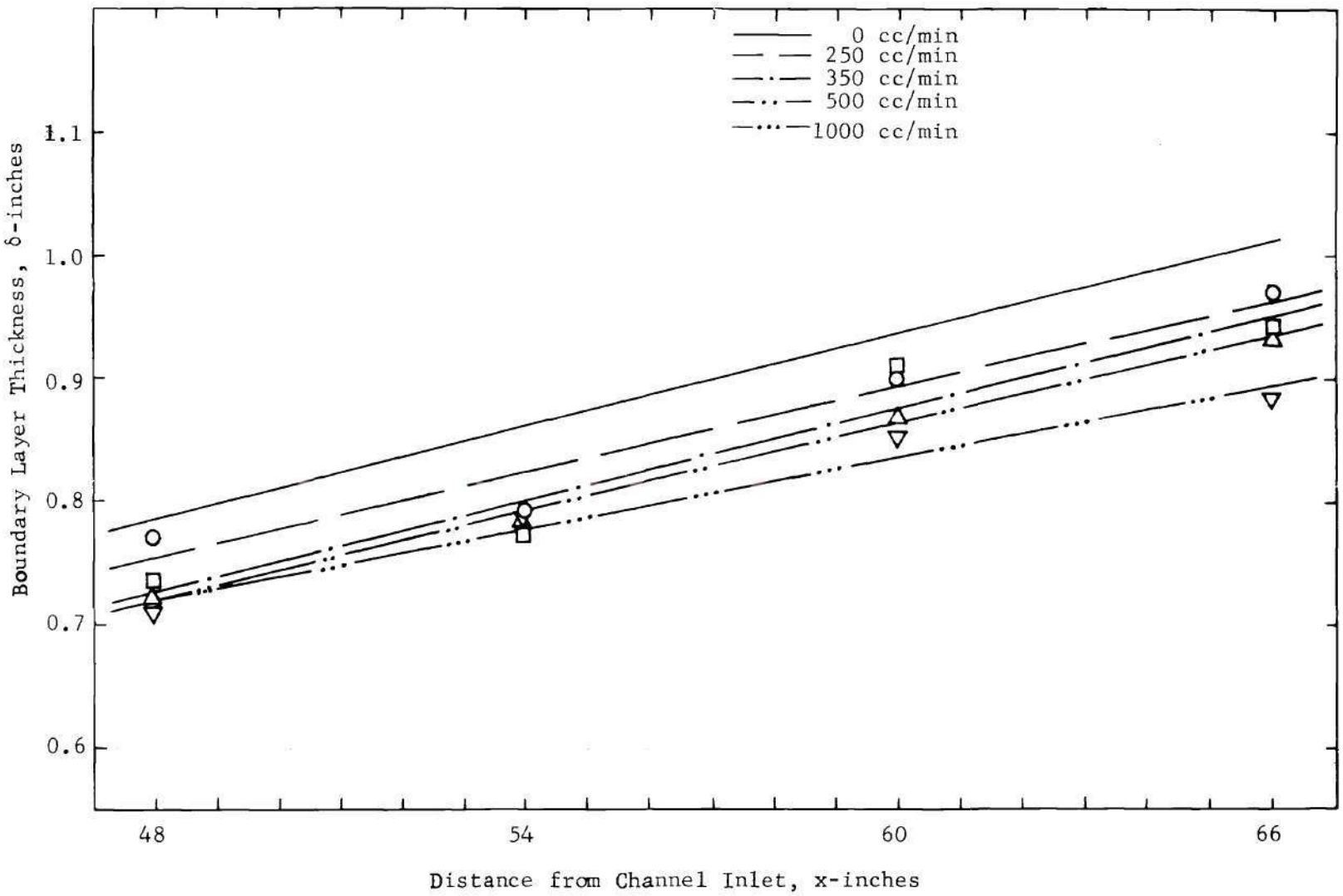

Figure 14. Boundary Layer Thickness, Injected Solution 2000 ppm PEO

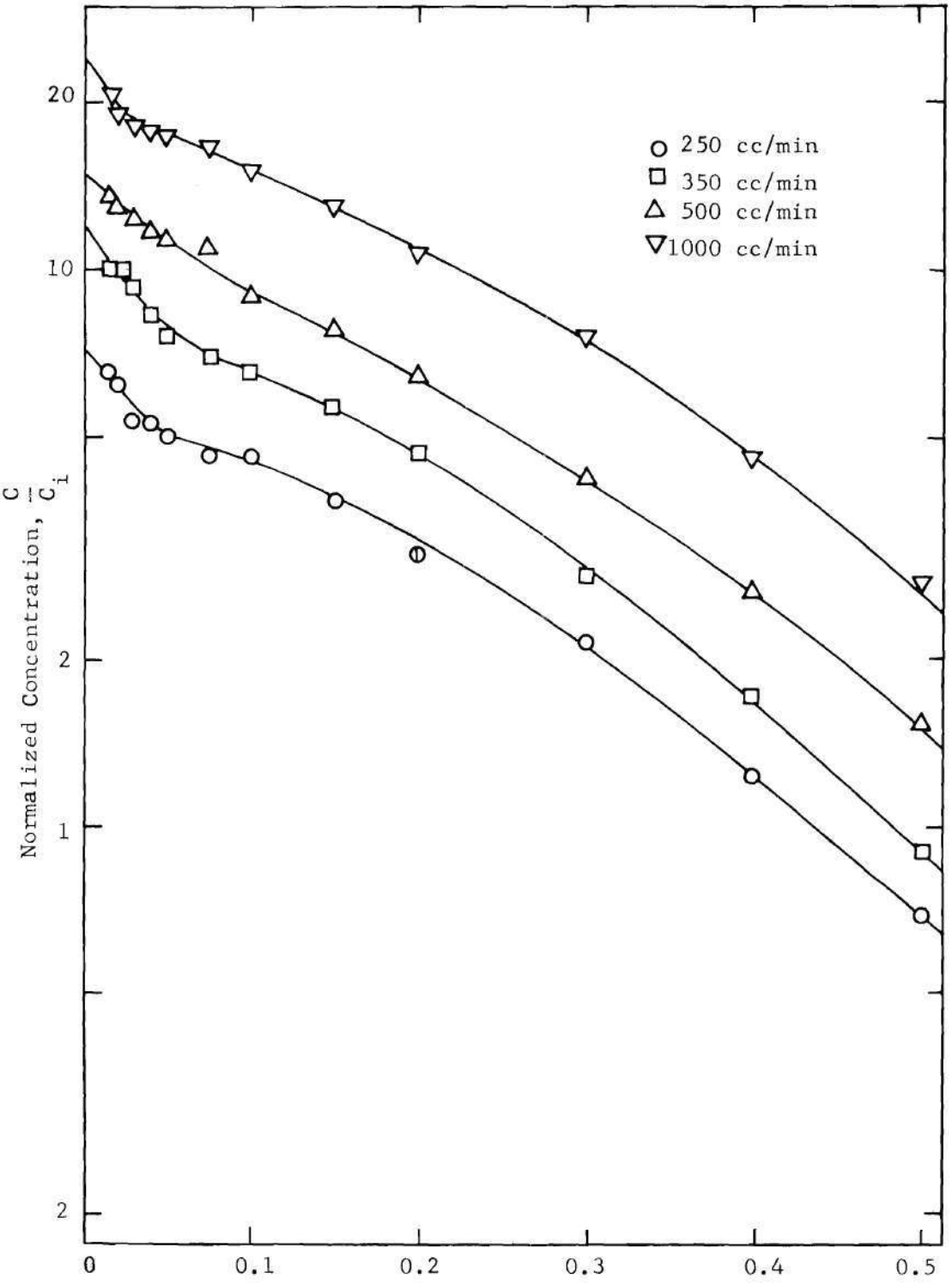

Figure 15. Typical Concentration Profile
Injected Solution-500 ppm PEO, Station 3

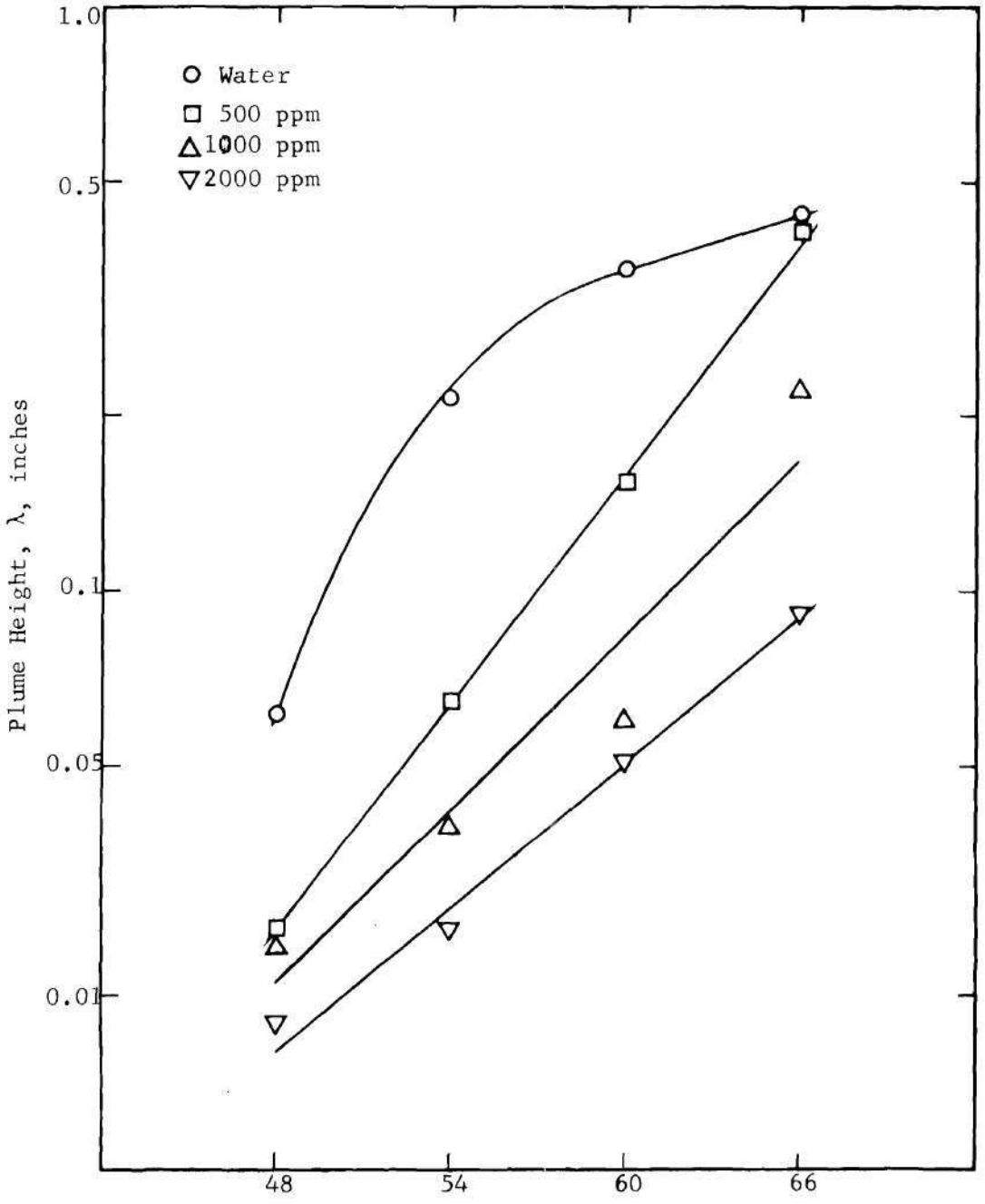

Figure 16. Concentration Boundary Layer Thickness

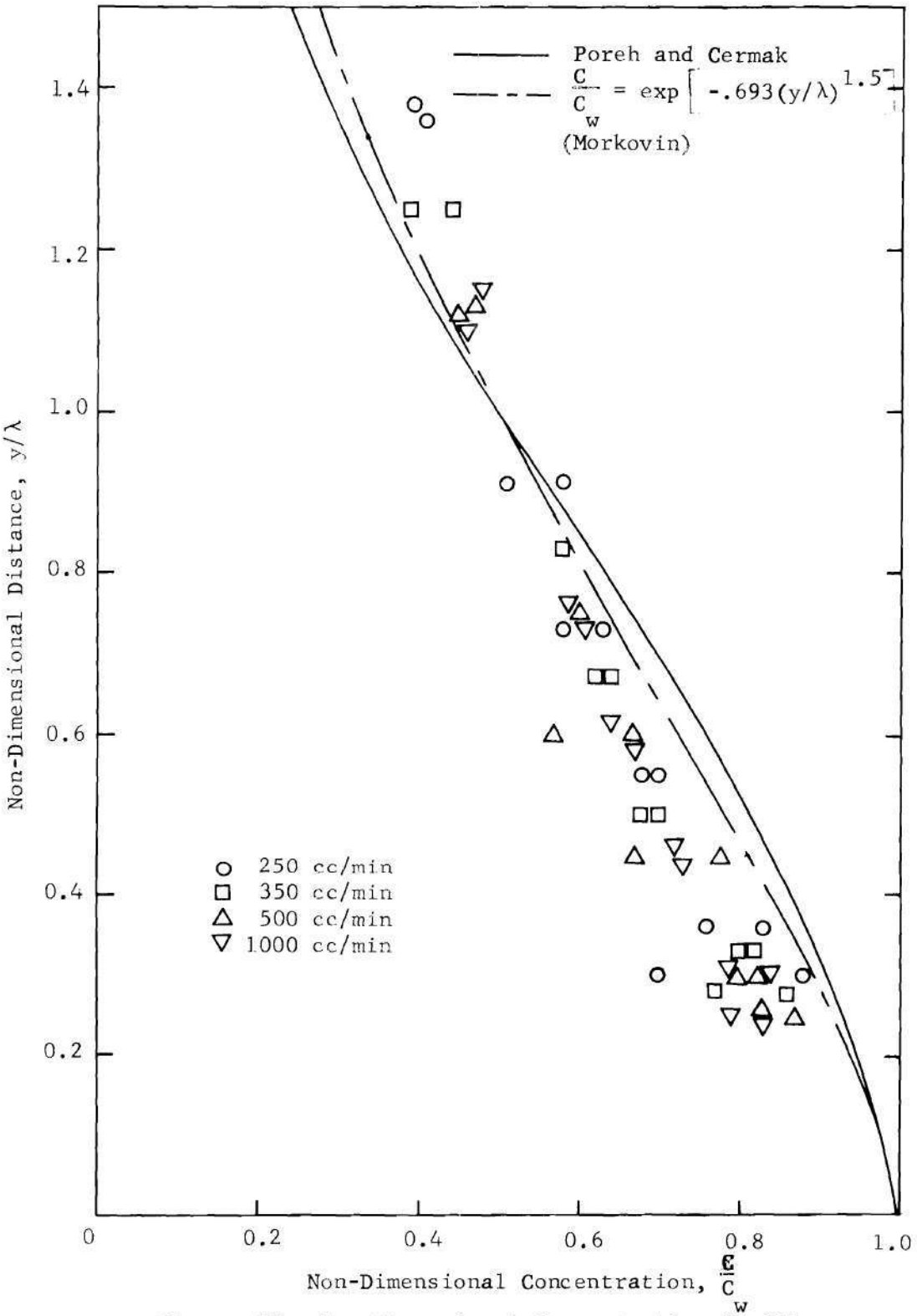

Figure 17. Non-Dimensional Concentration Profile Injected Solution-Water, Station 1

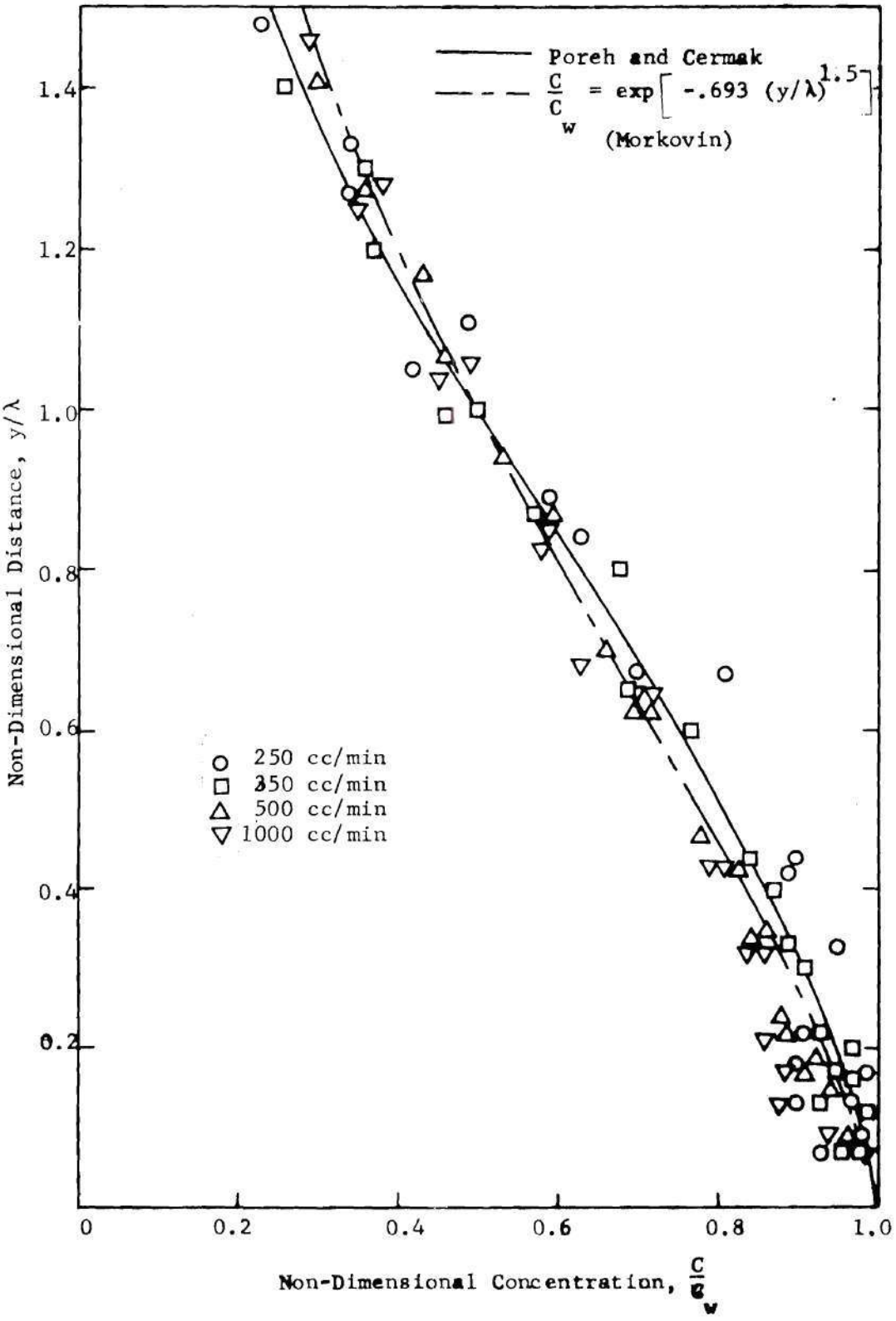

Figure 18. Non-Dimensional Concentration Profile Injected Solution-Water, Station 2

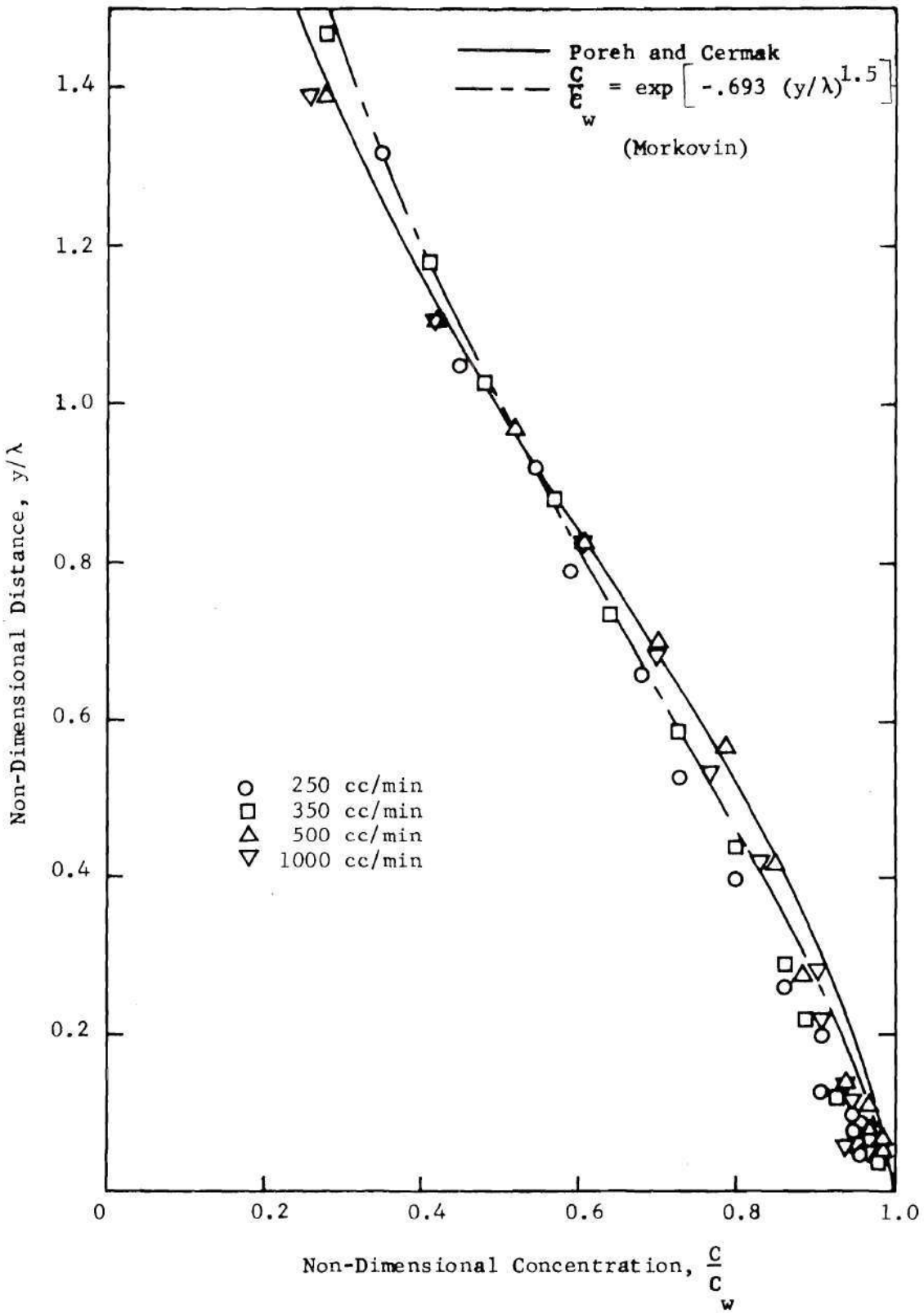

Figure 19. Non-Dimensional Concentration Profile Injected Solution-Water, Station 3

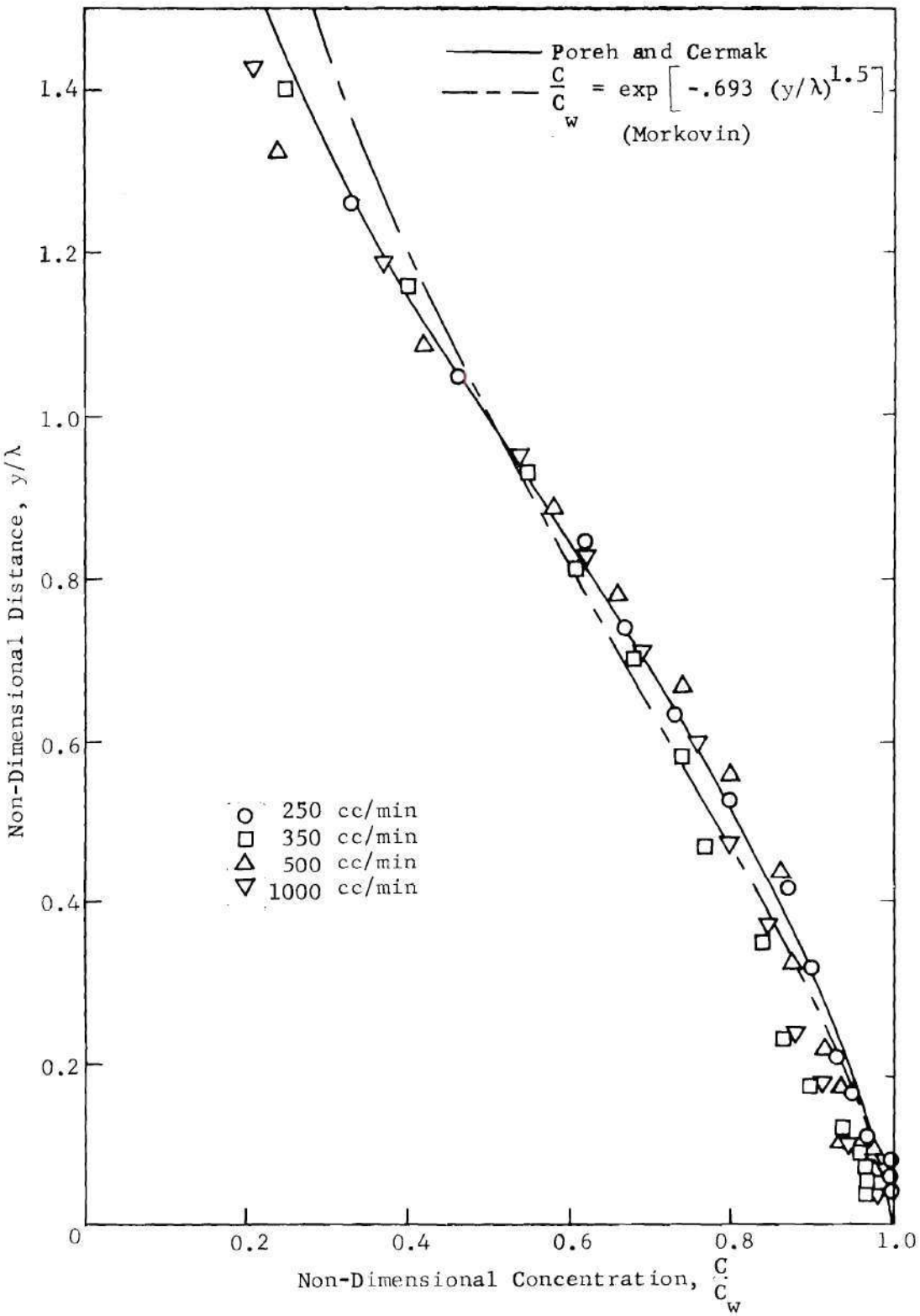

Figure 20. Non-Dimensional Concentration Profile Injected Solution-Water, Station 4

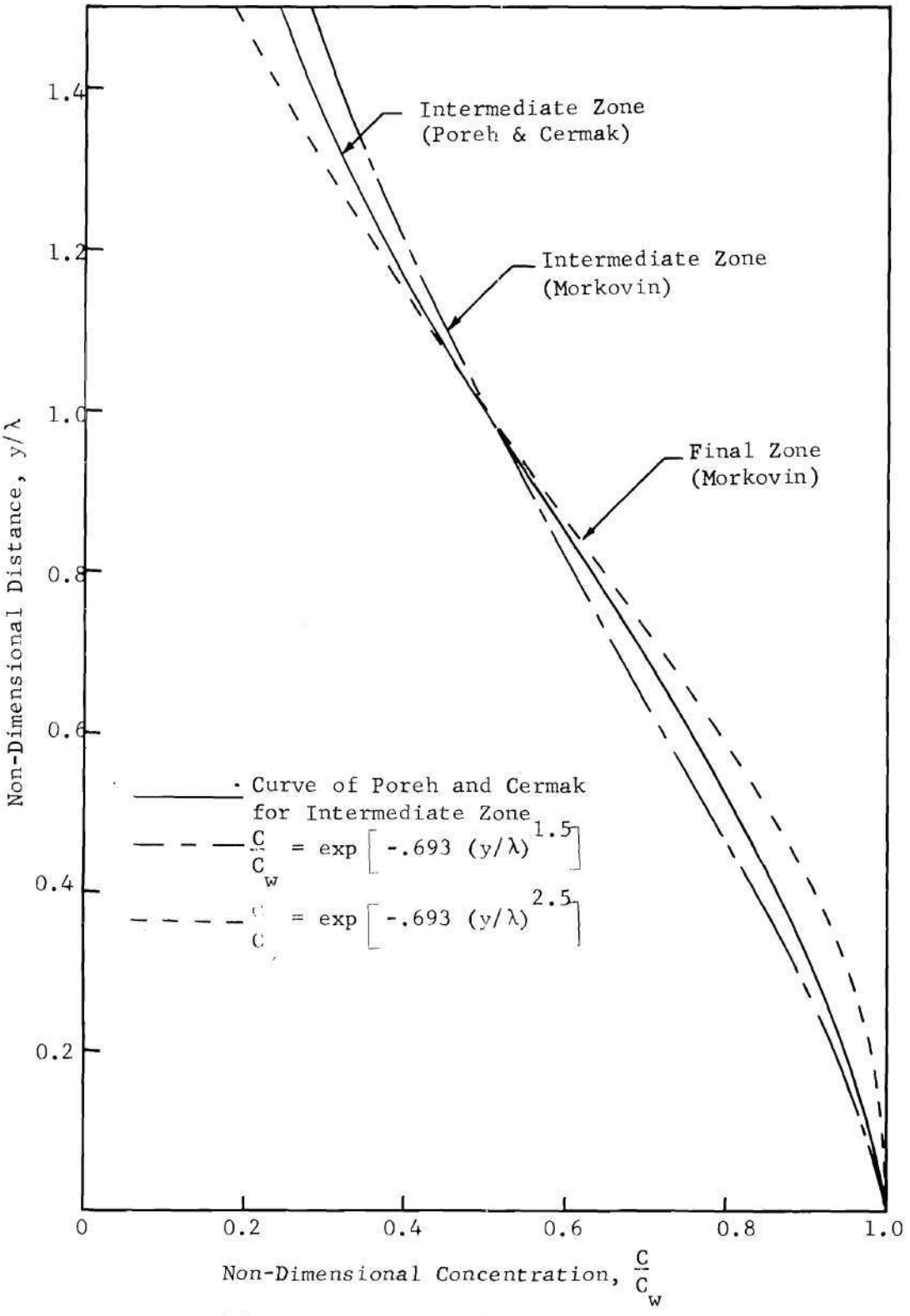

Figure 21. Comparison of Non-Dimensional Concentration Curves for Intermediate and Final Zones

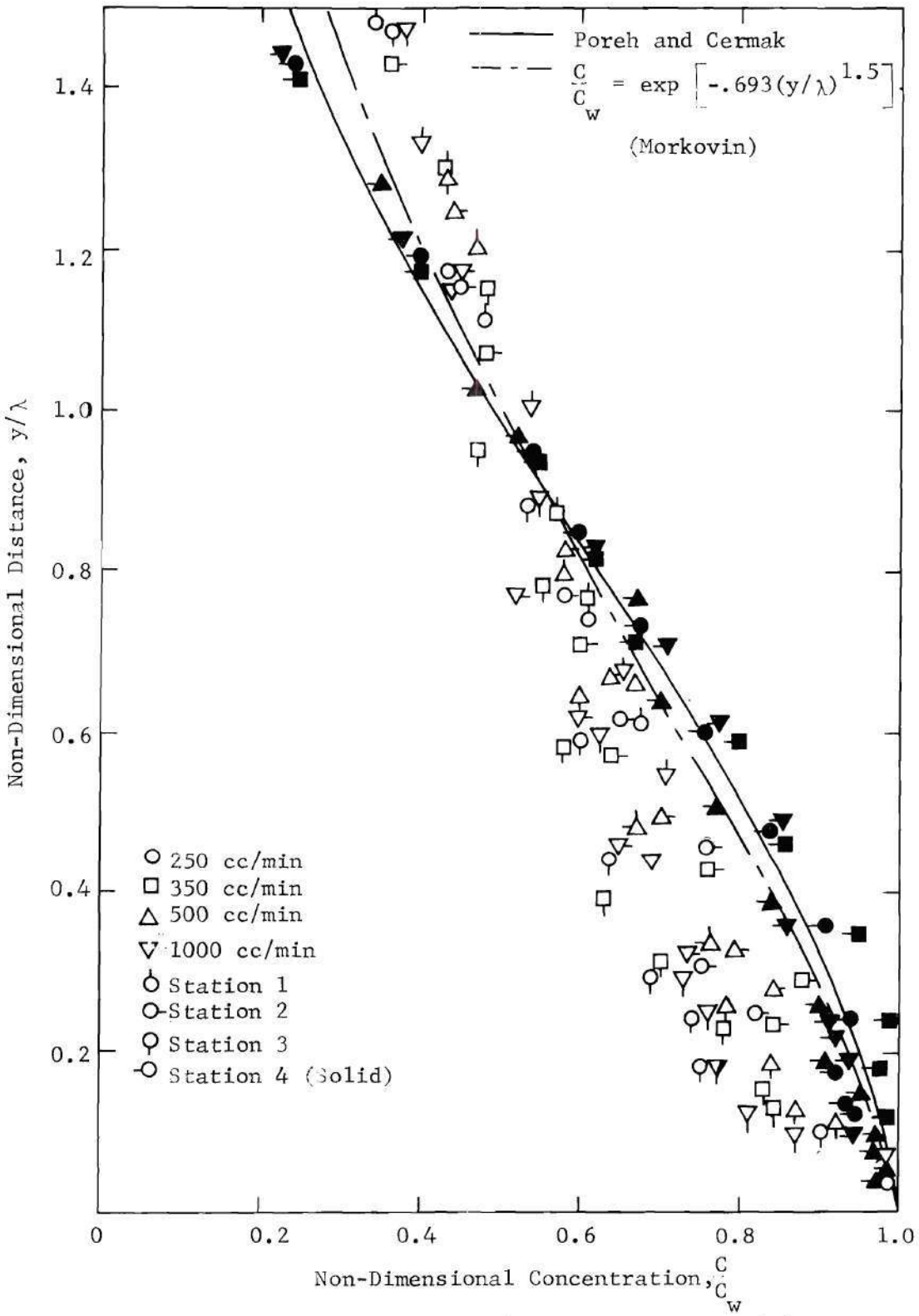

Figure 22. Non-Dimensional Concentration Profile
Injected Solution-500 ppm PEO

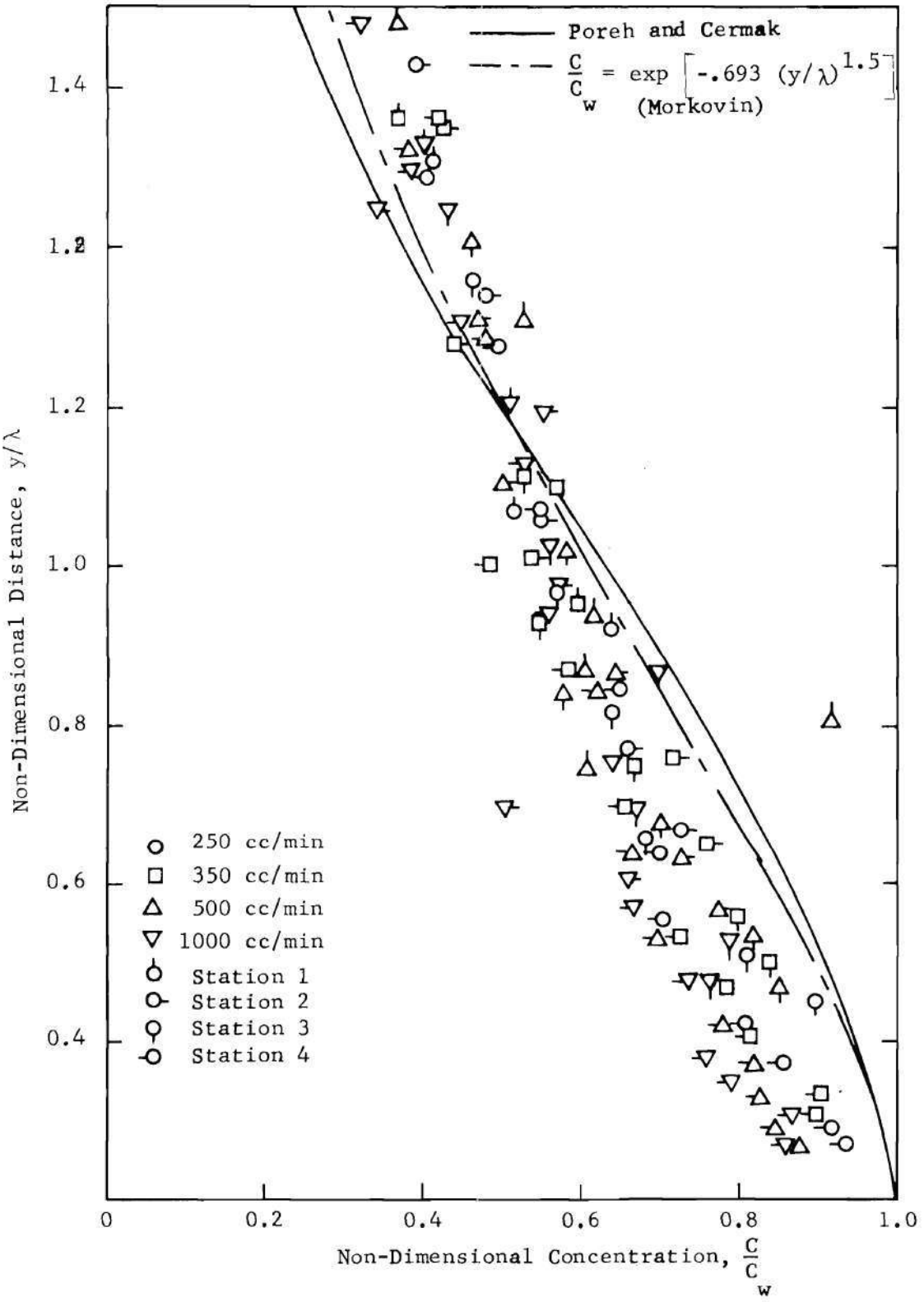

Figure 23. Non-Dimensional Concentration Profile
Injected Solution-1000 ppm PEO

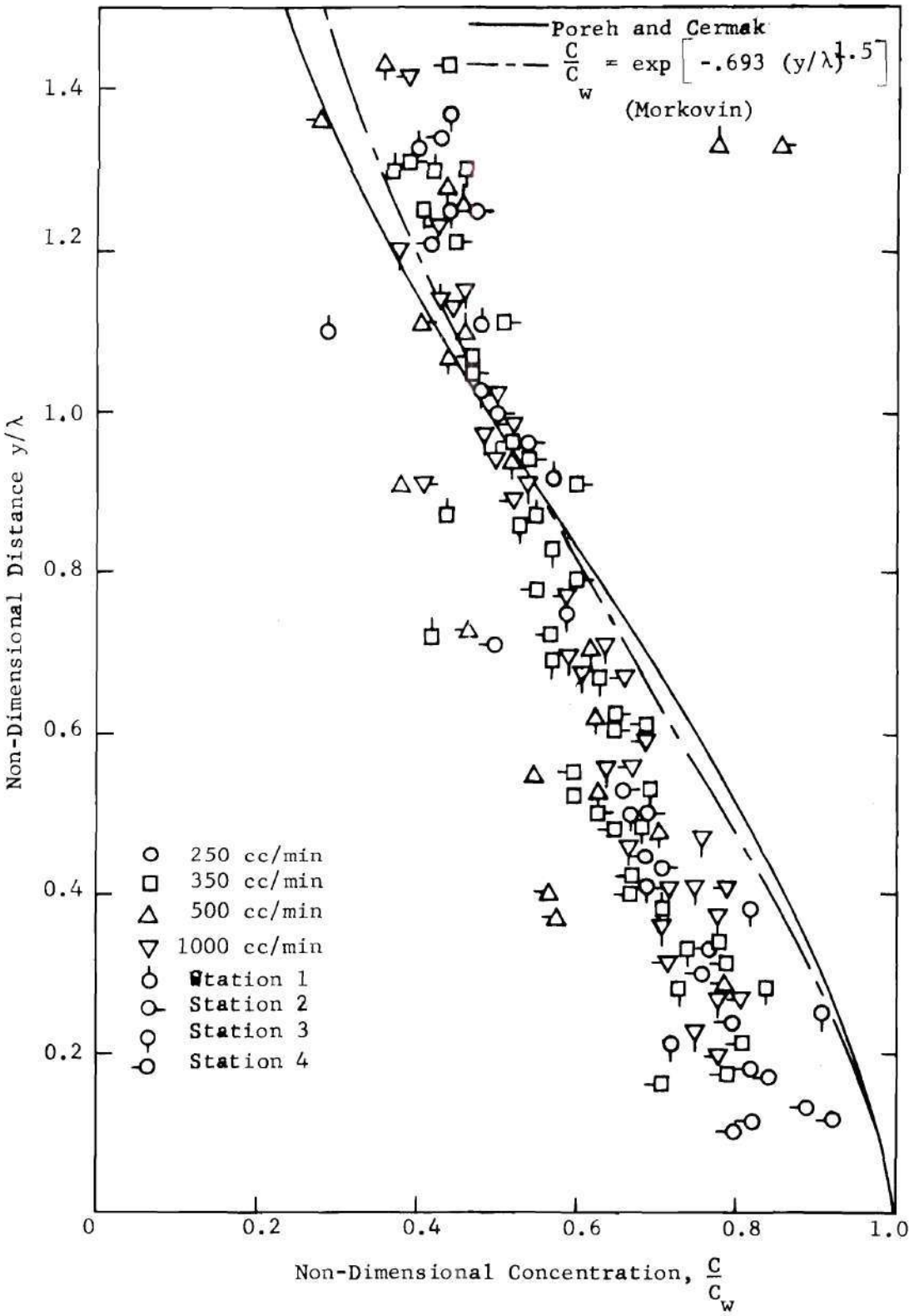

Figure 24. Non-Dimensional Concentration Profile
Injected Solution-2000 ppm PEO

Table 3. Summary of Experiments

Run No.	Concentration of Injected Solution (ppm)	Injection Rate cc/min	Kinematic Viscosity x 10^6 (ft^2/sec)
1	0	0	14.5
2	0	0	14.5
3	0	0	14.5
4	0	0	13.5
5	0	0	12.6
6	0	0	12.6
7	0	0	12.6
8	0	0	11.0
9	0	0	11.2
10	0	0	11.2
101	500	250	11.2
102	500	250	11.2
111	500	350	11.0
112	500	350	11.0
113	500	350	11.2
121	500	500	11.0
122	500	500	11.0
123	500	500	11.2
131	500	1000	11.0
132	500	1000	11.2
201	1000	250	10.8
202	1000	250	11.0
211	1000	350	10.8
212	1000	350	10.8
213	1000	350	12.0
214	1000	350	12.0
215	1000	350	11.5
216	1000	350	11.2
221	1000	500	10.8
222	1000	500	11.2
231	1000	1000	12.0
232	1000	1000	11.2

Table 3. (Continued)

Run No.	Concentration of Injected Solution (ppm)	Injection Rate cc/min	Kinematic Viscosity x 10^6 (ft^2/sec)
301	2000	250	14.5
302	2000	250	14.5
303	2000	250	14.5
304	2000	250	12.0
305	2000	250	11.0
311	2000	350	14.5
312	2000	350	14.5
313	2000	350	14.5
314	2000	350	13.5
315	2000	350	11.2
321	2000	500	12.6
322	2000	500	12.6
323	2000	500	12.6
324	2000	500	10.8
331	2000	1000	12.6
332	2000	1000	12.6
333	2000	1000	12.6
334	2000	1000	11.0

Table 4. Displacement Thickness, No Polymer Injection

Run Number	Displacement Thickness (inches x 10^3) Station 1	Station 2	Station 3	Station 4
1	134.3	144.3	159.5	178.7
2	132.7	146.2	164.2	173.8
3	134.1	147.4	162.2	176.9
4	130.4	145.1	159.2	176.7
5	126.2	134.3	156.5	173.3
6	132.3	145.0	154.5	168.8
7	134.5	143.0	157.9	177.1
8	133.1	136.6	159.1	173.0
9	135.1	145.0	158.8	173.2
10	139.5	147.4	161.7	181.1

Table 5. Momentum Thickness, No Polymer Injection

Momentum Thickness (inches x 10^3)				
Run Number	Station 1	Station 2	Station 3	Station 4
1	91.5	99.9	111.5	124.5
2	92.1	100.6	114.3	120.8
3	92.9	102.1	113.5	124.2
4	89.8	100.6	110.8	123.4
5	87.4	93.7	108.4	120.0
6	91.2	100.3	107.7	118.6
7	93.2	99.6	109.5	123.9
8	92.0	95.5	111.6	121.8
9	95.1	101.4	111.8	121.9
10	97.2	102.8	113.4	126.4

Table 6. Boundary Layer Thicknesses, No Polymer Injection

Run Number	Boundary Layer Thickness (inches)							
	Station 1		Station 2		Station 3		Station 4	
	δ	δ_∞	δ	δ_∞	δ	δ_∞	δ	δ_∞
1	.707	.741	.844	.899	.900	.950	1.010	1.064
2	.792	.847	.845	.909	.982	1.068	.984	1.049
3	.802	.859	.905	1.015	.971	1.049	1.009	1.069
4	.766	.818	.855	.920	.937	1.015	1.063	1.164
5	.757	.811	.789	.837	.924	1.004	1.022	1.124
6	.813	.900	.940	.900	.837	.925	.968	1.034
7	.774	.822	.848	.913	.929	.993	1.046	1.120
8	.796	.817	.793	.838	.929	.993	1.042	1.135
9	.874	.960	.857	.918	.939	1.011	1.042	1.135
10	.813	.864	.868	.929	.940	1.002	1.043	1.116
Average	.787	.844	.844	.908	.929	1.008	1.023	1.101

Table 7. Wall Shear (lb_f/ft^2), No Polymer Injection
Method A - Law of the Wall
Method B - Ludweig Tillmann Equation
Method C - Least Squares Fit, θ vs x, Individual θ's
Method D - Least Squares Fit, θ vs x, θ Averaged at Each Station

RUN	STATION 1				STATION 2				STATION 3				STATION 4			
	A	B	C	D	A	B	C	D	A	B	C	D	A	B	C	D
1	.024	.024	.025	.027	.026	.025	.025	.027	.026	.025	.025	.028	.024	.024	.025	.028
2	.024	.025	"	"	.026	.024	"	"	.024	.024	"	"	.027	.024	"	"
3	.026	.025	"	"	.023	.024	"	"	.026	.025	"	"	.026	.025	"	"
4	.025	.024	"	"	.023	.024	"	"	.024	.024	"	"	.024	.024	"	"
5	.024	.024	.018	.026	.021	.025	.021	.026	.026	.024	.025	.026	.024	.023	.028	.026
6	.024	.024	"	"	.025	.024	"	"	.023	.024	"	"	.022	.024	"	"
7	.025	.024	"	"	.021	.024	"	"	.027	.024	"	"	.026	.023	"	"
8	.022	.023	.022	.025	.022	.024	.024	.025	.023	.023	.026	.025	.020	.023	.028	.025
9	.022	.024	"	"	.016	.023	"	"	.019	.023	"	"	.020	.023	"	"
10	.022	.023	"	"	.022	.023	"	"	.022	.023	"	"	.021	.022	"	"

Table 8. Wall Shear Stress Data, No Injection

RUN NO.	STATION 1		STATION 2		STATION 3		STATION 4	
	u_*	B	u_*	B	u_*	B	u_*	B
1	.112	5.4	.115	5.0	.115	5.1	.110	5.5
2	.112	5.7	.115	4.9	.110	5.6	.117	4.3
3	.115	4.9	.108	6.1	.115	5.0	.108	5.9
4	.114	5.1	.109	5.8	.110	5.5	.110	5.4
5	.111	5.6	.104	7.0	.116	4.4	.110	5.1
6	.111	5.4	.107	6.1	.109	5.8	.107	5.8
7	.114	4.9	.105	6.6	.117	4.3	.117	4.1
8	.106	5.8	.107	5.9	.109	5.2	.109	5.1
9	.105	6.3	.090	9.2	.099	7.4	.101	6.8
10	.106	5.7	.106	5.7	.106	5.7	.105	5.5
$B_{ave.}$		5.5		6.2		5.0		5.0

Table 9. Evaluation of Pressure Gradient Parameters

$$\Delta = \int_0^\infty \left(\frac{U - u}{u_*}\right) dy$$

$$G = \int_0^\infty \left(\frac{U - u}{u_*}\right)^2 d\left(\frac{y}{\Delta}\right)$$

RUN	STATION 1		STATION 2		STATION 3		STATION 4	
	G	Δ	G	Δ	G	Δ	G	Δ
1	6.71	3.08	6.40	3.26	6.35	3.64	6.81	4.28
2	6.38	3.04	6.51	3.26	6.70	3.90	6.39	3.99
3	6.27	2.99	6.76	3.52	6.32	3.70	6.76	4.31
4	6.35	2.92	6.66	3.34	6.67	3.77	6.77	4.08
5	6.36	2.89	6.83	3.34	6.43	3.53	6.90	4.16
6	6.56	3.04	6.53	3.33	6.73	3.72	6.73	4.12
7	6.25	3.01	6.85	3.53	6.36	3.53	6.48	4.08
8	6.71	3.18	6.56	3.28	6.53	3.78	7.16	4.51
9	6.46	3.27	7.85	4.14	7.13	4.17	7.16	4.51
10	6.60	3.33	6.69	3.56	6.76	3.96	7.07	4.53
Ave.	6.5	3.08	6.8	3.46	6.6	3.77	6.82	4.26
$\frac{\Delta_{ave.}}{\delta_{ave.}}$		3.91		4.09		4.06		4.16

Table 10. Boundary Layer Thicknesses
Injected Solution-500 ppm PEO

Injection Rate cc/min	Run No.	Boundary Layer Thickness (inches) Station 1		Station 2		Station 3		Station 4	
		δ	δ_∞	δ	δ_∞	δ	δ_∞	δ	δ_∞
250	101	.859	.934	.860	.927	.894	.944	.959	1.008
	102	.786	.838	.826	.891	.933	.985	.951	1.011
	Ave	.786	.886	.843	.909	.914	.965	.959	1.010
350	111	.834	.892	.825	.895	.878	.928	.952	1.006
	112	.777	.829	.860	.925	.971	1.041	.944	1.004
	113	.717	.757	.751	.793	.856	.902	.924	.971
	Ave	.776	.826	.813	.871	.902	.957	.940	.993
500	121	.795	.846	.782	.825	.874	.935	.930	.981
	122	.825	.901	.774	.818	.919	.981	.901	.947
	123	.717	.759	.750	.792	.847	.897	.906	.955
	Ave	.779	.835	.769	.812	.880	.938	.912	.961
1000	131	.763	.810	.748	.786	.856	.903	.909	.960
	132	.745	.793	.777	.823	.872	.922	.889	.933
	Ave	.754	.802	.762	.804	.864	.912	.899	.946

Table 11. Boundary Layer Thicknesses
Injected Solution-1000 ppm PEO

Injection Rate cc/min	Run No.	Boundary Layer Thickness (inches) Station 1		Station 2		Station 3		Station 4	
		δ	δ_∞	δ	δ_∞	δ	δ_∞	δ	δ_∞
250	201	.829	.886	.912	.995	.953	1.018	.959	1.016
	202	.787	.828	.883	.962	.892	.939	1.00	1.057
	Ave	.808	.857	.898	.957	.922	.978	.980	1.036
350	211	.786	.839	.873	.937	.963	1.034	.958	1.014
	212	.763	.814	.788	.834	.893	.942	.963	1.017
	213	.753	.800	.784	.892	.882	.932	1.002	1.078
	214	.702	.741	.760	.802	.881	.933	.964	1.023
	215	.766	.810	.840	.897	.872	.925	.964	1.023
	216	.802	.845	.854	.916	.918	.991	.970	1.030
	Ave	.762	.808	.817	.870	.902	.960	.970	1.031
500	221	.784	.832	.835	.894	.949	1.017	.947	1.004
	222	.774	.821	.845	.905	.907	.958	.963	1.002
	Ave	.779	.826	.840	.900	.928	.988	.955	1.013
1000	231	.788	.834	.821	.878	.909	.960	.948	1.010
	232	.785	.835	.804	.848	.933	.996	.960	1.016
	Ave	.786	.834	.812	.863	.921	.978	.954	1.013

Table 12. Boundary Layer Thicknesses
Injected Solution-2000 ppm PEO

Injection Rate cc/min	Run No.	Boundary Layer Thickness (inches) Station 1 δ	Station 1 δ_∞	Station 2 δ	Station 2 δ_∞	Station 3 δ	Station 3 δ_∞	Station 4 δ	Station 4 δ_∞
250	301	.729	.778	.781	.820	.883	.937	.967	1.026
	302	.756	.804	.796	.841	.873	.923	.952	1.012
	303	.769	.818	.808	.859	.881	.929	.982	1.042
	304	.750	.803	.777	.822	.872	.922	.971	1.035
	305	.849	.921	.800	.852	.986	1.055	.966	1.022
	Ave	.771	.825	.792	.839	.900	.943	.968	1.027
350	311	.716	.755	.751	.794	.874	.924	.925	.976
	312	.753	.805	.768	.810	.853	.899	.947	1.006
	313	.707	.744	.802	.846	.911	.987	.941	1.006
	314	.733	.784	.772	.817	.938	1.041	.940	.999
	315	.773	.826	.765	.805	.970	1.036	.957	1.014
	Ave	.736	.783	.772	.814	.909	.977	.942	1.000
500	321	.682	.721	.764	.802	.863	.913	.971	1.043
	322	.705	.746	.768	.813	.909	.966	.959	1.019
	323	.755	.815	.924	.888	.810	.848	.907	.954
	324	.746	.795	.805	.858	.895	.942	.909	.957
	Ave	.722	.769	.790	.840	.869	.917	.937	.993
1000	331	.676	.716	.735	.774	.847	.887	.885	.932
	332	.744	.818	.790	.837	.880	.928	.878	.914
	333	.662	.695	.816	.889	.818	.855	.877	.922
	334	.757	.804	.807	.855	.865	.911	.896	.940
	Ave	.710	.758	.787	.839	.852	.895	.884	.927

Table 13. Reduction of Boundary Layer Growth in Test Solution Due to PEO Injection

C_i ppm	Injection Rate cc/min	δ Station 4	% Reduction* in δ
500	250	.959	22.1
	350	.940	28.6
	500	.912	38.3
	1000	.899	42.8
1000	250	.980	14.8
	350	.970	18.3
	500	.955	23.4
	1000	.954	23.4
2000	250	.968	19.0
	350	.942	27.9
	500	.937	29.6
	1000	.884	47.9

$$\% \ \delta \text{ Red.} = \frac{\delta^{p}_{66} - \delta^{\circ}_{45}}{\delta^{\circ}_{66} - \delta^{\circ}_{45}}$$

δ^{p}_{66} = Boundary Layer thickness, station 4, with polymer injection.

δ°_{66} = Boundary Layer thickness, station 4, no injection.

δ°_{45} = Boundary Layer thickness at injection point, 45 inches from channel inlet.

Table 14. Wall Shear Stress
Injected Solution-500 ppm PEO

Injection Rate cc/min	Run No.	Station 1		Station 2		Station 3		Station 4	
		τ_w^p	τ_w^p/τ_w^o	τ_w^p	τ_w^p/τ_w^o	τ_w^p	τ_w^p/τ_w^o	τ_w^p	τ_w^p/τ_w^o
250	101	.0181	.83	.0182	.82	.0256	1.14	.0315	1.47
	102	.0226	1.04	.0175	.80	.0226	1.00	.0247	1.15
350	111	.0208	.95	.0194	.89	.0319	1.42	.0335	1.57
	112	.0225	1.03	.0213	.98	.0204	.91	.0278	1.30
	113	.0308	1.41	.0287	1.30	.0337	1.50	.0398	1.86
500	121	.0250	1.15	.0261	1.19	.0275	1.23	.0361	1.69
	122	.0180	.83	.0282	1.28	.0217	.97	.0400	1.87
	123	.0243	1.11	.0278	1.26	.0314	1.40	.0375	1.75
1000	131	.0249	1.14	.0344	1.56	.0318	1.42	.0283	1.32
	132	.0223	1.02	.0237	1.08	.0302	1.35	.0430	2.01

Table 15. Wall Shear Stress
Injected Solution- 1000 ppm PEO

Injection Rate cc/min	Run No.	Station 1		Station 2		Station 3		Station 4	
		τ_w^p	τ_w/τ_w^o	τ_w^p	τ_w/τ_w^o	τ_w^p	τ_w/τ_w^o	τ_w^p	τ_w/τ_w^o
250	201	.0211	.97	.0193	.88	.0230	1.03	.0270	1.26
	202	.0273	1.25	.0168	.76	.0329	1.47	.0311	1.45
350	211	.0219	1.00	.0196	.89	.0221	.99	.0318	1.49
	212	.0194	.89	.0261	1.19	.0319	1.42	.0346	1.62
	213	.0226	.93	.0253	1.18	.0326	1.29	.0219	.93
	214	.0274	1.13	.0295	1.37	.0318	1.26	.0258	1.10
	215	.0263	1.21	.0206	.94	.0288	1.29	.0258	1.21
	216	.0274	1.26	.0202	..92	.0224	1.00	.0283	1.32
500	221	.0219	1.00	.0207	.94	.0202	.90	.0334	1.56
	222	.0235	1.08	.0224	1.02	.0266	1.19	.0238	1.11
1000	231	.0263	1.21	.0200	.93	.0315	1.41	.0235	1.10
	232	.0243	1.11	.0310	1.44	.0247	1.10	.0305	1.43

Table 16. Wall Shear Stress
Injected Solution-2000 ppm PEO

Injection Rate cc/min	Run No.	Station 1		Station 2		Station 3		Station 4	
		τ_w^p	τ_w/τ_w^o	τ_w^p	τ_w/τ_w^o	τ_w^p	τ_w/τ_w^o	τ_w^p	τ_w/τ_w^o
250	301	.0219	.88	.0365	1.51	.0256	1.04	.0301	1.25
	302	.0238	.96	.0268	1.11	.0311	1.26	.0256	1.07
	303	.0237	.95	.0254	1.05	.0341	1.39	.0304	1.27
	304	.0193	.80	.0274	1.28	.0308	1.22	.0245	1.04
	305	.0169	.78	.0229	1.04	.0225	1.00	.0257	1.20
350	311	.0260	1.04	.0276	1.14	.0340	1.24	.0335	1.42
	312	.0230	.92	.0320	1.32	.0316	1.28	.0269	1.12
	313	.0251	1.01	.0286	1.18	.0328	1.33	.0264	1.10
	314	.0206	.83	.0270	1.12	.0170	.69	.0288	1.20
	315	.0216	.99	.0321	1.46	.0217	.97	.0329	1.54
500	321	.0243	1.00	.0317	1.47	.0281	1.12	.0234	1.00
	322	.0253	1.04	.0260	1.21	.0255	1.01	.0314	1.34
	323	.0171	.70	.0189	.88	.0325	1.29	.0320	1.36
	324	.0218	1.00	.0229	1.06	.0334	1.49	.0387	1.81
1000	331	.0238	.98	.0309	1.44	.0358	1.42	.0325	1.38
	332	.0159	.65	.0300	1.40	.0338	1.34	.0609	2.59
	333	.0325	1.34	.0178	.83	.0427	1.69	.0394	1.68
	334	.0235	1.08	.0251	1.17	.0301	1.19	.0404	1.89

Table 17. Concentration Boundary Layer Thickness

Concentration ppm	Injection Rate	Plume Height (λ) inches Station 1	Station 2	Station 3	Station 4
0	250	.055	.23	.38	.48
		.055	.24		
	350	.060	.23	.34	.43
		.060	.25		
	500	.067	.21	.36	.45
		.067	.23		
	1000	.068	.24	.36	.42
		.065	.24		
500	250	.027	.065	.17	.42
	350	.023	.070	.13	.42
	500	.025	.060	.15	.39
	1000	.030	.065	.17	.42
1000	250	.023	.035	.065	.23
	350	.022	.037	.055	.15
	500	.027	.045	.062	.23
	1000	.030	.040	.060	.27

Table 17. (Continued)

Concentration ppm	Injection Rate	Plume Height (λ) inches Station 1	Station 2	Station 3	Station 4
2000	250	.018	.038	.080	.165
		.015	.040	.073	.150
	350	.023	.032	.060	.095
		.023	.033	.058	.105
	500	.015	.015	.032	.045
				.028	.055
	1000	.018	.018	.044	.075
				.042	.053

Table 18. Determination of Growth Rate Parameter for Momentum Boundary Layers

Injected Concentration (ppm)	Injection Rate cc/min	Distance from Channel Inlet (in)	δ_{ave}	δ_{fit}	$\frac{d\delta}{dx}$	L_δ^*
0	0	48.0	.787	.776	.0137	57.7
		54.0	.844	.857	.0133	63.3
		60.0	.929	.936	.0131	71.2
		66.0	1.023	1.014	.0128	79.9
500	250	48.0	.786	.786	.0102	77.3
		54.0	.843	.847	.0099	84.9
		60.0	.914	.906	.0097	94.0
		66.0	.959	.963	.0095	100.5
500	350	48.0	.776	.770	.0100	77.5
		54.0	.813	.829	.0098	83.2
		60.0	.902	.887	.0096	94.2
		66.0	.940	.944	.0094	100.1
500	500	48.0	.779	.758	.0088	88.8
		54.0	.769	.810	.0086	89.8
		60.0	.880	.861	.0084	104.9
		66.0	.912	.911	.0082	110.8
500	1000	48.0	.754	.739	.0092	81.6
		54.0	.762	.794	.0090	84.4
		60.0	.864	.847	.0088	97.7

Table 18.(Continued)

Injected Concentration (ppm)	Injection Rate cc/min	Distance from Channel Inlet (in)	δ_{ave}	δ_{fit}	$\frac{d\delta}{dx}$	L_{δ}^{*}
		66.0	.899	.900	.0087	103.7
1000	250	48.0	.808	.820	.0093	86.7
		54.0	.898	.876	.0091	98.7
		60.0	.922	.930	.0089	103.5
		66.0	.980	.983	.0087	112.1
1000	350	48.0	.762	.756	.0122	62.4
		54.0	.817	.828	.0119	68.5
		60.0	.902	.899	.0117	77.2
		66.0	.970	.968	.0115	84.7
1000	500	48.0	.779	.782	.0106	73.3
		54.0	.840	.845	.0104	80.9
		60.0	.928	.907	.0102	91.3
		66.0	.955	.967	.0100	95.8
1000	1000	48.0	.786	.776	.0106	74.4
		54.0	.812	.838	.0103	78.7
		60.0	.921	.900	.0101	91.2
		66.0	.954	.960	.0099	96.3

Table 18.(Concluded)

Injected Concentration (ppm)	Injection Rate cc/min	Distance from Channel Inlet (in)	δ_{ave}	δ_{fit}	$\frac{d\delta}{dx}$	L^*_δ
2000	250	48.0	.771	.752	.0121	63.6
		54.0	.792	.824	.0119	66.9
		60.0	.900	.894	.0116	77.6
		66.0	.970	.963	.0114	85.2
2000	350	48.0	.736	.726	.0130	56.6
		54.0	.772	.803	.0127	60.8
		60.0	.909	.878	.0124	73.1
		66.0	.942	.952	.0122	77.2
2000	500	48.0	.722	.720	.0125	57.9
		54.0	.790	.794	.0122	64.8
		60.0	.869	.866	.0119	72.8
		66.0	.937	.937	.0117	80.0
2000	1000	48.0	.710	.719	.0101	70.1
		54.0	.787	.780	.0099	79.5
		60.0	.852	.838	.0097	87.9
		66.0	.884	.896	.0095	93.0

$$*L_\delta = \frac{\delta_{ave}}{\frac{d\delta}{dx}}$$

Table 19. Determination of Growth Rate Parameter for Concentration Boundary Layer

Injected Concentration ppm	Distance from Channel Inlet (in)	λ_{ave}	λ_{fit}	$\frac{d\lambda}{dx}$	L^*_λ
0	48	.062		0.033	1.9
	54	.233		0.032	7.2
	60	.360		0.013	27.8
	66	.444		0.015	29.6
500	48	.026	.026	.0040	6.64
	54	.065	.065	.0099	6.59
	60	.155	.162	.0246	6.30
	66	.414	.403	.0614	6.74
1000	48	.025	.021	.0025	10.33
	54	.039	.043	.0049	7.98
	60	.060	.085	.0098	6.17
	66	.220	.170	.0195	11.26
2000	48	.018	.016	.0015	11.52
	54	.026	.029	.0027	9.53
	60	.052	.051	.0047	10.72
	66	.093	.089	.0083	11.08

* $L_\lambda = \frac{\lambda_{ave}}{\frac{d\lambda}{dx}}$

Table 20. Summary of Wall Concentration Results

Injected Concentration C_i ppm	Injection Rate cc/min	Wall Concentration $(C_w/C_i) \times 10^3$ Station 1	Station 2	Station 3	Station 4
0	250	15.5	3.4	2.2	1.5
		14.5	3.5		
	350	25.0	6.1	4.4	3.1
		22.0	6.8		
	500	37.0	10.2	6.6	5.0
		37.0	11.8		
	1000	68.0	18.0	10.5	8.4
		55.0	18.8		
500	250	40.0	15.0	7.2	2.5
	350	66.0	22.5	12.0	3.9
	500	90.0	33.0	15.0	5.7
	1000	140.0	56.0	24.0	9.6
1000	250	76.0	27.5	16.4	6.2
	350	115.0	46.0	29.0	10.2
	500	200.0	66.0	36.0	12.0
	1000	250.0	115.0	60.0	17.0
2000	250	33.0	20.0	11.5	4.5
		22.0	16.0	10.5	5.4
	350	37.0	32.0	18.0	8.5
		58.0	26.0	21.0	9.5
	500	180.0	160.0	58.0	38.0
				29.0	32.0
	1000	400.0	400.0	105.0	62.0
				48.0	38.0

Table 21. Relative-Rate Parameter and Ratio of Plume Height to Boundary Layer Thickness
Injected Solution-Water

Distance from Channel Inlet (in)	Injection Rate cc/min	β	$\frac{\lambda_{ave}}{\delta}$
48		.033	.079
54		.114	.276
60		.390	.388
66		.370	.434

Table 22. Relative-Rate Parameter and Ratio of Plume Height to Boundary Layer Thickness
Injected Solution-500 ppm PEO

Distance from Channel Inlet (in)	Injection Rate cc/min	β	$\frac{\lambda_{ave}}{\delta}$
48	250	0.086	.033
	350	0.086	.034
	500	0.075	.033
	1000	0.081	.034
	Ave	0.082	.034
54	250	0.078	.077
	350	0.079	.080
	500	0.073	.085
	1000	0.078	.085
	Ave	0.077	.082
60	250	0.067	.170
	350	0.067	.172
	500	0.060	.176
	1000	0.064	.179
	Ave	0.064	.174
66	250	0.067	.432
	350	0.067	.440
	500	0.061	.378
	1000	0.065	.461
	Ave	0.065	.428

Table 23. Relative-Rate Parameter and Ratio of Plume Height to Boundary Layer Thickness
Injected Solution-1000 ppm PEO

Distance from Channel inlet (in)	Injection Rate cc/min	β	$\frac{\lambda_{ave}}{\delta}$
48	250	.119	.031
	350	.165	.033
	500	.141	.032
	1000	.139	.032
	Ave	.141	.032
54	250	.081	.043
	350	.116	.048
	500	.099	.046
	1000	.088	.048
	Ave	.096	.046
60	250	.060	.065
	350	.080	.067
	500	.068	.065
	1000	.068	.065
	Ave	.069	.066
66	250	.100	.224
	350	.133	.227
	500	.117	.230
	1000	.117	.231
	Ave	.117	.228

Table 24. Relative-Rate Parameter and Ratio of Plume Height to Boundary Layer Thickness Injected Solution-2000 ppm PEO

Distance from Channel Inlet (in)	Injection Rate cc/min	β	$\frac{\lambda_{ave}}{\delta}$
48	250	.181	.023
	350	.203	.025
	500	.199	.025
	1000	.163	.025
	Ave	.186	.024
54	250	.142	.033
	350	.157	.034
	500	.147	.033
	1000	.120	.033
	Ave	.142	.033
60	250	.138	.058
	350	.147	.057
	500	.147	.060
	1000	.122	.061
	Ave	.138	.059
66	250	.130	.096
	350	.144	.099
	500	.139	.099
	1000	.119	.105
	Ave	.133	.100

BIBLIOGRAPHY

1. Toms, B. A., "Some Observations on the Flow of Linear Polymer Solutions through Straight Tubes at Large Reynolds Numbers", Proceedings of International Congress on Rheology, Vol 2, North Holland Publishing Company, p. 135 (1948).

2. Hoyt, J. W., "The Effect of Additives on Fluid Friction", Trans. ASME, J. Basic Engineering, 94, D, 258 (1972).

3. Shaver, R. G., and E. W. Merrill, "Turbulent Flow of Pseudoplastic Polymer Solutions in Straight Cylindrical Tubes", AIChE J., 5, p. 181 (1959).

4. Dodge, D. W., and A. B. Metzner, "Turbulent Flow of Non-Newtonian Systems", AIChE J. 5, p. 189 (1959).

5. Ousterhout, R. S., and C. D. Hall, Jr., "Reduction of Friction Loss in Fracturing Operations", J. of Petroleum Technology, 13, p. 217 (1961).

6. Vogel, W. M. and A. M. Patterson, "An Experimental Investigation of the Effects of Additives Injected into the Boundary Layer of an Underwater Body", Proc. 5th Symposium on Naval Hydrodynamics, Bergen, ONR-ACR-112, p. 975 (1964).

7. Fabula, A. G., "The Toms Phenomenon in the Turbulent Flow of Very Dilute Polymer Solutions", Proceedings Fourth International Congress on Rheology, 1963, Part 3, E. H. Lee ed. Interscience Publishers, New York, p. 455 (1965).

8. Kowalski, T., "Reduction of Frictional Drag by Non-Newtonian Additives", Naval Engineers Journal, 78, p. 293 (April 1966).

9. Anon., "Friction Reducing Agent Improves Water Flow", Chemical Engineering, p. 36 (1 Aug. 1966).

10. Green, J. H., "Effect of Polymer Additives on Noozle Stream Coherence: A Preliminary Study", Naval Undersea R & D Center TN 504 (1971).

11. Schlichting, H., Boundary Layer Theory, McGraw-Hill, New York, 6th ed (1968).

12. Hinze, J. O., Turbulence, McGraw-Hill, New York (1959).

13. Bird, R. B., W. E. Stewart, and E. N. Lightfoot, Transport Phenomena, Wiley, New York (1960).

14. Head, M. R., "Entrainment in the Turbulent Boundary Layer", ARC RM 3152 (1958).

15. Kline, S. J., Ed., Proceedings, Computations of Turbulent Boundary Layers - AFOSR-IFP - Stanford Conference, Vol. I,Stanford Press (1969).

16. Clauser, F. H., "The Turbulent Boundary Layer", Vol. IV, Advances in Fluid Mechanics, Academic Press, New York, p. 2 (1956).

17. Ludweig, H. and W. Tillmann, "Investigations of the Wall Shearing Stress in Turbulent Boundary Layers", NACA TM 1285 (1950).

18. Clauser, F. H., "Turbulent Boundary Layers in Adverse Pressure Gradients", J. Aero. Sci., 21, 2,p. 91 (Feb., 1954).

19. Coles, D., "The Law of the Wake in the Turbulent Boundary Layer", J. Fluid Mech., 1, 2, p. 191 (1956).

20. Fabula, A. G., and T. J. Burns, "Dilution in a Turbulent Boundary Layer with Polymeric Friction Reduction", Naval Undersea Research and Development Center, San Diego, NUC TP 171 (1970).

21. Hama, F. R., Society Naval Architects Marine Engrs. Trans., 62, 333 (1954) Cited in Reference 12, p. 481.

22. Granville, P. S., "The Frictional Resistance and Velocity Similarity Laws of Drag-Reducing Dilute Polymer Solutions", NSRDC Report 2502, (1967).

23. Meyer, W. A., "A Correlation of the Frictional Characteristics for Turbulent Flow of Dilute Viscoelastic Non-Newtonian Fluids in Pipes", AIChE J., 12, p. 522 (1966).

24. Wetzel, J. M., and J. F. Ripken, "Shear and Diffusion in a Large Boundary Layer Injected with Polymer Solution", Univ. of Minn., St. Anthony Falls Hydraulic Laboratory, Project Report, 114 (1970).

25. Hulsebos, J., "An Investigation of a Turbulent Boundary Layer with Homogeneous Polymer Injection", Ph.D. Thesis, Georgia Institute of Technology (1968).

26. Poreh, M., and K. S. Hsu, "Diffusion of Drag Reducing Polymers in a Turbulent Boundary Layer", J. Hydronautics, 6, 1, p. 27 (1972).

27. White, F. M., "An Analysis of Flat Plate Drag with Polymer Additives", J. Hydronautics, 2, 4, p. 181 (1968).

28. Poreh, M., and J. E. Cermak, "Study of Diffusion from a Line Source in a Turbulent Boundary Layer", Int. J. Heat Mass Transfer, 7, p. 1083 (1964).

29. Morkovin, M. V., "On Eddy Diffusivity, Quasi-Similarity and Diffusion Experiments in Turbulent Boundary Layers", Int. J. Heat Mass Transfer, 8, p. 129 (1965).

30. Lumley, J. L., "Drag Reduction by Additives", in W. R. Sears, ed. Annual Review of Fluid Mechanics, Volume 1, Annual Reviews, Inc., Palo Alto, p. 367 (1969).

31. Patterson, G. K., J. L. Zakin, and J. M. Rodriquez, "Drag Reduction: Polymer Solutions, Soap Solutions and Solid Particle Suspensions in Pipe Flow", Industrial and Engineering Chemistry, 61, p. 22, (1969).

32. Granville, P. S., "Progress in Frictional Drag Reduction, Summer 1969 to Summer 1970", NSRDC, Ship Performance Department, Technical Note 184, (1970).

33. Granville, P. S., "Progress in Frictional Drag Reduction, Summer 1970 to Summer 1971", NSRDC, Ship Performance Department, Report 3761 (1972).

34. Granville, P. S., "Progress in Frictional Drag Reduction, Summer 1971 to Summer 1972", NSRDC, Ship Performance Department, Report 3994 (1973).

35. Pruitt, G. T., C. M. Simmons, G. H. Neill, and H. R. Crawford, "A Method to Minimize Costs of Pumping Fluids Containing Friction Reducing Additives", J. of Petroleum Technology, 17, p. 641 (1965).

36. Virk, P. S., "The Toms Phenomenon-Turbulent Pipe Flow of Dilute Polymer Solutions", Sc. D. Thesis Massachusetts Institute of Technology, (1967).

37. Goren, Y. and J. F. Norbury, "Turbulent Flow of Dilute Aqueous Polymer Solutions", Trans. ASME, J. Basic Engineering, 89, Series D, p. 814 (1967).

38. Ripkin, J. F. and M. Pilch, "Studies of the Reduction of Pipe Friction with the Non-Newtonian Additive CMC", Univ. of Minn. St. Anthony Falls Hydraulic Laboratory, Technical Paper No. 42, Series B (1963).

39. Pruitt, G. T. and H. R. Crawford, "Effect of Molecular Weight and Segmental Constitution on the Drag Reduction of Water Soluble Polymers", Western Co. Report No. DTMB-1 (1965).

40. Ernst, W. D., "Investigations of the Turbulent Shear Flow of Dilute Aqueous CMC Solutions", AIChE Journal, 12, p. 581 (1966).

41. Ernst, W. D., Investigation of the Turbulent Shear Flow of Dilute Aqueous CMC Solutions, NASA CR-395, Contract No. NASw-729, LTV Research Center, Dallas, Texas (1966).

42. Metzner, A. B., and M. G. Park, "Turbulent Flow Characteristics of Viscoelastic Fluids", J. Fluid Mechanics, 20, p. 291 (1964).

43. Whitsitt, N. F., L. J. Harrington, and H. R. Crawford, "Effect of Wall Shear Stress on Drag Reduction of Viscoelastic Fluids", C. S. Wells, Ed. Viscous Drag Reduction, Plenum Press, N. Y., p. 265 (1969).

44. White, W. D., "Drag-Reduction Measurements for Three Polymers at 4°C", in C. S. Wells, ed. Viscous Drag Reduction, Plenum Press, N. Y., p. 173 (1969).

45. Savins, J. G., "Drag Reduction Characteristics of Solutions of Macromolecules in Turbulent Pipe Flow", Society of Petroleum Engineering Journal, 4, p. 203 (1964).

46. Hoyt, J. W. and A. G. Fabula, "The Effect of Additives on Fluid Friction", Proceedings Fifth Symposium of Naval Hydrodynamics, Bergen, Norway, Office of Naval Research ACR-112, p. 947 (1964).

47. Virk, P. S., H. S. Mickley, and K. A. Smith, "The Ultimate Asymptote and Mean Flow Structure in Toms' Phenomenon". Trans. ASME, J. Applied Mechanics, 37, p. 488 (1970).

48. Virk, P. S., E. W. Merrill, H. S. Mickley, and K. A. Smith, "The Critical Wall Shear Stress for Reduction of Turbulent Drag in Pipe Flows by Poly(ethylene oxide) in Dilute Solution", in Modern Developments in the Mechanics of Continua, Academic Press, Inc., N. Y. (1966).

49. White, W. D., and D. M. McEligot, "Transition of Mixtures of Polymers in a Dilute Aqueous Solution Trans ASME, J. Basic Engineering, 92, D, p. 411 (1970).

50. Castro, W., and W. Squire, "The Effect of Polymer Additives on Transition in Pipe Flow", Applied Scientific Research, 18, p. 81 (1967).

51. Virk, P. S., "Drag Reduction in Rough Pipes", J. Fluid Mechanics, 45, p. 225 (1971).

52. Wells, C. S., "Turbulent Heat Transfer in Drag Reducing Fluids", AIChE J., 14, p. 406 (1968).

53. Sidahmed, G. H., and R. G. Griskey, "Mass Transfer in Drag Reducing Fluid Systems", AIChE J., 18, p. 138 (1972).

54. Elata, C., J. Lehrer, and A. Kahanovitz, "Turbulent Shear Flow of Polymer Solutions", Israel Journal of Technology, 4, p. 87 (1966).

55. Granville, P. S., "Limiting Conditions to Similarity-Law Correlations for Drag-Reducing Polymer Solutions", NSRDC Report 3635 (1971).

56. Gilbert, C. G., and J. F. Ripken, "Drag Reduction on a Rotating Disk", in C. S. Wells, ed. Viscous Drag Reduction, Plenum Press, N. Y., p. 251 (1969).

57. Giles, W. B., "Similarity Laws of Friction-Reduced Flows", J. Hydronautics, 2, p. 34, (1968).

58. Shin, H., "Reduction of Drag in Turbulence by Dilute Polymer Solutions", ScD. Thesis, Massachusetts Institute of Technology (1965).

59. Astarita, G., and L. Nicodemo, "Velocity Distributions and Normal Stresses in Viscoelastic Turbulent Pipe Flow", AIChE J. 12, p. 478 (1968).

60. Metzner, A. B., and G. Astarita, "External Flow of Viscoelastic Materials: Fluid Property Restriction on the Use of Velocity-Sensitive Probes", AIChE J., 13, p. 550 (1967).

61. Wetzel, J. M., and F. Y. Tsai, "Impact Tube Measurements in Dilute Polymer Solutions", AIChE J., 14 p. 663 (1968).

62. Frumen, D., P. Sulmont, and G. Loiseau, "Mesure des vitesses dans les fluides viscoelastiques au moyen de tubes de Pitot", J. de Mecanique, 8, p. 463 (1969).

63. Friehe, C. A. and W. H. Schwartz, "The Use of Pitot Static Tubes and Hot-Film Anemometers in Dilute Polymer Solutions", in C. S. Wells, ed. Viscous Drag Reduction, Plenum Press, N. Y., p. 281, (1969).

64. Granville, P. S., "Maximum Drag Reduction at High Reynolds Number for a Flat Plate Immersed in Polymer Solution", J. Hydronautics, 6, p. 58 (1972).

65. Levy, J. and S. Davis, "Drag Measurements on a Thin Plate in Dilute Polymer Solutions", International Shipbuilding Progress, 14, p. 166, (1967).

66. McCarthy, J. H., "Flat Plate Frictional Drag Reduction with Polymer Injection", NSRDC Report 3290 (1970).

67. Granville, P. S., "Drag Reduction of Flat Plates with Slot Ejection of Polymer Solutions", NSRDC Report 3158 (1969).

68. Elata, C., "Reduction of Friction on Submerged Bodies by Polymer Additives", Proc. 11th International Towing Tank Conf., Tokyo, p. 81 (1966).

69. White, D. A., "The Flow of a Dilute Polymer Solution in a Turbulent Boundary Layer on a Flat Plate", in C. S. Wells, ed. Viscous Drag Reduction, Plenum Press, N. Y., p. 351 (1969).

70. Poreh, M. and K. S. Hsu, "Diffusion of Drag Reducing Polymers in a Turbulent Boundary Layer", J.Hydronautics, 6, p. 27 (1972).

71. Poreh, M. and K. S. Hsu, "Diffusion from a Line Source in a Turbulent Boundary Layer", Int. J. Heat and Mass Transfer, 14, p. 1473 (1971).

72. Wells, C. S., "An Analysis of Uniform Injection of a Drag-Reducing Fluid into a Turbulent Boundary Layer", in C. S. Wells, ed. Viscous Drag Reduction, Plenum Press, N. Y., p. 361 (1969).

73. Emerson, A., "Model Experiments Using Dilute Polymer Solutions Instead of Water", Trans., N. E. Coast Inst. of Engineers and Shipbuilders, 81, p. 201 (1965).

74. Wu., J., "Drag Reduction in External Flows of Additive Solutions", in C. S. Wells, ed. Viscous Drag Reduction, Plenum Press, N. Y., p. 331 (1969).

75. Tagori, T., and I. Ashidate, "Some Experiments on Friction Reduction on Flat Plate by Polymer Solutions", Proc. 12th International Towing Tank Conference, Rome, p. 132 (1969).

76. Merrill, E. W., K. A. Smith, and R. Y. C. Chung, "Drag Augmentation by Polymer Addition", AIChE J., 12, p. 809 (1966).

77. White, A., "Effect of Polymer Additives on Boundary Layer Separation and Drag of Submerged Bodies", Nature, 208, p. 1390 (1966).

78. Lang, T. G., and H. V. L. Patrick, "Drag of Blunt Bodies in Polymer Solutions", Paper presented at the Winter Annual Meeting and Energy Systems Exposition of ASME, New York (1966).

79. Thurston, S. and R. D. Jones, "Experimental Model Studies of Non-Newtonian Soluble Coatings for Drag Reduction", AIAA J. of Aircraft, (March/April 1965).

80. Sarpkaya, T. and P. G. Rainey, "Flow of Dilute Polymer Solutions about Circular Cylinders", Naval Postgraduate School Report NPS-59SL1021A (1971).

81. Love, R. H., "The Effect of Ejected Polymer Solutions on the Resistance and Wake of a Flat Plate in a Water Flow", Hydronautics, Inc., Tech. Report 353-2 (1965).

82. Wells,C. S., Jr., and J. G. Spangler, "Injection of a Drag-Reducing Fluid into Turbulent Pipe Flow of a Newtonian Fluid", Physics of Fluids, 10, p. 1890 (1967).

83. Maus, J. R. and L. R. Wilhelm, "Effect of Polymer Injection on Frictional Drag in Turbulent Pipe Flow", J. Hydronautics, 4, p. 35 (1970).

84. Baronet, C. N., and W. H. Hoppman II, "Drag Reduction Caused by High Polymer Solutions Injected into Water Flowing Around Cylindrical Bodies", Rensselaer Polytechnic Inst., Dept. of Mechanics, Report to ONR on Contract Nonr-591 (20), AD 636158 (1966).

85. Latto, B. and C. H. Shen, "Effect of Dilute Polymer Solution Injection on External Boundary Layer Phenomena", Canadian J. Chem. Engr., 48, p. 34 (1970).

86. Wu, J. and M. Tulin, "Drag Reduction by Ejecting Additive Solutions into a Pure-Water Boundary Layer", Hydronautics Inc., Tech. Report 353-7 (1970).

87. Wu, J., "Some Techniques of Ejecting Additive Solutions for Drag Reduction", Hydronautics, Inc., Technical Report 7101-1 (1971).

88. Walters, R. R., and C. S. Wells, "An Experimental Study of Turbulent Diffusion of Drag Reducing Polymer Additives", J. Hydronautics, 5, p. 65 (1971).

89. Walters, R. R., and C. S. Wells, "Effects of Distributed Injection of Polymer Solutions on Turbulent Diffusion", J. Hydronautics, 6, p. 69 (1972).

90. Wu, J., "Suppressed Diffusion of Drag-Reducing Polymer in a Turbulent Boundary Layer", J. Hydronautics, 6, p. 46 (1972).

91. Tullis, J. P., and L. F. Lindeman, "Polymer Injection for Drag Reduction", Colorado State University, Contract N00014-67-A-0299-0013, Project No. 2322 (July 1972).

92. Oldroyd, J. G., "A Suggested Method of Detecting Wall Effects in Turbulent Flow Through Tubes", Proceedings of the First International Congress on Rheology, Vol. 2, North Holland Publishing Company, p. 130 (1948).

93. Davies, G. A., and A. B. Ponter,"Turbulent Flow Properties of Dilute Polymer Solutions", Nature, 212, p. 65 (1966).

94. Sl'perin, I. T., and B. M. Smol'skil, Vesti Akad. Navuk Belarusk. SSR Ser. Fix.-Tekhn., Navak, 2, 39 (1965). Cited in Reference 93.

95. Little, R. C., "Drag Reduction by Dilute Polymer Solutions in Turbulent Flow". Naval Research Laboratory Report 6542, (1967).

96. Little, R. C., "Displacement of Aqueous Drag-Reducing Polymer Solutions", I & EC Fundamentals, 8, p. 520 (1969).

97. Patterson, G. K. and J. L. Zakin, "Prediction of Drag Reduction with Viscoelastic Model", AIChE J., 14, p. 434 (1968).

98. Elata, C. and M. Poreh, "Momentum Transfer in Turbulent Shear Flow of an Elastico-Viscous Fluid", Rheological Acta, 5, p. 148 (1966).

99. Boggs, F. W., and J. Thompson, "Flow Properties of Dilute Solutions of Polymers, Part 1-Mechanism of Drag Reduction", U.S. Rubber Co. Research Center Report on Contract No. Nonr-3120 (00), (1966).

100. Lockett, F. J., "Fluid Dynamics Approach to the Toms Effect", Nature, 222, p. 937 (1969).

101. Black, T. J., "Viscous Drag Reduction Examined in the Light of a New Model of Wall Turbulence , in C. S. Wells, ed. Viscous Drag Reduction, Plenum Press, N. Y., p. 383 (1969).

102. Ellis, A. T., R. Y. Ting, and R. H. Nadolink, "Some Effects of Storate and Shear History on the Friction Reducing Properties of Dilute Polymer Solutions", J. Hydronautics, 6, p. 66 (1972).

103. Lumley, J. L., "The Toms Phenomenon: Anomalous Effects in Turbulent Flow of Dilute Solutions of High Molecular Weight Linear Polymers", Applied Mechanics Review, 20, p. 1139 (1967).

104. Paterson, R. W., and F. H. Abernathy, "Turbulent Flow Drag Reduction and Degration with Dilute Polymer Solutions", J. Fluid Mechanics, 43, p. 689 (1970).

105. Peterlin, A., "Molecular Model of Drag Reduction of Polymer Solutes" Nature, 227, p. 598 (1970).

106. Tulin, M. P., Hydrodynamic Aspects of Macromolecular Solutions", Proc. 6th Symposium on Naval Hydrodynamics Washington, UNR ACR-136, p. 3 (1966). Cited in ref. 2.

107. Gordon, R. J., "On the Explanation and Correlations of Turbulent Drag Reduction in Dilute Macromolecular Solutions", J. App. Polymer Science, 14, p. 2097 (1970).

108. Millward, A., "Turbulent Pressure Fluctuations in Water with Additives", University of Southhampton Department of Aeronautics and Astronautics, Contract Number F61052 67 C 0086, AD 736634 (1971).

109. Gadd, G. E., "Reduction of Turbulent Friction in Liquids by Dissolved Additives", Nature, 212, p. 874 (1966).

110. Gadd, G. E., "Turbulence Damping and Drag Reduction Produced by Certain Additives in Water", Nature, 206, p. 463 (1965).

111. Johnson, B., and R. H. Barchi, "Effect of Drag-Reducing Additives on Boundary-Layer Turbulence", J. Hydronautics, 2, p. 108 (1968).

112. Walsh, M., III, "On the Turbulent Flow of Dilute Polymer Solutions", Ph.D. Thesis, California Institute of Technology, (1967).

113. Black, T. J., "Some Practical Applications of a New Theory of Wall Turbulence", Proceedings of the 1966 Heat Transfer and Fluid Mechanics Institute, Stanford University Press, p. 366 (1966).

114. Union Carbide Corp., "How to Dissolve Polyox Water-Soluble Resins", Bulletin F-42933.

115. Stone, F. W., and J. J. Stratta, "Ethylene Oxide Polymers", Encyclopedia of Polymer Science and Technology, Wiley, New York (1967).

116. Eichholz, G. G., A. N. Galli, and L. W. Elston, "Problems in Trace Element Analysis in Water", Water Resources Research, 2, 3, p. 561 (1966).

117. Eichholz, G. G., R. B. Hughes, and A. E. Nagel, "Adsorption of Ions in Dilute Aqueous Solutions on Glass and Plastic Surfaces", Georgia Institute of Technology, Technical Report NE-2 (1964).

118. Draper, N. R., and H. Smith, Applied Regression Analysis, Wiley, New York (1966).

119. MacMillan, F. A., "Viscous Effects on Flattened Pitot Tubes at Low Speeds", J. Royal Aeronautical Society, 58, p. 837 (1954).

120. Knudsen, J. G., and D. L. Katz, Fluid Dynamics and Heat Transfer, McGraw-Hill, New York(1958).

121. Shaw, R., "The Influence of Hole Dimensions on Static Pressure Measurements", J. Fluid Mech., 7, p. 550 (1960).

VITA

Dermot Joseph Collins was born November 22, 1942 in Corner Brook, Newfoundland, Canada, and graduated from high school there in 1959. He attended Saint Francis Xavier University and Nova Scotia Technical College, where he received a Bachelor of Engineering in Chemical Engineering in 1964.

Mr. Collins worked for Cynamid of Canada in Niagara Falls and the Linde Division of Union Carbide in Tonawanda, New York, before entering graduate school at Georgia Tech in 1967. He received a M.S. in Chemical Engineering in 1968. He was employed by Shell Oil and Esso Production Research, both in Houston, Texas, during the summers of 1968 and 1969, respectively. In 1970, he was employed part time as an engineering consultant in the field of process research. He represented Georgia Tech in bridge at the Southeast College Regional Tournaments in 1971 and 1973. He is a member of Sigma Xi.

Mr. Collins married the former Paula Mills of Sparta, Georgia, and they have a daughter, Cecilia Nicole.